# Characterization of neuronal activity in the auditory brainstem of rats: An optical imaging approach

Dissertation

zur Erlangung des Doktorgrades der

Naturwissenschaften

Fachbereich Biologie
Technische Universität Kaiserslautern

vorgelegt von

**Geetha Srinivasan**

Juni 2004

Vorsitzender: Prof. Dr. Joachim W. Deitmer (Technische Universität Kaiserslautern)

Betreuer: Prof. Dr. Eckhard Friauf (Technische Universität Kaiserslautern)

Koreferent: Prof. Dr. Rüdiger Köhling (Rheinische Friedrich-Wilhelms-Universität Bonn)

Tag der Disputation: Juli 2004

I, Geetha Srinivasan, do hereby declare that this submission is my own work and that, to the best of my knowledge and belief, it contains no material previously published by another person, nor material which to a substantial extent has been accepted for the award of any other degree or diploma of a university or other institute of higher learning.

Kaiserslautern, 14th June 2004.

# Table of contents

# 1 General introduction

The brain is a huge ensemble of neurons and glial cells, which control specific functions like emotion, memory, and judgement. Specific parts of the brain relay information throughout the body so that the body can perform its day to day functions. There are about $10^{12}$ neurons, interconnected by at least $10^{15}$ synapses. These synaptic connections play a major role in performing different tasks. This thesis addresses neuronal ensemble activity in the auditory brainstem, by optical imaging with voltage-sensitive dyes (VSD).

## 1.1 Auditory pathway – an overview

The ear converts and translates sound into neuronal information (transduction) and the brain processes this information in order to obtain meaningful knowledge (computation). The computation process is carried out in a number of stages by different neural structures. Neurons that process sound information are the extreme timing machines of the brain. They were designed for speed, to preserve and analyze the very rapid neuronal signals that encode sound signals. Through the ear, the acoustic signals are transformed into electrical signals by the cochlea. In the cochlea, the basilar membrane carries out a frequency analysis of the incoming sound wave, such that each frequency within the auditory spectrum causes a maximum displacement to occur at a particular place on the basilar membrane. Sensory receptors, known as hair cells, reside on the basilar membrane and generate potentials. Communication of hair cell responses to the nervous system is achieved via the auditory nerve. The distribution of auditory nerve fibers is a duplicate of the sound spectrum, and the characteristic frequencies from the basal end (high

frequency) to the apical end (low frequency) of the membrane. Thus, auditory nerve fibers convey a tonotopic representation of sound to the brain. Comprehensive reviews of the auditory system are given by Irvine (1986; 1992), Cant (1997), and Oliver (2000).

The tonotopic organization of the cochlea is retained at all levels of the central auditory system (review: Irvine, 1986). Projections from the cochlea innervate the cochlear nucleus (CN). CN neurons send their output through three different fiber tracts, namely dorsal, ventral, and intermediate acoustic striae, innervating several distinct groups of neurons, each projecting to different nuclei (review: Cant, 1991). Acoustic information is processed by at least six parallel ascending pathways that are integrated in the inferior colliculus (IC). The output of the IC is conveyed to the medial geniculate nucleus. This in turn, projects to the auditory cortex, the pinnacle of the auditory processing pathway necessary for the perception of sound. As mentioned above, at all levels of processing, connections are topographically ordered on the basis of frequency (tonotopy).

## 1.2 Superior olivary complex - an integral part of the central auditory system

The CN projects to the superior olivary complex (SOC) and the IC (review: Thompson and Schofield, 2000). The SOC is the first station where the information from both ears converge (review: Illing et al., 2000). The SOC consist of several nuclei, mainly the lateral superior olive (LSO), the medial superior olive (MSO), the medial nucleus of the trapezoid body (MNTB), the superior paraolivary nucleus (SPN) and the periolivary nucleus (PON). The PON is comprised of the lateral nucleus of the trapezoid body (LNTB), and the ventral nucleus of the trapezoid body (VNTB). The inputs to these nuclei are described in Chapter 3.1.

**1.2.1 MNTB - a sign-inverting relay station in the auditory pathway**

The MNTB is a conspicuous structure in the mammalian auditory brainstem, which possesses one of the most powerful presynaptic terminals in the central nervous system, i.e., the calyx of Held (Friauf and Ostwald, 1988; Smith et al., 1998). The majority of the cells in the MNTB are principle cells with globular somata and relatively few dendrites (Sommer et al., 1993). MNTB neurons are monoaural and
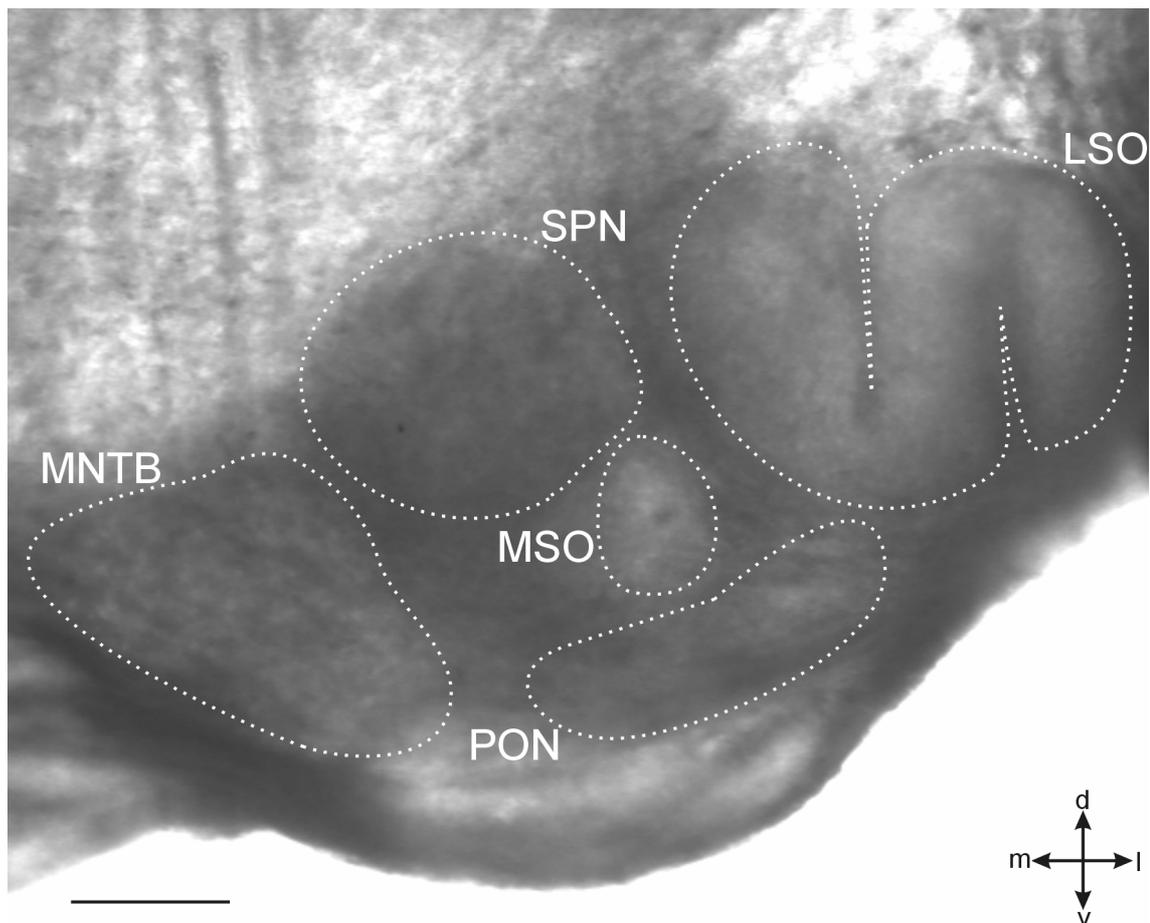


**Fig. 1.1: Videomicrograph of the superior olivary complex (SOC)**

Videomicrograph of a 300 µm thick acute brainstem slice of a P10 rat, showing the major nuclei of the SOC, i.e., the lateral superior olive (LSO), the medial superior olive (MSO), the medial nucleus of the trapezoid body (MNTB), the superior paraolivary nucleus (SPN), and the periolivary nucleus (PON). v = ventral; d = dorsal; l = lateral; m = medial; scale bar = 200 µm.

respond only to contralateral acoustic stimulation (Sommer et al., 1993). Synaptic transmission at the calyx synapse is mediated by glutamate acting on ionotropic glutamate receptors (Forsythe and Barnes-Davies, 1993a,b), and the transmission is such that each presynaptic action potential (AP) results in an postsynaptic AP (Borst et al., 1995). MNTB neurons themselves are inhibitory (Wenthold, 1991) i.e., they provide glycinergic input to the postsynaptic neurons of various nuclei as described in Chapter 4.1. Thus, principle neurons of the MNTB sign invert their glutamatergic inputs from the contralateral CN (Moore and Caspary, 1983; Spangler et al., 1985; Smith et al., 1998; Kim and Kandler, 2003). Additionally, the MNTB itself is inhibited by its recurrent collaterals (Guinan and Li, 1990) and also by neurons in the VNTB (review: Thompson and Schofield, 2000). The frequency gradient in the MNTB is arranged such that high frequencies are represented in the medial part and low frequencies in the lateral part (Fig. 4.1; Vater and Feng, 1990).

## 1.2.2 LSO – processing of interaural level differences

In carnivores and rodents, the LSO has a peculiar S-shape and is located laterally in the SOC (Fig. 1.1; Schwarz, 1992). It is evident that LSO neurons process differences in sound level between the two ears (Sanes, 1993; Tollin and Yin, 2002a,b). In the rat, Rietzel and Friauf (1998) described seven classes of LSO neurons. The bipolar neurons and multipolar neurons are the two most frequent types. The small multipolar neurons, banana-like neurons, bushy neurons, unipolar neurons and marginal neurons are the less frequent types. The spherical bushy neurons of the ventral CN provide glutamatergic input to the ipsilateral LSO in a tonotopic fashion (Cant and Casseday, 1986; Friauf and Ostwald, 1988; Cant, 1991; Suneja et al., 1995). On the other hand, the globular bushy cells in the ventral CN

deliver glycinergic inputs to the contralateral LSO via the MNTB (Warr, 1972). Accordingly, the majority of neurons respond to acoustic stimuli, presented to either ear, as follows: stimulation of the ipsilateral ear causes an increase, yet stimulation of the contralateral ear a decrease in the firing rate of a given LSO neuron. The LSO contains a detailed map of sound frequency, i.e., LSO neurons respond best for a characteristic frequency of sound (Sanes et al., 1990). The tonotopic organization of the LSO is such that high frequencies are represented in the medial limb and low frequencies in the lateral limb (Fig. 4.1; Tolbert et al., 1982a,b; Wenthold, 1991; Vater, 1995; Kelly et al., 1998).

### 1.2.3 MSO – processing of interaural time differences

In the MSO, three types of neurons were described, namely the principle bipolar neurons, marginal neurons and the MSO core neurons with multipolar dendritic trees (Smith, 1995). Principle neurons receive low frequency information from both ears. The MSO has been considered as the primary site for processing interaural time differences (ITD) by coincidence detection of incoming bilateral synaptic excitation. The supporting data include converging afferents from both anteroventral CN (Stotler, 1953; Warr, 1966; Goldberg and Brown, 1968) with identical types of synapses from either side (Clark, 1969a,b; Perkins, 1973). The majority of principle MSO neurons are excited by sound stimulation of either ear (Goldberg and Brown, 1969; Caird and Klinke, 1983; Langford, 1984). Anatomical results suggest that the MSO also receives inhibitory afferents, mainly from the ipsilateral MNTB (Spangler et al., 1985; Kuwabara and Zook, 1991; Grothe et al., 1992). There is also a second presumed inhibitory projection to MSO neurons from the periolivary nucleus (PON; Cant & Hyson, 1992). The MSO is tonotopically organized such that high frequencies

are represented in the ventral part and low frequencies in the dorsal part (Fig. 4.1; Grothe, 1994; Kelly et al., 1998). A detailed account of the MSO with respect to ITD coding is described in Chapter 5.1.

### 1.2.4 SPN - its role in sound localization

The SPN is composed of mainly GABAergic and some glycinergic neurons (Saint Marie and Baker, 1990; Thompson and Schofield, 2000; Kulesza et al., 2003). Typical SPN neurons are medium to large multipolar cells with long, scarcely branched and smooth dendrites that extend over long distances within a nearly parasagittal plane (Saldana and Berrebi, 2000). They receive excitatory inputs from the ipsi- and contralateral CN (Behrend et al., 2002; Dehmel et al., 2003; Kulesza et al., 2003) and inhibitory input from the ipsilateral MNTB (Kulesza et al., 2003). The glycinergic MNTB input to the SPN is well documented (Spangler et al., 1985; Banks and Smith, 1992; Kuwabara and Zook, 1992; Sommer et al., 1993). Physiological studies suggest that the majority of SPN neurons are excited by stimulation of either ear, and that many SPN neurons receive convergent inputs from the two CN (Finlayson and Adam, 1997). In the SPN, at least a significant proportion of the neurons are directly involved in sound localization (Behrend et al., 2002). The tonotopic organization of the SPN is such that high frequencies are represented medially and low frequencies laterally (Fig. 4.1; Kelly et al., 1998; Kulesza et al., 2003).

In general, for addressing physiological questions in these auditory brainstem nuclei, conventional patch-clamp recordings have been used. This technique allows recording from a single or few cells at a time. Therefore, in order to study a population of cells, an alternative method is needed. In several systems excluding

the auditory brainstem, multisite optical recording has been demonstrated, which allows recording from a population of neurons with high temporal resolution. So, I attempt to establish optical imaging for the auditory brainstem slice. Establishment of this technique is described in Chapter 2.

## 1.3 Multisite optical recording of the SOC

The optical recording technique used in this study consisted of an array of 464 photodiodes, to measure dynamic changes in transmembrane potentials of SOC nuclei stained with VSDs. This technique enables to understand the spatio-temporal profiles of the information processing occurring in complex and intact neural structures directly (Neunlist et al., 1999). The temporal resolution is in the tens of microsecond range (reviews: Grinvald et al., 1988; Ebner and Chen, 1995), sufficient to study action potentials and synaptic potentials. Usage of VSDs has made it possible to monitor electrical activity in small cells, which is difficult or impossible by conventional electrophysiological means.

### 1.3.1 Voltage-sensitive dyes

The VSDs are a heterogeneous group of chemical compounds, which have in common the ability to act as molecular transducers by transforming changes in membrane potential into changes in optical signal (review: Ebner and Chen, 1995). The choice of the optimal dye for a given preparation is an important consideration for optical recordings. The wave length dependence (i.e., the excitation and emission wavelength spectra of the dye should match with optical filter settings and spectra of the lamp), dye toxicity, signal size, signal-to-noise ratio, osmotic behaviour, and the utility of dyes for long-term recording were taken into consideration with respect to

the selection of the dye (review: Ebner and Chen, 1995). The ideal VSD is (1) sensitive to changes in transmembrane potential: the signal size and the signal-to-noise ratio are large; (2) the optical response follows a voltage change rapidly; (3) little or no tendency to harm the preparation as a result of pharmacological or phototoxic action; and (4) little and/or slow photobleaching of the dye. A detailed account of VSDs is given in Chapter 2.1.

## 1.4 Aim of this thesis

The aim of this doctoral thesis was to study synaptic transmission simultaneously in a large population of neurons in the SOC, which is possible by optical imaging. This study focus on the following four specific projects:

1.  Establishment of a multisite optical imaging technique for auditory brainstem slices.

2.  Elucidating the functional glycinergic and glutamatergic inputs to the major nuclei of the SOC, namely the LSO, MSO, and SPN.

3.  Characterization of the action of glycine development in the LSO, MSO, SPN, and MNTB.

4.  The role of MSO in coincidence detection was investigated.

Each project will be treated in a separate Chapter, which will be organized such that each Chapter (2 to 5) will have its own Introduction, Materials and methods, Results, and Discussion section.

_____

# 2 Establishment of optical imaging with voltage-sensitive dye in auditory brainstem slices

## 2.1 INTRODUCTION

Understanding the spatio-temporal features of the information processing in the brain requires monitoring and analyzing of the activity in populations of neurons. Classical intracellular and extracellular electrophysiological techniques have provided important insights into the function of neural circuits and neuronal populations in the brain. However, it is difficult to study the neuronal activity in a population of neurons at a single time point using conventional electrophysiological techniques. Therefore, complementary techniques are required. Optical imaging using voltage-sensitive dyes (VSDs) has made it possible to monitor the electrical activity of populations of neurons (review: Ebner and Chen, 1995). Therefore, it is necessary to establish optical imaging techniques for every region of interest in the brain. In the present study, optical imaging of auditory brainstem using VSDs had to be established in a first step before scientific questions could be addressed.

VSDs are classified as slow dyes and fast dyes (Fig. 2.1) based on the speed, size and mechanism of the potential-dependent optical change (Waggoner, 1979a,b).
*Slow dyes*: The slow dyes (or redistribution dyes) respond to membrane potential changes in time frames of seconds. They can permeate membranes and work by a mechanism involving potential-dependent redistribution of the charged dye molecules between the medium and the inside of the cell (Fig. 2.1A). Slow dyes have a voltage sensitivity in the order of 1-2% change in light intensity per mV change in membrane potential (Ebner and Chen, 1995).
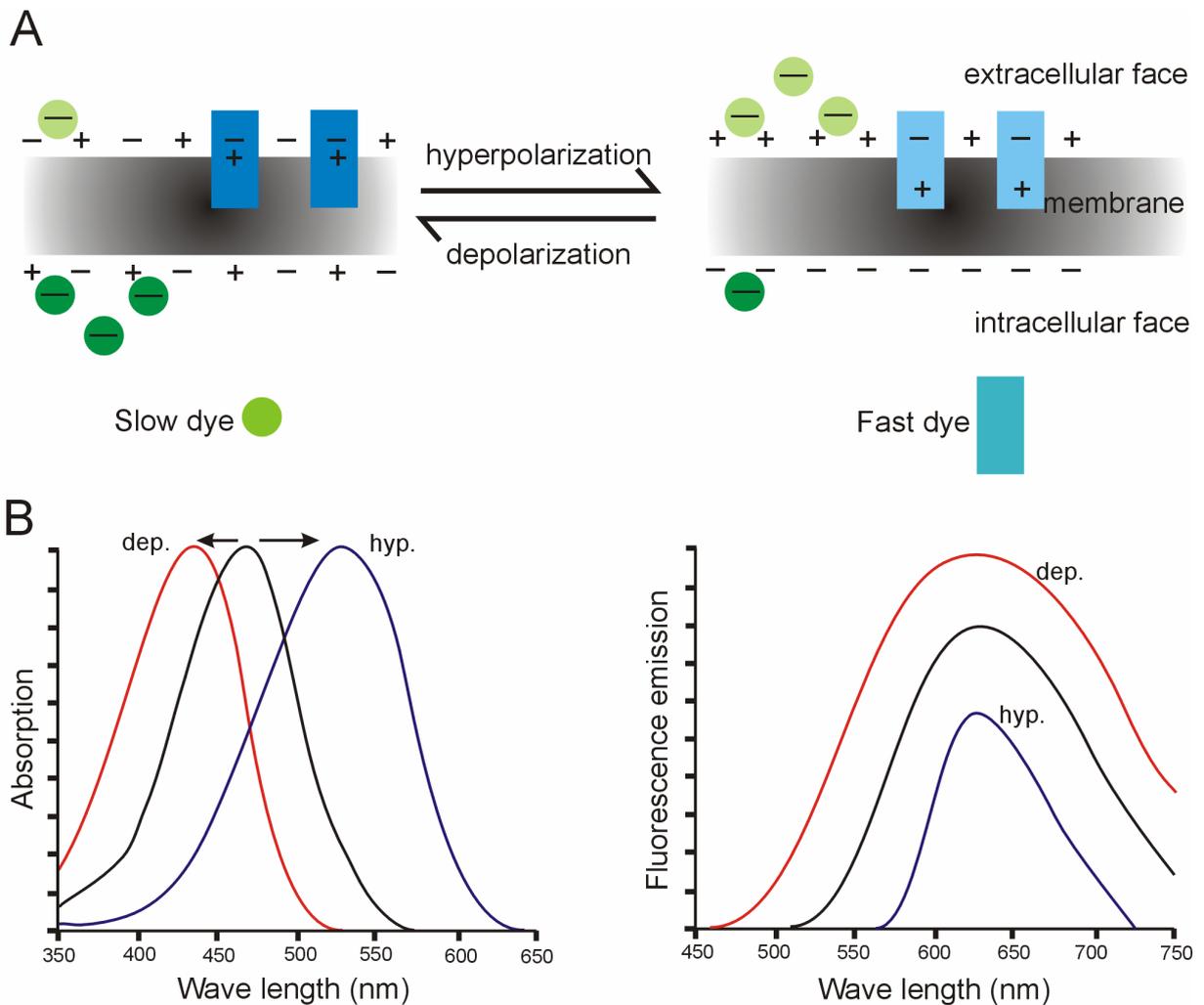
**Fig. 2.1: Mechanisms of fluorescence changes of voltage-sensitive dyes (VSDs) upon membrane potential**

(A) Slow and fast dyes are the two types of VSDs. Slow dyes are lipophilic anions (as depicted in this illustration) or cations that are membrane permeable, and can thus change their transmembrane distribution (slow transmembrane movement of entire molecules) upon membrane de- and hyperpolarizations. Fluorescence changes associated with transmembrane redistribution are represented by color changes in the illustration (cf. Fig. 2.1B). In contrast, the fast dyes bind to phospholipid bilayer membranes and change their electronic structure (fast intramolecular redistribution of electrons) upon de- and hyperpolarizations. The changes in the spectral profile are represented by color changes in the illustration. (B) Absorption (left graph) and emission (right graph) spectra of a typical fast dye (Di-8-ANEPPS; black curves) and its changes upon depolarization (dep., red curves) and hyperpolarization (hyp., blue curves). The absorption and emission maximum of this dye is at 467 nm and 631 nm, respectively, when bound to membranes. The dye responds to hyperpolarization with a decrease in fluorescence emission and to depolarization with an increase in fluorescence emission (modified from Handbook of fluorescent probes and research products, Molecular probes).

_____

*Fast dyes*: The fast dyes respond to membrane potential changes in less than a millisecond (review: Grinvald et al., 1988). They bind to the membrane and work by potential-dependent changes of the charge distribution (Fig. 2.1A). The changes in charge distribution influence the spectral properties (absorption and emission) of the dye (Fig. 2.1B). Fast dyes have a voltage sensitivity in the order of 2-10% change in light intensity per 100 mV change in membrane potential (Ebner and Chen, 1995).

Understanding the spatio-temporal features of the information processing in the SOC expands our knowledge of auditory processing. This requires monitoring and analyzing the electrical activity in a population of neurons. Although conventional electrophysiological techniques provided important insights into the functioning of the SOC, optimal techniques for studying the spatio-temporal features in neuron population lacked. Thus, establishing optical recordings of electrical activity in the SOC is essential. Therefore, optical recordings with RH795 (reviews: Ebner and Chen, 1995; Momose-Sato et al., 2001; Grinvald et al., 1988), a fast voltage-sensitive dye on acute brainstem slices in combination with electrical stimulation of SOC inputs were done in the present thesis. This approach allows the comparative measurement of electrical activity of cell ensembles with high spatio-temporal resolution. RH795 is one of an extensive group of dialkylaminophenylpolyenylpyridinium dyes, that are principally used for functional imaging of neurons (deBeer, 1997). RH795 produced negligible side effects when tested *in vitro* using hippocampal slices and in *in vivo* experiments on cat and monkey visual cortices (Grinvald et al., 1994). In contrast to dye Di-8-ANEPPS (Fig. 2.1), RH795 responds to hyperpolarization with a increase in fluorescence emission and to depolarization with an decrease in fluorescence emission.

In this Chapter 2 of the present study, in order to establish an optical imaging technique to study neuronal activity in the SOC, the following parameters were tested: (1) extracellular potassium concentration, (2) power supplies, (3) amplifier adjustment time, (4) dye concentration, and I also characterized the optical signals in terms of presynaptic and postsynaptic components. This part of the present study shows that optical recordings with VSDs can be used for detecting neuronal activity in auditory brainstem slices.

Part of the data presented in this Chapter has been accepted for publication (Srinivasan et al., 2004b).

## 2.2 MATERIALS AND METHODS

### Acute slice preparation

Brainstem and cortex slices were prepared from Sprague-Dawley rat pups of either gender between postnatal day (P) 3 and P19 (the day of birth was defined as P0). The animals were bred and housed in the animal facility in accordance with the current German animal protection law. All protocols were approved by the animal care and use committees responsible for our institution. The animals were deeply anesthetized with an overdose of ketamine (1 mg $g^{-1}$ body weight i.p.), decapitated, and their brain was carefully dissected. The following preparation steps were done in cold (~4 °C) preparation solution (for composition, see below): regarding the brainstem, 300 µm-thick coronal or horizontal brainstem slices containing the SOC and regarding the cortex, 300 µm-thick sagittal slices were cut with a vibrating microtome (VT-1000, Leica, Bensheim, Germany) and transferred into a chamber filled with carboxygenated (95% $O_2$, 5% $CO_2$) storage solution (for composition, see below). After 60 min at ~34 °C, the slices were kept at room temperature (20-23 °C)

for 30 min. The slices were then transferred into carboxygenated recording solution (for composition, see below) supplemented with 50 or 100 μM of the voltage-sensitive dye RH795. Some brainstem slices were also tested with 100 μM RH414 and 50 μM Di-8-ANEPPS; dyes were obtained from Molecular Probes, Leiden, The Netherlands. After dye incubation for 30 min, the slices were placed in a recording chamber, which was continuously perfused with recording solution ($\cong$ 3-4 ml min$^{-1}$). In some experiments, the slices were placed in a chamber with carboxygenated recording solution for 50 min to wash out unbound dye molecules. Then they were transferred to the recording chamber.

**Solutions and drug applications**

The preparation solution contained [mM]: NaHCO$_3$, 25; NaH$_2$PO$_4$, 1.25; KCl, 2.5; MgCl$_2$, 1; CaCl$_2$, 2; D-glucose, 260; Na-pyruvate, 2; *myo*-inositol, 3; and kynurenic acid, 1 (pH 7.4 when bubbled with 95% O$_2$, 5% CO$_2$). The storage solution had the following composition [mM]: NaCl, 125; NaHCO$_3$, 25; NaH$_2$PO$_4$, 1.25; KCl, 2.5; MgCl$_2$, 1; CaCl$_2$, 2; D-glucose, 10; Na-pyruvate, 2; *myo*-inositol, 3; ascorbic acid, 0.4 (pH 7.4 when bubbled with 95% O$_2$, 5% CO$_2$). The recording solution used for dye incubation and recordings contained 122.5 mM NaCl and 5 mM KCl. In case of recordings with different concentrations of KCl, KCl was replaced by an equimolar concentration of NaCl. To pharmacologically isolate stimulus-evoked and action-potential mediated signals, the Na$^+$ channel blocker tetrodotoxin (TTX, Tocris, Germany; 0.5 μM) was added to the recording solution. In case of recordings with Ca$^{2+}$-free solution, Ca$^{2+}$ was replaced by an equimolar concentration of Mg$^{2+}$. Ca$^{2+}$-free solution and TTX were bath applied for 15 minutes before the recording began.

**Optical recording setup**

The arrangement of the optical recording setup is schematically illustrated in figure 2.2. Slices were placed into the recording chamber mounted on an upright microscope (Axioskop2 FS, Zeiss, Jena, Germany) and continuously perfused with recording solution. The microscope was equipped with differential interference contrast/fluorescent optics (Achroplan objectives, Zeiss) and a camera system containing a charge coupled diode (CCD) camera (VC 45, PCO, Kelheim, Germany) and a PC frame grabber card (DT 3155, Data Translation, Bietigheim-Bissingen, Germany). Images of the slices were digitized (Fig. 2.3A) and all relevant identifiable structures, i.e., the SOC nuclei, the border of the slice, and the tips of the stimulus electrodes (SE), were outlined with graphic software (CorelDraw, version 9.0, Corel, Ottawa, Canada; Fig. 2.3B). During optical recordings, the slices were illuminated with light from a mercury arc light bulb (HBO103, Osram, München, Germany). The light pathway contained a shutter (VS25, Uniblitz, Vincent Ass., Rochester, NY), which was controlled by the acquisition software (Neuroplex 3.01, RedShirtImaging, Fairfield, CT), and a set of fluorescent filters (excitation: 546 ± 12 nm, beam splitter: 580 nm, emission: 590 nm; Zeiss). Emitted light was detected by a photodiode array (PDA; Neuroplex, RedShirtImaging), containing 464 hexagonally arranged diodes with a physical dimension of approximately 1.8 cm $\times$ 1.8 cm (750 µm x 750 µm diode area). Depending on the magnification of the objective (10x-40x), the area covered by a single photodiode ranged from 75 µm x 75 µm to 18.75 µm x 18.75 µm (Fig.2.3).
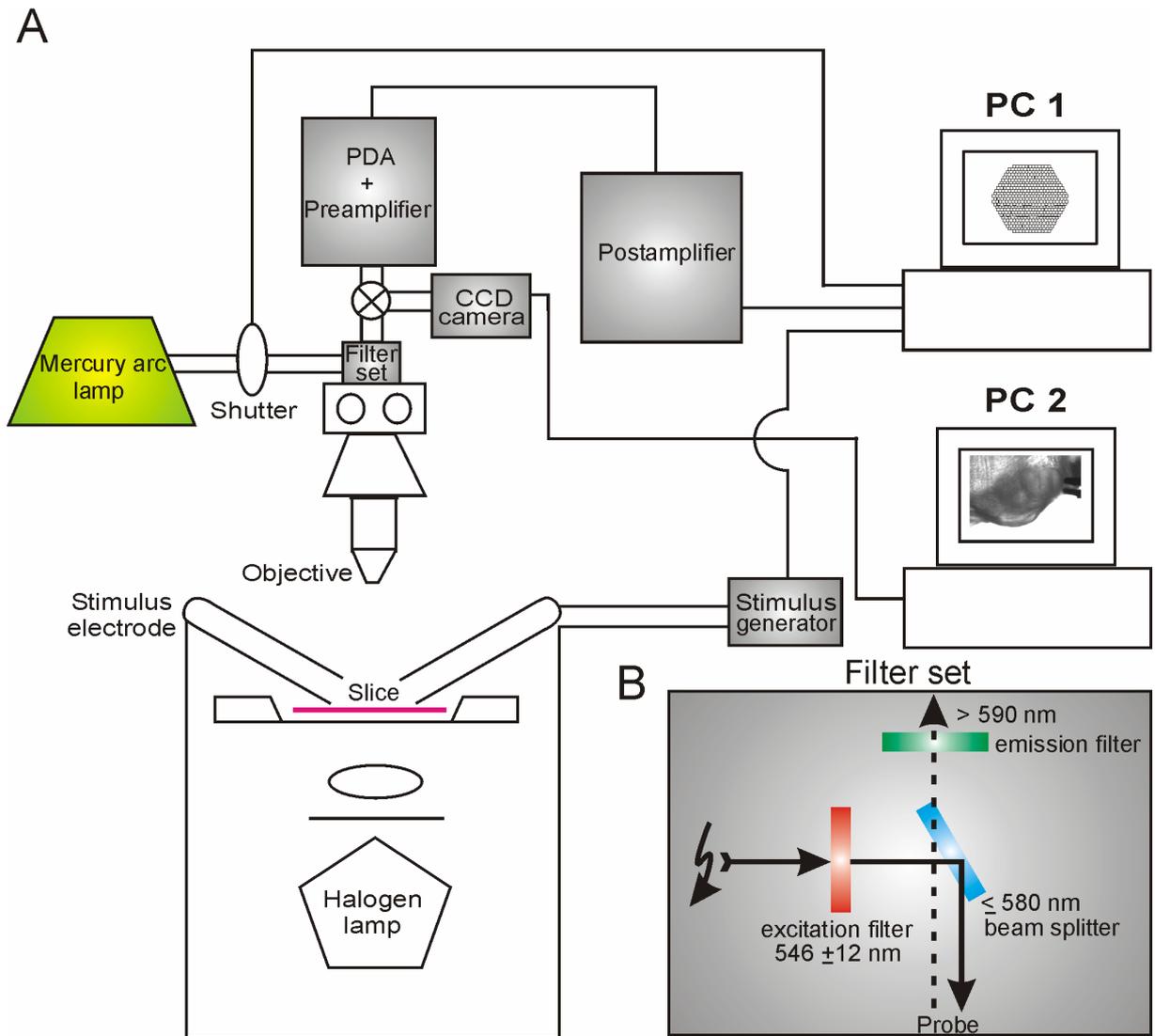
**Fig. 2.2: Schematic diagram of the setup for optical recordings with VSDs**

(A) Schematic diagram of the setup for measuring electrical activity with a hexagonally arranged 464 photodiode array (PDA). Slices were illuminated from below with a halogen lamp to take videomicrographs (like the one shown in A, PC 2 screen) with a CCD camera, connected to a personal computer (PC 2). For detecting electrical activity, dye-loaded slices were illuminated from above with light from a mercury arc lamp that had been passed through a filter set. Electrical stimuli were generated by a stimulus generator and applied via bipolar stimulus electrodes. Emitted fluorescent light was detected by the PDA, pre- and postamplified, digitized, and analyzed with a personal computer (PC 1). (B) Schematic diagram of the filter set. Light enters the excitation filter (red, BP 546), through which passes light of $546 \pm 12$ nm. The beam splitter (blue, FT 580) reflects light $\leq 580$ nm onto the probe. The emitted light from the probe will arrive at the emission filter (green, LP 590), through which only light of > 590 nm can pass, that reaches the PDA.
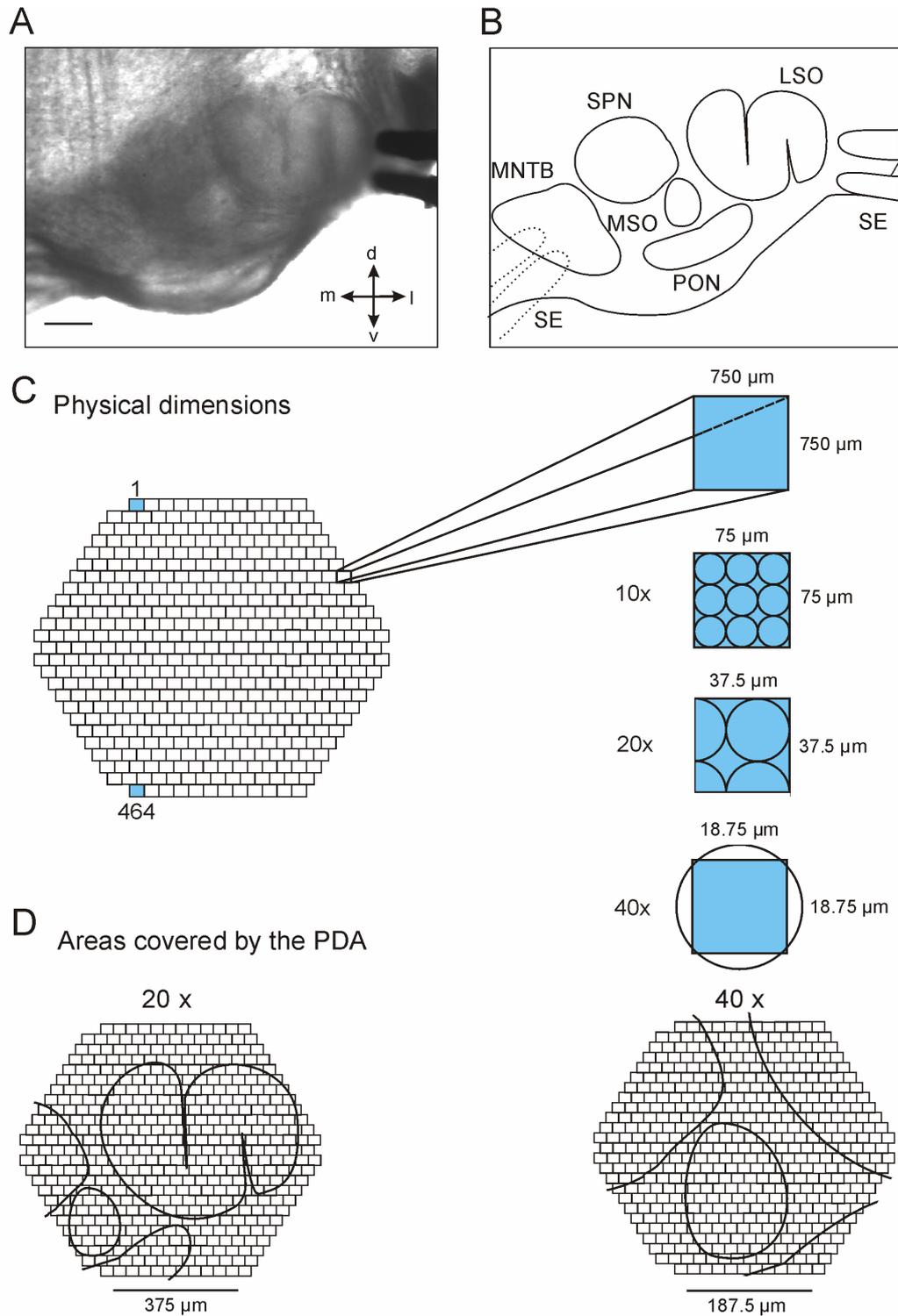
**Fig. 2.3: Spatial resolution of the PDA**

(A) Videomicrograph of a rat brainstem slice (P10) containing the SOC as used for optical recordings with electrical stimulation. The bipolar stimulus electrode is seen lateral to the S-shaped LSO. Scale bar = 200 µm. (B) Five SOC nuclei are outlined from the image shown in A: MNTB, SPN, MSO, LSO, and PON. The ventral border of the slice and the bipolar stimulus electrode (SE), which was placed lateral to the LSO to stimulate the inputs from the ipsilateral side, are also outlined. Stimulation of the inputs from the contralateral side was done via a stimulus electrode placed within the MNTB (indicated

_____

by the SE drawn with dotted lines). (C) The PDA contained 464 hexagonally arranged photodiodes, each with a physical dimension of 750 µm x 750 µm. Depending on the magnification of the objective (10x-40x), the area covered by a photodiode ranged from 75 µm x 75 µm to 18.75 µm x 18.75 µm. Circles schematically indicate circular cell bodies i.e., each with a size of 20 µm. (D) With a 20x objective, the entire LSO and MSO as well as the lateral part of the SPN and PON from the slice shown in panels A and B were covered by the PDA (left half of panel D). With a 40x objective, the entire MSO and a part of LSO, PON, and SPN were covered (right half of panel D).

## Data acquisition and analysis

Optical signals were amplified, digitized by an analog-to-digital converter, and low-pass filtered at 1 kHz before storage. In recordings from all 464 diodes, the frame rate (= sample rate) was 1.66 kHz (Fig. 2.4). In some cases, only signals from a subset of diodes were recorded, thus the frame rate was correspondingly higher (Fig. 2.13). One recording is considered as one trial. To reduce noise from the recordings, 10 subsequent trials were (temporally) averaged, with an interval of 20 seconds between subsequent trials. Such a recording is considered as 10 trials (Fig. 2.8).

Recordings from an individual diode are considered as `single diode recording´. In some experiments the recordings were averaged from several spatially related diodes. Such a recording is considered a `multiple diode recording´ of several diodes (Fig 2.13). To assign the optical recordings to anatomical structures, a frame with the recordings of all responding diodes was superimposed with the above-mentioned drawings of the recognized structures in a slice (Fig. 2.3D).

The voltage-sensitive dye RH795 shows a fluorescence decrease upon membrane depolarization and a fluorescence increase upon hyperpolarization. Optical signals are presented as the ratio $\Delta F/F$ (in %) of the fluorescence change ($\Delta F$) and the fluorescence baseline level (F). F was measured for each diode immediately before the acquisition of the stimulus-induced optical signals. To be in accordance with electrophysiological conventions, the optical signals were inverted such that upward

A

Diode interval = 1.3 µs

1

464

Frame #1
Frame #2
Frame #3

Frame interval = 0.613 ms
(464 × 1.3 µs)

≅

Frame rate = 1.66 kHz
(when all 464 diodes are used)

1 2 3

represented in
pseudocolors

high

low

B

1 2 3          16

0 ms          0.613 ms          1.262 ms          1.839 ms          2.452 ms

3.06 ms          3.678 ms          4.291 ms          4.904 ms

• • •
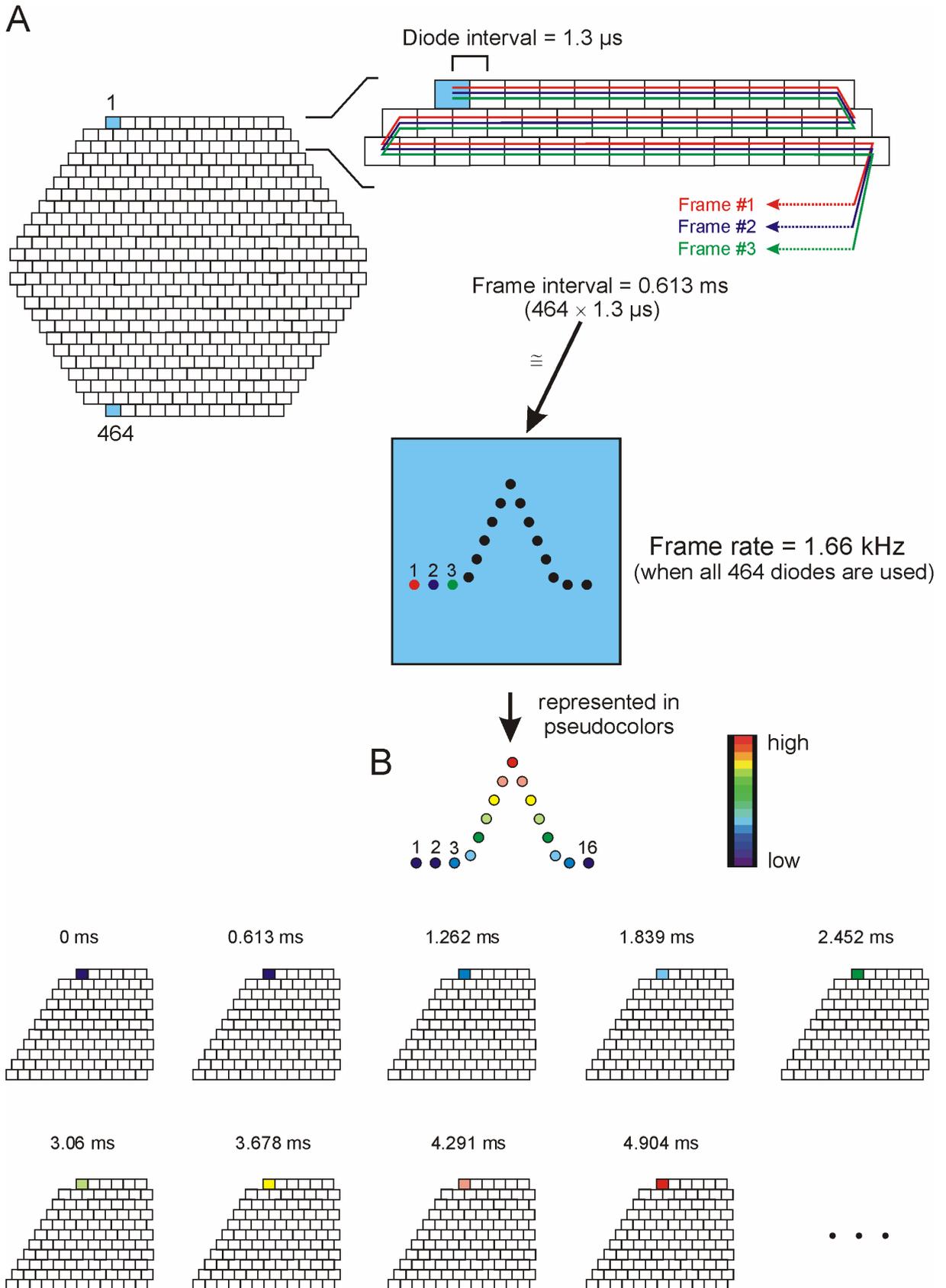
**Fig. 2.4: Temporal resolution of the PDA**

(A) Each photodiode consist of a defined number of frames (sample points), with a certain interval. The acquisition starts from the 1<sup>st</sup> frame of the 1<sup>st</sup> photodiode and moves to the 1<sup>st</sup> frame of the 2<sup>nd</sup>

_____

photodiode and so on, up to the 1st frame of the 464th photodiode. In recordings from all 464 diodes, the frame interval is 0.613 ms (464 × 1.3 µs diode interval), corresponding to a frame rate of 1.6 kHz. (B) The optical signals can be represented in pseudocolors, where the warm and cold colors represent high and low amplitudes of fluorescence change in each frame, respectively.

deflections correspond to depolarizations and downward deflections correspond to hyperpolarizations.

**Electrical stimulation of SOC input fibres**

Bipolar stainless steel electrodes (Rhodes NEX 200, Science Products, Hofheim, Germany) were placed lateral to the LSO and within the MNTB to stimulate the inputs originating from the ipsilateral and contralateral cochlear nucleus (CN), respectively (Fig. 2.3B). Single or double current shocks of 0.2 ms duration and 1-3 mA amplitude were used. In case of double shocks, 80 ms stimulus interval was used (Fig. 2.9A).

**2.3 RESULTS**

**Influence of extracellular potassium concentration ($[K^+]_e$) on optical recording**

For patch-clamp recordings in SOC slices, 2.5 mM $[K^+]_e$ was used in the recording solutions. With the same $[K^+]_e$ in the incubation and recording solutions, optical signals were observed upon synaptic stimulation in the cortex slices, yet not in the SOC slices (Fig. 2.5A).

A total of 93 SOC slices were incubated with RH795 and recorded at different $[K^+]_e$ of 2.5 mM (n = 53), 5 mM (n = 13), 10 mM (n = 22), and 20 mM (n = 5). At 2.5 mM $[K^+]_e$, 85% of the SOC slices did not show any response (Fig. 2.5A bottom) upon synaptic stimulation. The remaining 15% of the slices showed weak responses only under direct stimulation i.e., when the stimulus electrode placed directly in the nuclei. In contrast, 90% of the cortex slices showed responses upon synaptic stimulation (Fig.

2.5A inset). At 5 mM $[K^+]_e$, 75% of the SOC slices showed responses to synaptic stimulation (Fig. 2.5B). At 10 mM $[K^+]_e$, 72% of the SOC slices also showed responses (Fig. 2.5C). At 20 mM $[K^+]_e$, none of the five slices showed any response in the SOC (Fig. 2.5D). In all the above cases, the baselines of the traces were not straight, this was rectified by proper amplifier settings (Fig. 2.7). Together, the results obtained with different $[K^+]_e$ show that 5 mM $[K^+]_e$ (for incubation of the slice in the dye and during optical recording) is necessary to observe the synaptically-evoked responses in the SOC.
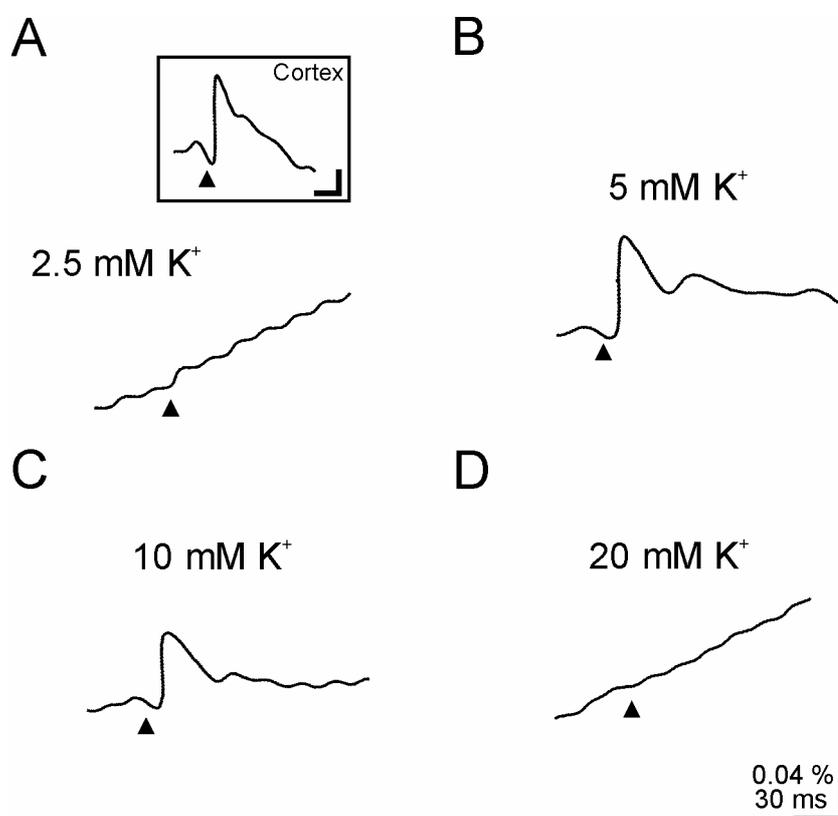


**Fig. 2.5: Extracellular potassium ($[K^+]_e$) influences optical signals in the SOC**

Single diode recording evoked by a single electrical pulse (2 mA, 200 µs) in P8 slices containing the SOC incubated in RH795 dye. Three subsequent trials were averaged at different $[K^+]_e$. (A) No profound response was observed at 2.5 mM $[K^+]_e$ in the SOC, whereas the cortex (inset) displayed a response. (B and C) At 5 and 10 mM $[K^+]_e$, responses were observed in the SOC. (D) At 20 mM $[K^+]_e$, no response was observed in the SOC. Arrow head = stimulus; optical signals were low pass filtered at 35 Hz (butterworth filter); scale bar in D holds also for A-C, its values hold also for the scale bars in inset.

_____

**Power supplies cause various noise levels**

In order to achieve a better signal-to-noise ratio, different power supplies were tested. Peak-to-peak scatter in the baseline is defined as noise. Optical noises were influenced by the lamp power supply (Fig. 2.6). The peak-to-peak amplitude of the noise from a single diode, while using a Zeiss mercury arc lamp power supply, is 1.5% (Fig. 2.6A middle panel), which was observed in all the 464 photodiodes (Fig. 2.6A left panel). Fast fourier transformation (FFT) spectrum displayed the frequencies and the magnitude of the noise, which appeared regularly in multiples of 100 Hz (Fig. 2.6A right panel). A drastic reduction in the noise (0.4%) was observed when using another mercury arc lamp power supply (Statron - model 3231, Statron elektronik GmbH, Fürstenwalde, Germany). The FFT spectrum displayed the elimination of the multiples of 100 Hz noise, but left the 50-60 Hz noise (Fig. 2.6B). The amplitude of the noise was further reduced to 0.1%, when the entire setup was plugged to a AC power source (5KVA AC power source, model - 5001i-400-4725, Zes Zimmer electronic system, California instruments, San Diego, USA) along with the Statron mercury arc lamp power supply. The FFT spectrum showed the reduction in the 50-60 Hz noise (Fig. 2.6C). Together, the results indicate that with an additional AC power supply, along with a Statron mercury arc lamp power supply, the conditions suited well for optical recording (Fig. 2.6C).
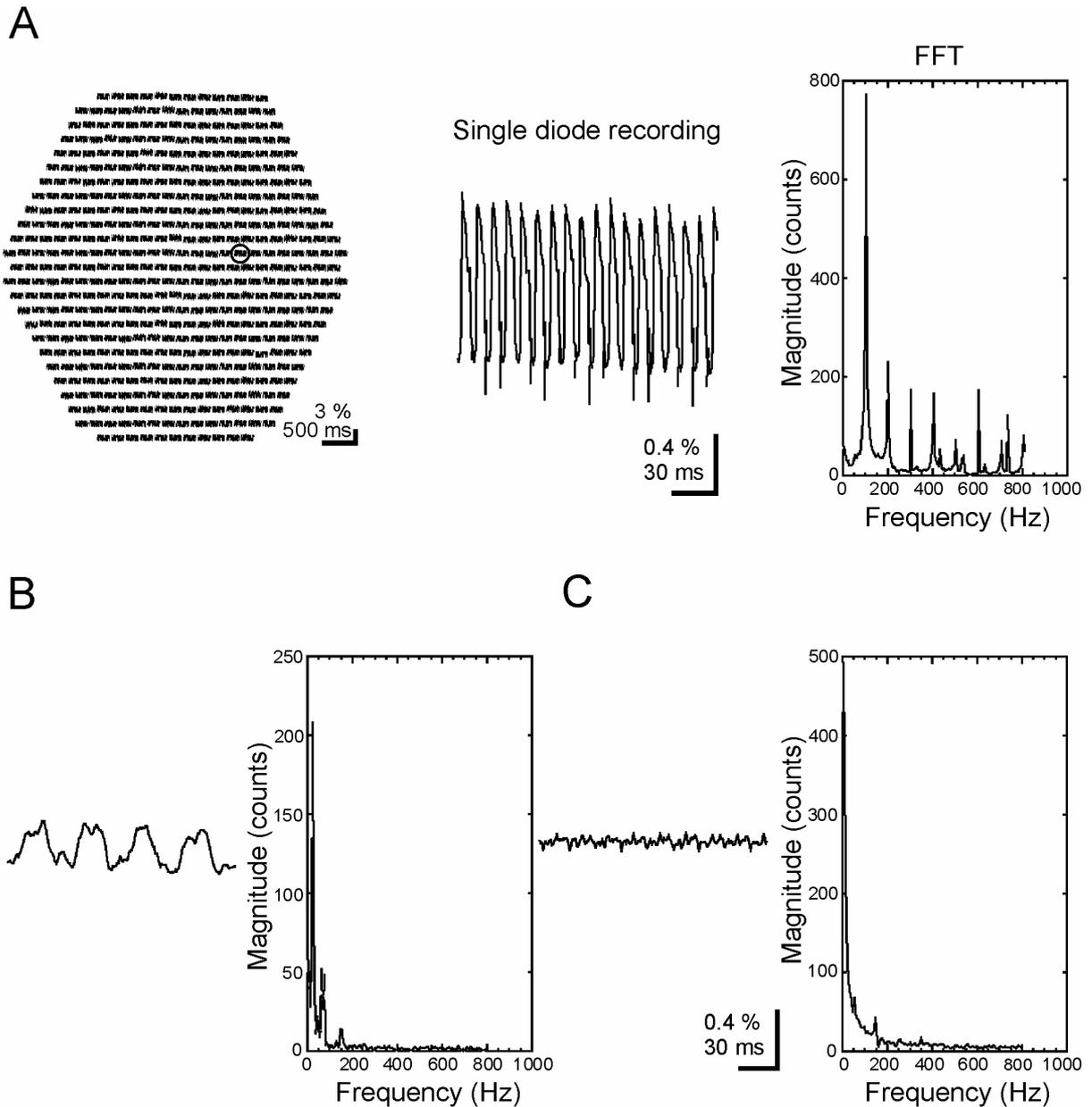
**Fig. 2.6: Characterization of noise level under different power supplies**

Noise levels in optical recordings are influenced by the power supply. (A) Noise level in 464 photodiodes (left panel), and in a single diode (middle panel) while using mercury arc lamp power supply from Zeiss. Note that the noise is present in all photodiodes. Fast fourier transformation (FFT) shows the frequency spectrum of the noise (right panel). (B) Noise level in a single diode while using mercury arc lamp power supply from Statron. A drastic reduction in the noise was observed while this power supply. (C) With additional power supply from Zes Zimmer electronic system (AC power source) along with Statron mercury arc lamp power supply the noise level was further reduced.

_____

**Achievement of straight baseline optical signals**

As already shown in Fig. 2.5, the baselines of the traces were not straight in the initial experiments, which was due to improper amplifier settings (Fig. 2.7). As illustrated in Fig. 2.7A, a certain time is needed to establish a straight baseline before starting the acquisition. But the reset time of 150 ms was not sufficient to bring the amplifier to the baseline level; therefore, an additional amplifier adjustment time is needed. This is the amount of time that the amplifier needs to `wait´ after the reset pulse and before the start of acquisition. Moreover, the amplifier has two modes, namely AC1 and AC2. Since, the time constants for the AC1 and AC2 modes are 500 ms and 100 ms, respectively, I used the AC2 mode to quickly achieve a straight baseline.

To achieve a straight baseline before acquisition, the amplifier adjustment time was standardized. With 0 ms amplifier adjustment time, the stimulus-evoked optical traces displayed an exponential baseline (Fig. 2.7B left panel). In this case, the total mercury arc lamp illumination time of the slice is 327 ms (reset time = 150 ms; acquisition time = 177 ms). With a 1000 ms amplifier adjustment time, the steepness of the exponential baseline is reduced (Fig. 2.7B1 middle panel). In this case, the total lamp illumination time of the slice is 1327 ms (150 ms + 1000 ms + 177 ms). With an amplifier adjustment time of 1500 ms, the baseline becomes straight, but the total illumination time is now 1827 ms (150 ms + 1500 ms + 177 ms; Fig. 2.7B1 right panel). Unfortunately, a long-lasting illumination will affect the healthiness of the slice. The consequence of exposing live cells to a high intensity illumination is direct damage to the cells (phototoxicity). Fluorophores react with oxygen molecules to release free radicals which cause cellular damage. This leads to the induction of stress responses in cells, which may affect the experimental outcome, and finally lead to the death of the cells. Another problem is photobleaching due to long-lasting

## A



## B
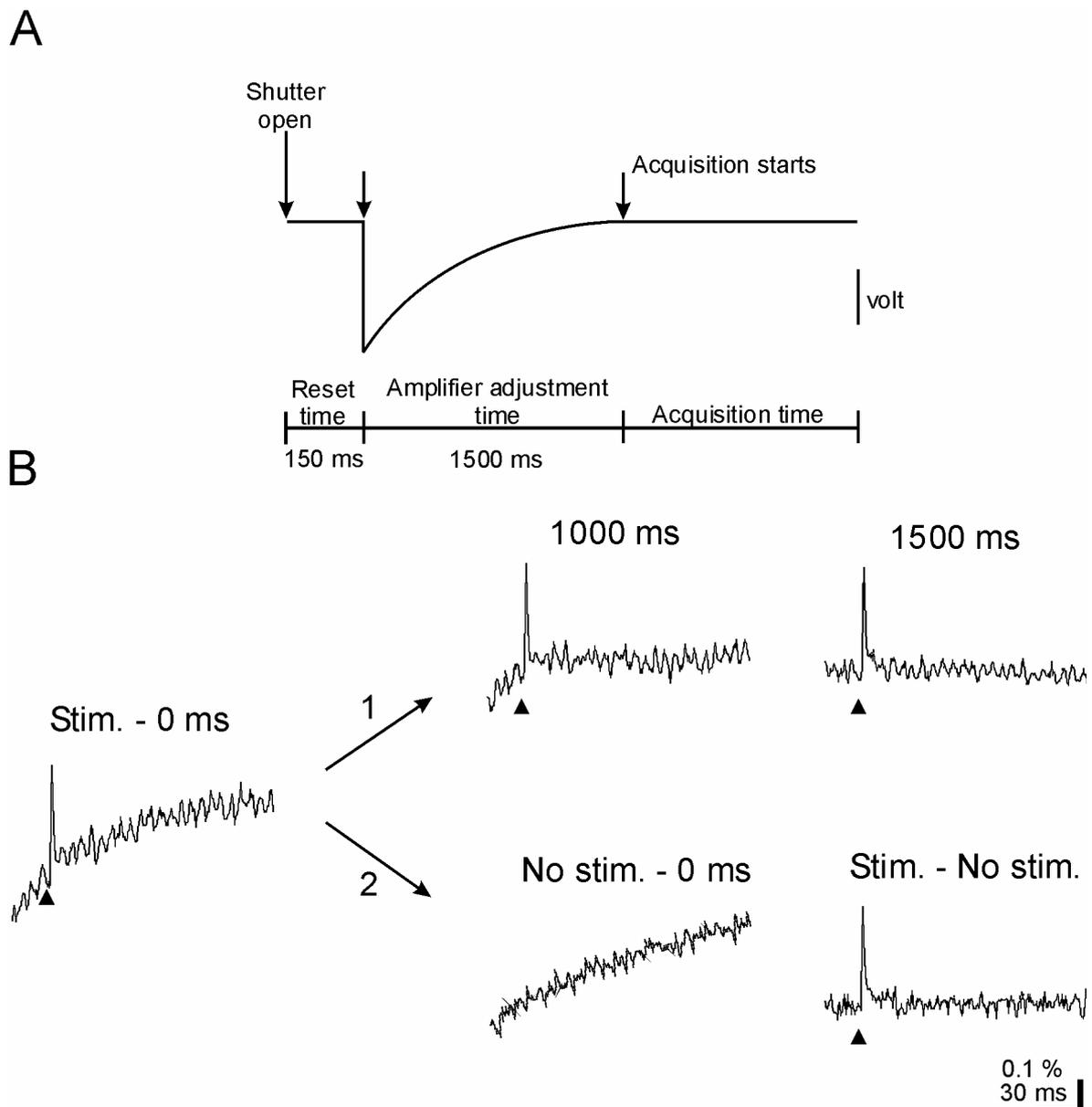


**Fig. 2.7: Characterization of optical signals**

Single diode recording evoked by a single electrical pulse (3 mA, 200 µs) in a P10 slice incubated in RH795 dye. Ten subsequent trials were averaged. Slices were recorded at different amplifier adjustment times. (A) Schematic illustration of the sequential functioning of the system. When the shutter opens, the fluorescent light enters and it excites the amplifier. A reset time of 150 ms was not sufficient to establish a baseline, therefore, an additional amplifier adjustment time is needed. After establishing the baseline, acquisition starts. (B left panel) Stimulus-evoked optical signal acquired with 0 ms amplifier adjustment time shows the time course of the exponential baseline. The baseline can become straight in two ways. (B1) Optical signals acquired after 1000 ms and 1500 ms amplifier adjustment time. Note that the baseline of the optical signal becomes straight with 1500 ms amplifier adjustment time. (B2) Optical signals without stimulation with the same 0 ms amplifier adjustment time also display the exponential baseline (middle panel). Upon subtracting the traces (stimulation – no

_____

stimulation) i.e., with and without stimulus, the baseline also becomes straight (right panel). Arrow head = stimulus.


illumination i.e., fluorophores irreversibly lose the ability to fluoresce due to photon-induced chemical damage and covalent modification.

Therefore, I opted a different approach to reduce the illumination time (Fig. 2.7B2). With 0 ms amplifier adjustment time (Fig. 2.7B left panel), the stimulus-evoked optical traces displayed exponential baseline with a total illumination time of 327 ms (reset time = 150 ms; acquisition time = 177 ms). Without stimulation (Fig. 2.7B2 middle panel) under the same amplifier adjustment time, the traces displayed also the exponential baseline with a total illumination time of 327 ms. Traces become straight (Fig. 2.7B2 right panel) by digital subtraction of the optical signals, with and without stimulation (stim. – no stim.). Thereby, the illumination time is reduced to 654 ms when compared to the previously described settings, where the illumination time totalled 1827 ms. Thus, a straight baseline was achieved along with minimum illumination time. This condition is suitable for optical recording and was used throughout all further experiments.


**Improvement of the signal-to-noise ratio by averaging**

In order to get a good signal-to-noise ratio, the subsequent trials were temporally averaged (Fig. 2.8). With 1 trial, the peak amplitude of the noise from the baseline was 0.1%, and the amplitude of the response from baseline was 0.3% (Fig. 2.8A). With 1 trial the signal-to-noise ratio was 0.3/0.1 = 3. Averaging over 3, 6, 10, and 20 trials increased the signal-to-noise ratio by 5, 5.8, 8.8, and 9.3, respectively. Averaging resulted in the reduction of the noise amplitude from 0.1% to 0.03% i.e., by 70%. But the amplitude of the response remained in the range of 0.30% to 0.28%.

These results show that the noise could be reduced by averaging subsequent recordings. Together, averaging of 10 trials is sufficient and effective for achieving *a* good signal-to-noise ratio with a considerably short illumination time.
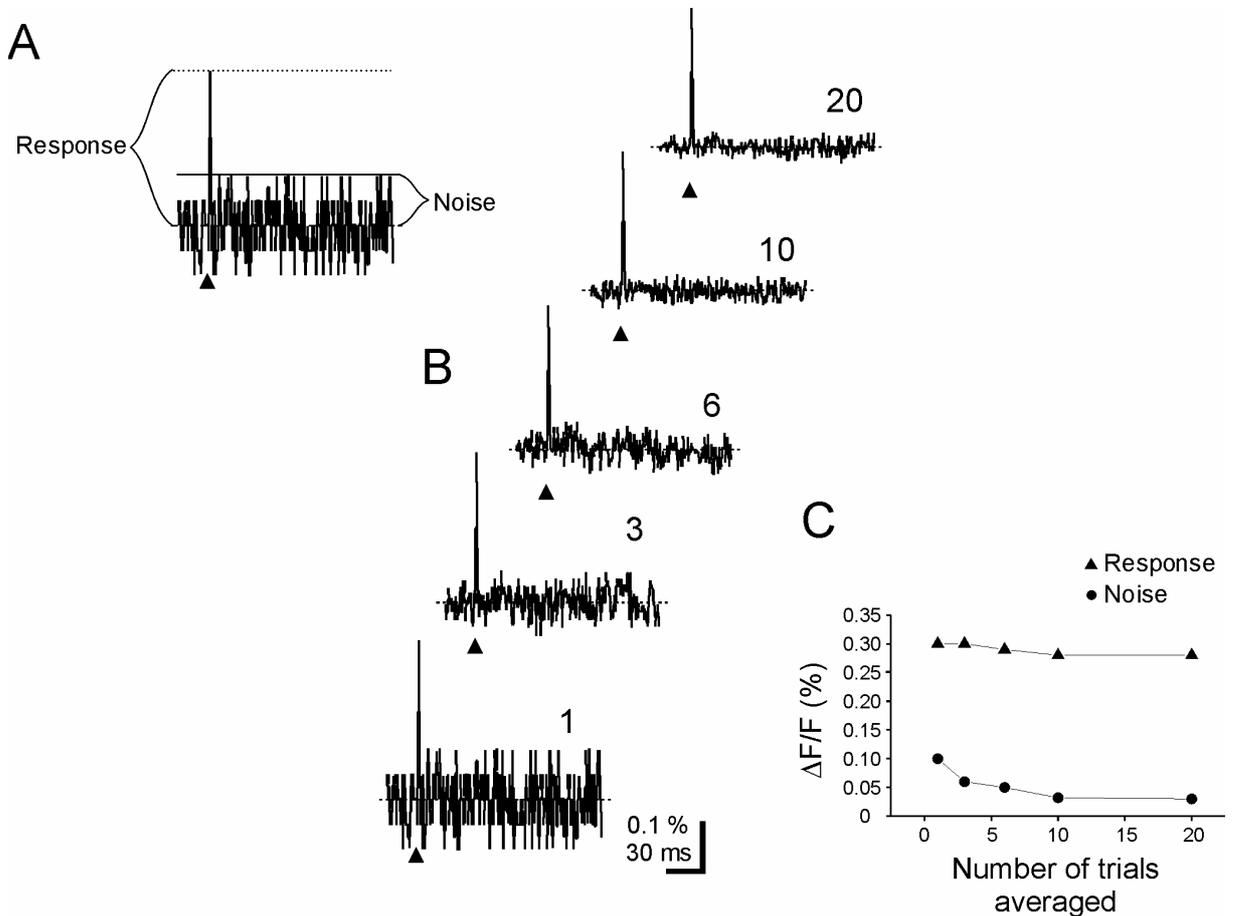


**Fig. 2.8: Better signal-to-noise ratio upon averaging trials**

(A) Stimulus-evoked optical signal which shows that the amplitude of the noise is measured from the baseline (horizontal broken line) to the peak of upward deflected noise (horizontal solid line), and the response is measured from baseline to the peak amplitude (horizontal dotted line). (B) Temporally averaged stimulus-evoked optical signals with different number of trials (1, 3, 6, 10, & 20). Note that the noise is getting reduced by averaging temporally. Arrow heads = stimulus. (C) Graph illustrating the amplitude of the stimulus-evoked response ( ▲ ) and of the noise ( ● ) plotted against the number of trials over which averaging was done.

**Correlation of resting light intensity (RLI) and response amplitude in SOC slices**

Experiments were done to understand the influence of RLI value (i.e., the baseline fluorescence level) on the response amplitude at different ages. In order to correlate
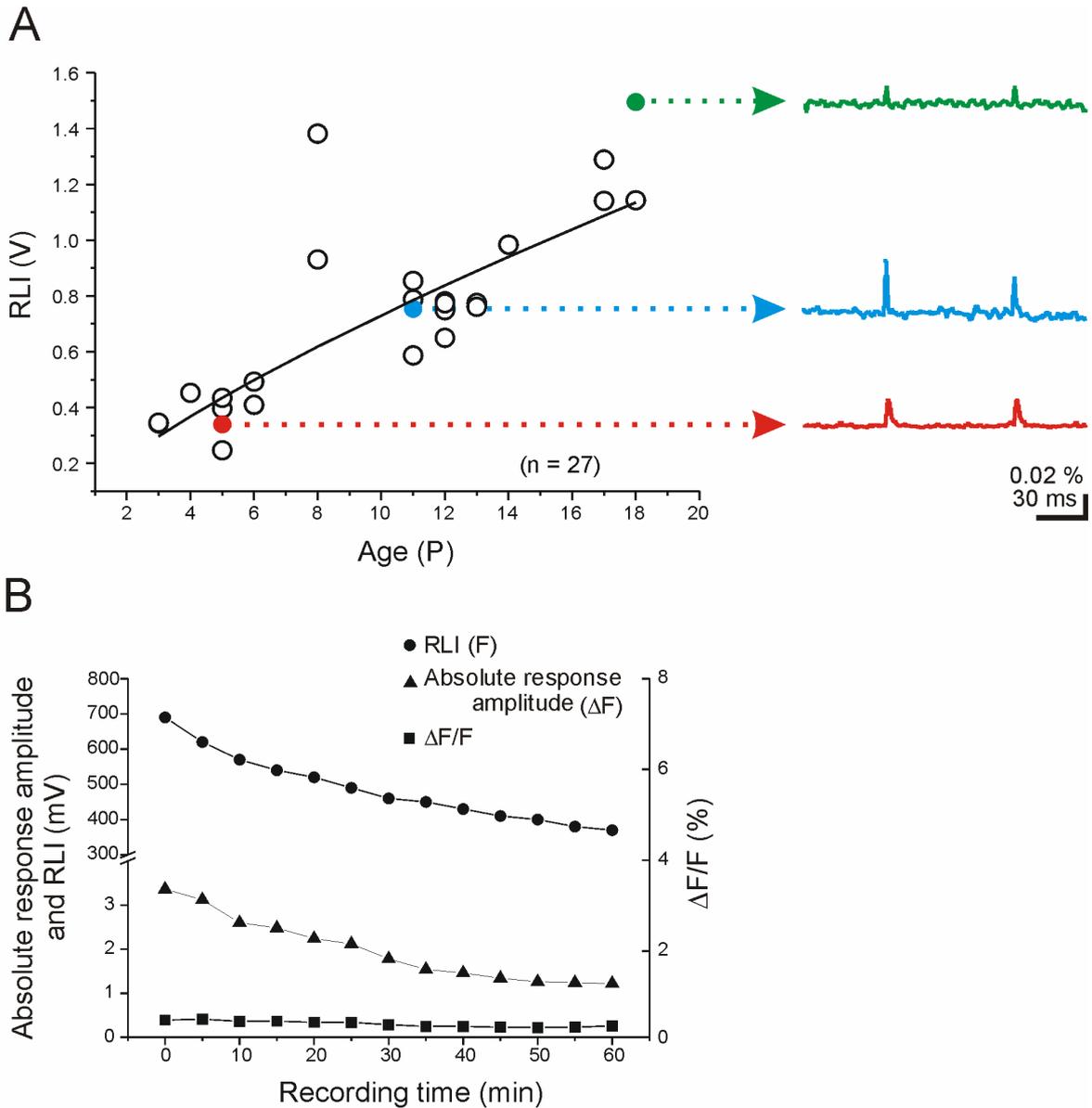


**Fig. 2.9: Resting light intensity (RLI) and response amplitude in SOC slices**

(A) Mean RLI values from the entire PDA (○) obtained from 27 SOC slices at different postnatal ages. RLI values correlate with age. Typical examples of multidiode recordings from the entire PDA at three different ages are shown on the right. Double current shocks of 2 mA amplitude for 0.2 ms duration, with an interval of 80 ms were used. (B) Typical example of a single diode recording illustrating the time course of the absolute response amplitude (▲), RLI (●), and ΔF/F (■) plotted against recording time.

the RLI values with respect to age, a total of 27 slices from different ages (P3-18) were imaged (Fig. 2.9A). The stimulus strength used was 2 mA and the stimulus duration was 200 µs. The RLI value increased with age, which means that more dye molecules are present in the slice. This may be due to an increase in the size of the neurons and or to the growth of glial cells in older animals. However, the amplitude of the signal did not necessarily increase with RLI as shown in Fig. 2.9A, indicating insignificant relation. The amplitude of the optical signals is assumed to depend on several parameters like fibre connection, healthiness of the slice, RLI, and stimulus condition.

Fig. 2.9B shows the relation of the RLI (F) and the absolute response amplitude (∆F) as a function of the recording time. The RLI decreased over time, presumably due to the wash out of the dye molecules. As a result, the amplitude of the signal is also declined. To normalize the signal size, it is necessary to use the ratio value i.e., ∆F/F. Thereby, the amplitude of the signal was expected to remain constant over time.

**Standardization of RH795 dye concentration for SOC slices**

To standardize the RH795 dye concentration for recording optical signals from SOC slices, 10 and 15 slices with 50 µM and 100 µM concentrations, respectively, were tested. Typical examples are shown in Fig. 2.10A. With a single electrical pulse (2 mA; 200 µs), the peak amplitude of the optical response from a single diode was measured over recording time up to 80 minutes (Fig. 2.10A). With 50 µM RH795, the amplitude of the response was reduced to 50% within 23 min from the initial value, and of totally vanished after 40 min. In contrast, when using 100 µM RH795, the amplitude of the response was reduced to 50% after 52 min from the initial value, and a signal was still detectable after 80 min. Thus, 100 µM dye concentration

enabled me to record for more than an hour, probably due to more dye molecules being bound to the membrane.

A



B
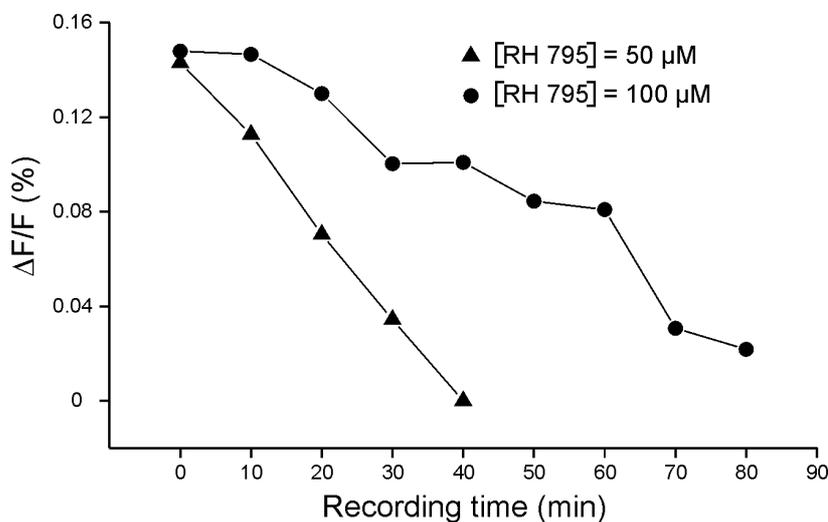


**Fig. 2.10: Standardization of RH795 dye concentration for SOC slices**

(A) The maximum amplitude of the responses from a single diode obtained from P8 slices were plotted against recording time. Slices were incubated with 50 µM (▲) or 100 µM (●) RH795, for 30 min before recording started.
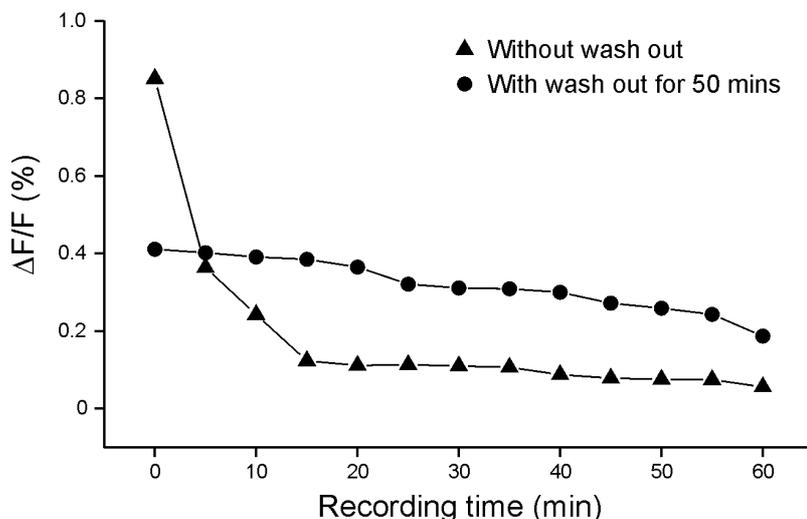
(B) The maximum amplitude of the responses from a single diode were plotted against recording time. Slices were incubated with 100 µM dye concentration for 30 min, and recorded after wash out for 50 min (●) or without wash out (▲) in extracellular solution. 0 = Start of the recording.

Rapid decline in the response amplitude over time may be due to washout of unbound dye molecules by perfusion of the recording solution in the beginning. It is very likely that the unbound dye molecules contribute only to the RLI but not to the response. To overcome this problem, after dye-incubation, slices (n = 5) were kept in the recording solution for 50 min, before recording. A typical example is shown in Fig.

_____

2.10B. The rapid decline in the response amplitude was reduced (Fig. 2.10B). Together, these results demonstrated that slices incubated with 100 µM RH795 with 50 min pre-wash allow one to record for more than 60 min.

So far, I have described the standardization of the optical imaging method for the auditory brainstem slices. Overall, the results demonstrate that this method allow one to image SOC slices with a good signal-to-noise ratio. As a next step, I characterized the optical signals in order to interpret the neuronal activity.

**Stimulus-evoked optical signals are TTX-sensitive**

Optical signals obtained from the SOC slice upon ipsilateral stimulation are illustrated in Fig. 2.11A. Optical responses were observed both inside and outside the nuclei of interest. In order to isolate the action potential (AP)-driven responses, pharmacological experiments were performed in 9 slices. Typical example is shown in Fig. 2.11. During control recordings, stimulus-evoked optical signals were observed (Fig. 2.11A). Upon 15 min bath application of the $Na^+$ channel blocker TTX (0.5 µM), optical signals disappeared (Fig. 2.11B). After washout of the drug, the optical signals recovered partially. This demonstrates that the optical signals were AP-driven.
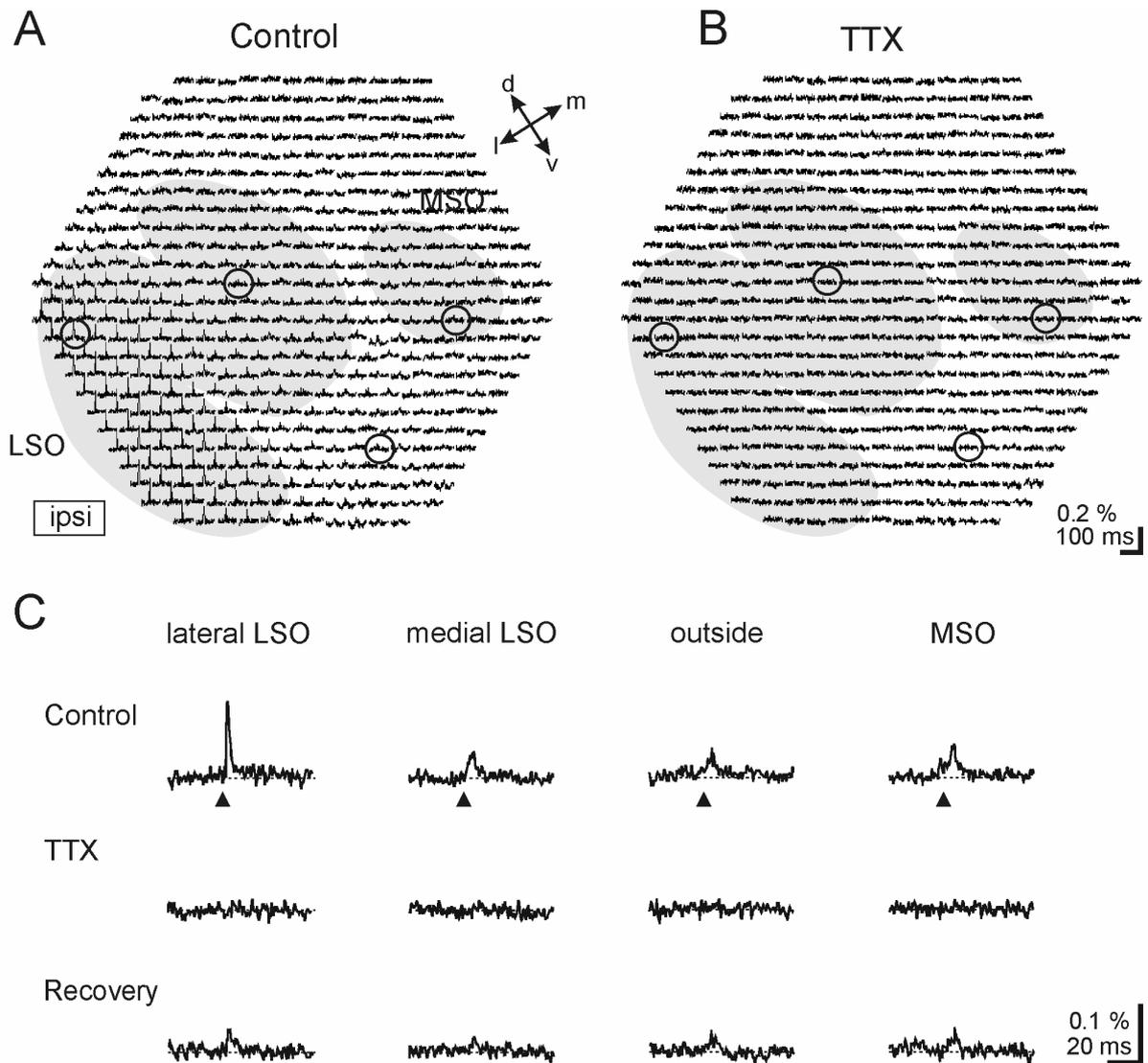
**Fig. 2.11: Pharmacology reveals TTX-sensitive optical signals**

(A) Example of the spatio-temporal pattern of optical signals evoked by ipsilateral stimulation. (B) Optical signals evoked by ipsilateral stimulation in the presence of TTX. All the stimulus-evoked signals are sensitive to TTX. (C) Single diode recordings obtained from four diodes (see circles in A and B), representing the lateral and medial LSO, the MSO, and the outside region (ventral to the LSO) under control conditions, upon TTX application and after recovery. The horizontal dotted lines represent the baseline fluorescence level. ipsi = site of stimulation; v = ventral; d = dorsal; l = lateral; m = medial; Arrow head = stimulus. Meaning of symbols holds also for figures 2.12 and 2.13.

**Optical signals reflect pre- and postsynaptic membrane potential changes**

To obtain a better understanding of the optical signals, it is mandatory to distinguish between $Ca^{2+}$-insensitive, presynaptic components and $Ca^{2+}$-sensitive, postsynaptic

components. To do so, 11 experiments were performed with $Ca^{2+}$-free recording solution while stimulating the ipsilateral (n = 3) or contralateral (n = 8) SOC inputs.

Fig. 2.12A illustrates the spatio-temporal pattern of optical signals in 4 different SOC nuclei following ipsilateral stimulation. Stimulus-evoked responses were observed in the LSO, the MSO, and the MNTB as well as in the internuclear region between the LSO and the MSO. No or only very small responses occurred in the SPN. To identify possible $Ca^{2+}$-sensitive components corresponding to transmitter-evoked postsynaptic responses, the recordings were repeated in $Ca^{2+}$-free recording solution. Digital subtraction of the responses under $Ca^{2+}$-free conditions from those under control conditions revealed the $Ca^{2+}$-sensitive response components. In the representative example shown (Fig. 2.12B), $Ca^{2+}$-sensitive response components occurred in the LSO and the MSO. In the MNTB, only a single response component could be detected which was unaffected by $Ca^{2+}$ removal (left column in Fig. 2.12C). Due to its single component and $Ca^{2+}$-insensitivity, I identified this response as an antidromic action potential (aAP), which was probably evoked by antidromically activated MNTB-LSO collaterals (Wu and Kelly, 1991). In contrast to the MNTB, two response components were obvious in the MSO and the LSO (middle and right column in Fig. 2.12C, respectively). They were attributable to an early presynaptic and a delayed postsynaptic component. Such $Ca^{2+}$-insensitive presynaptic components and $Ca^{2+}$-sensitive postsynaptic components were detected in all 11 experiments.
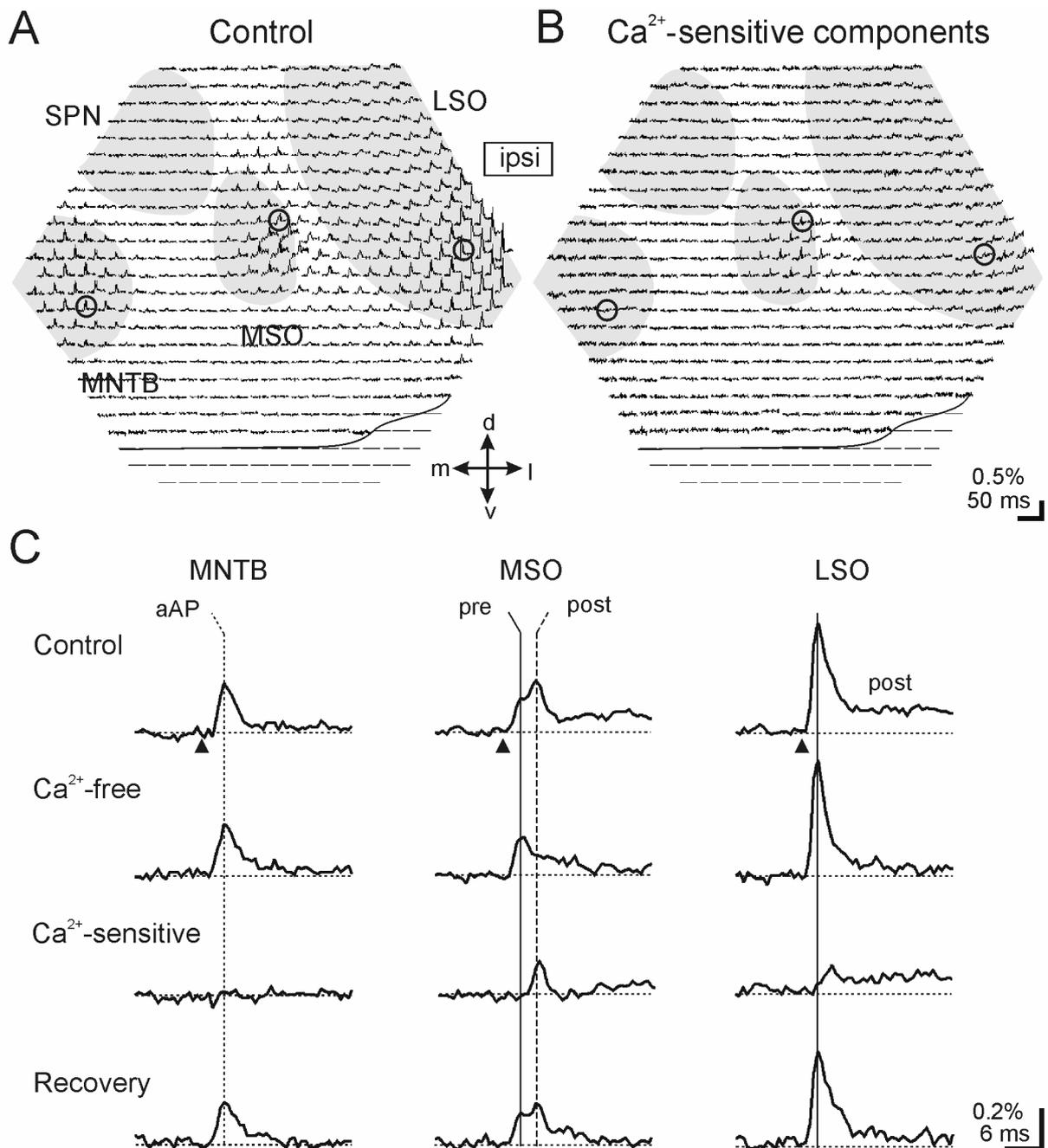
**Fig. 2.12: Optical signals in the SOC comprise pre- and postsynaptic components**

(A) Example of the spatio-temporal pattern of optical signals evoked by ipsilateral stimulation. (B) $Ca^{2+}$-sensitive components revealed by subtracting the responses under $Ca^{2+}$-free conditions from the responses under control conditions (A). Under the stimulus conditions used, $Ca^{2+}$-sensitive responses were primarily observed in the MSO and in the ventral part of the medial limb of the LSO. (C) Individual responses obtained from three diodes (see circles in A), scanning areas in the MNTB, the MSO, and the LSO. The horizontal dotted lines represent the baseline fluorescent level. The optical signal obtained in the MNTB was not influenced by the $Ca^{2+}$-free solution, whereas the signals in the MSO and the LSO were considerably affected when $Ca^{2+}$ was removed from the recording solution. The differences in $Ca^{2+}$-sensitivity between the three nuclei are clearly shown by the traces in the row

labeled `Ca$^{2+}$-sensitive´. ipsi = site of stimulation; v = ventral; d = dorsal; l = lateral; m = medial; dotted vertical line labeled `aAP´ points to antidromic action potentials; solid vertical lines labeled `pre´ = presynaptic components; broken vertical line labeled `post´ = postsynaptic components; Arrow head = stimulus.

To further characterize the nature of the pre- and postsynaptic optical signals, they were correlated with the anatomical structures lying underneath the
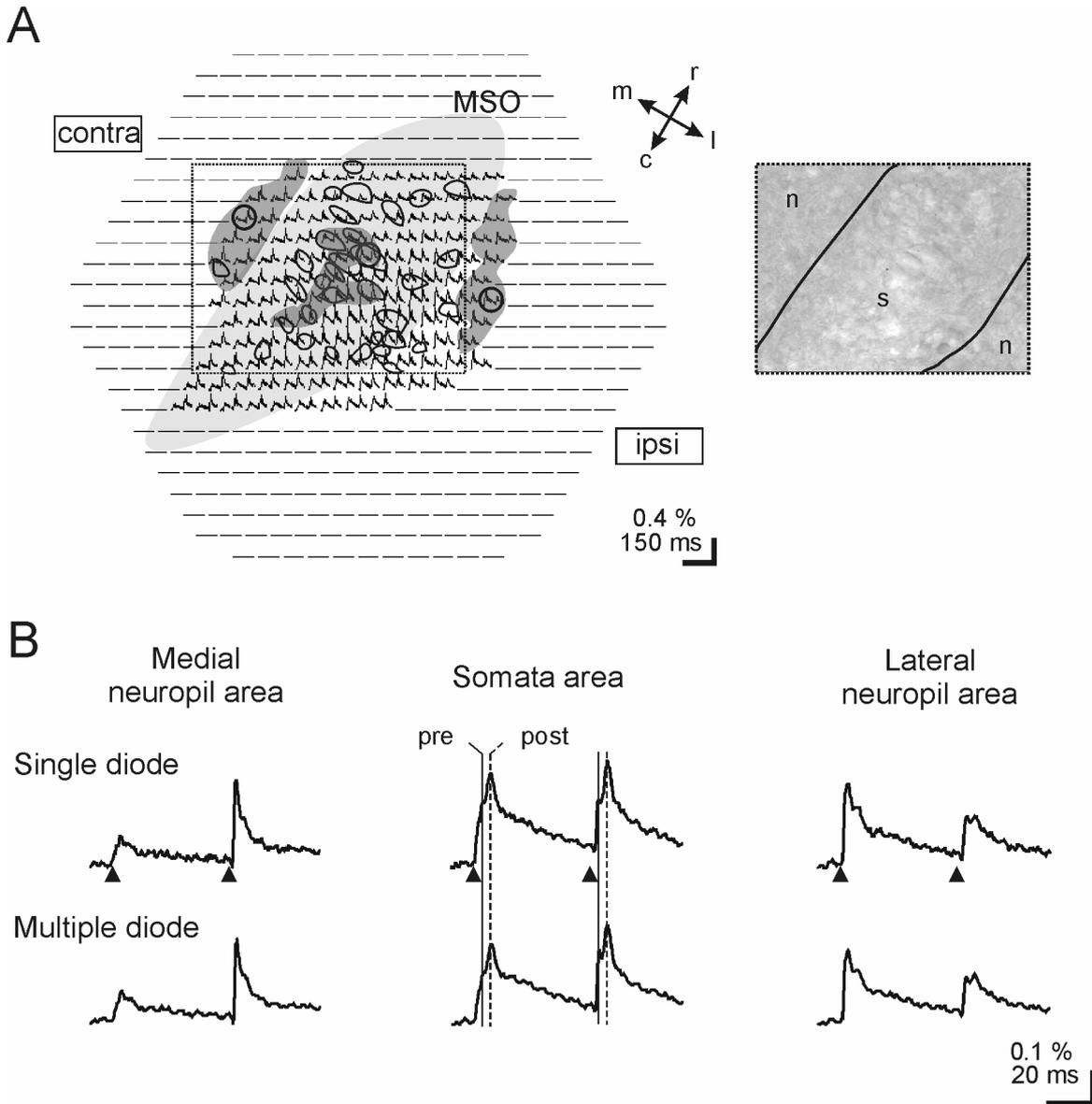


**Fig. 2.13: Locations of pre- and postsynaptic optical signals correspond to locations of neuropil and somata**

(A) Optical signals obtained from 132 diodes (equivalent to a sample rate of 5.83 kHz; cf. Materials and Methods) were superimposed with the graphical representation of the somata area of the MSO

(light gray area) and its peripheral neuropil area in a horizontal section. The videomicrograph (~210 µm x ~160 µm) was used for identifying the somata area (s) and the medially and laterally flanked neuropil area (n) in the region marked by the frame. In this region, a total of 34 somata were visually identified and outlined (30/34 in the somata area). (B) Comparison of `single diode recordings´ (circles in A) and `multiple diode recordings´ (dark gray areas in A) obtained from three different areas. Two neuropil areas, medial and lateral to the somata area, containing no and only one visible soma, respectively, were scanned by 10 diodes. The third area was within the somata area and contained 10 visible somata. All traces depict responses to an ipsilateral stimulus followed by a contralateral stimulus after 50 ms (both 3 mA amplitude, 200 µs duration). contra, ipsi = site of stimulation; r = rostral; c = caudal; l = lateral; m = medial; Arrow head = stimulus.

scanning diodes. This was done in 23 slices in which the MSO was stimulated both ipsi- and contralaterally. The MSO was selected because of its cytoarchitecture with densely piled up somata flanked medially and laterally by neuropil, i.e. a high density of dendrites and axons (Fig. 2.13A). The optical signals obtained from the neuropil showed dominant presynaptic components in response to the ipsilateral (first) pulse and the contralateral (second) pulse (Fig. 2.13B). Within the somata area, the postsynaptic response was always larger than the presynaptic following both ipsi- and contralateral stimulation (Fig. 2.13B). The `multiple diode recordings´ obtained via 10 spatially related diodes (areas marked in dark gray in Fig. 2.13A) are compared with `single diode recordings´ from the same regions (sites marked by a circle in Fig. 2.13A).

No differences between the `single diode recordings´ and `multiple diode recordings´ responses were observed (Fig. 2.13B). Together, the data indicate that the location of pre- and postsynaptic response components indeed corresponds to the location of neuropil and somata regions in the MSO. Furthermore, the response from a *single diode* at a 40x objective magnification is composed of pre- and postsynaptic components. Finally, responses from spatially related diodes, which scan

anatomically related structures, can be averaged to describe the characteristic response pattern of distinct slice regions.

## 2.4 DISCUSSION

Several factors were analyzed and standardized for achieving optical recordings with VSDs in the SOC: (1) $[K^+]_e$ of 5 mM is necessary during the incubation and optical recordings in order to observe the synaptically-evoked responses in the SOC. (2) By employing different power supplies, the amplitude of the noise was reduced by 93%. (3) Averaging of 10 subsequent trials yields a better signal-to-noise ratio. (4) RH795 of *100 µM with 50 min prewash* is sufficient to image SOC slices for recording times of more than 60 min.

Moreover, the optical signals from VSD imaging were characterized in order to interpret in terms of neuronal activity. (1) Stimulus-evoked optical signals were TTX sensitive revealing AP-driven input. (2) Synaptically-evoked optical signals were characterized to be composed of pre- and postsynaptic components. (3) Optical signals are well correlated with anatomical structures.

### $[K^+]_e$ is critical for optical imaging with voltage-sensitive dyes

A crucial factor in the establishment of VSD recordings in the SOC was the incubation and recording with an increased $[K^+]_e$ (Fig. 2.5) compared to the storage solution (5 mM $K^+$ instead of 2.5 mM $K^+$). Profound responses were observed with 5 mM $[K^+]_e$. The baseline fluorescence level was similar in storage and recording solution. The increase in $[K^+]_e$ leads to a depolarization of the resting membrane potential ($V_m$) of ~14 mV (calculated by Goldman-Hodgkin-Katz equation). It is conceivable that the incorporation of the VSDs into the membrane depends on the

_____

$V_m$, and thus their potency to change fluorescence increased by raising the $[K^+]_e$. But with 20 mM $[K^+]_e$, no profound response was observed, which may be due a relatively high depolarizing $V_m$ at which the voltage-gated $Na^+$ channels cannot be opened again until the $V_m$ returns to a negative value near threshold (-40 mV). VSD imaging with 2.5 mM and 5 mM $[K^+]_e$ have been described. For example, 2.5 mM $[K^+]_e$ was used in rat hippocampal slices (Inoue et al., 2001) and rat somatosensory neocortical slices (Antic et al., 1999). On the other hand, 5 mM $[K^+]_e$ was used in guinea pig visual neocortex (Albowitz and Kuhnt, 1993), mice thalamocortical slices (Llinas et al., 2002), and rat barrel cortex (Petersen et al., 2003). So there are region-specific requirements, and that my results demonstrate that the SOC neurons need a higher $[K^+]_e$ to display satisfactory VSD signals.


**Signal-to-noise ratio relies on power supplies**

Fluctuation in the output of the light source causes noise, which is common in optical imaging (Wu et al., 1998). Initially, my setup was equipped with a Zeiss mercury arc lamp power supply. The optical signals obtained with this power supply had a bad signal-to-noise ratio, which could be improved by using a Statron mercury arc lamp power supply. In addition with the Statron mercury arc lamp power supply, when the entire setup was run with a AC power source, a good signal-to-noise ratio was achieved.

In order to further improve the signal-to-noise ratio, subsequent recordings were temporally averaged. But there are some drawbacks in averaging, for example photobleaching due to long illumination time, and broadening of APs due to temporal jitter. So, in order to reduce these drawbacks, I limited the averaging. Average of 10 subsequent trials yielded a good signal-to-noise ratio.

**RH795 is an appropriate dye for imaging auditory brainstem slices**

VSD recordings are species-specific and sometimes also brain region-specific (Spors and Grinvald, 2002). Among the dyes tested for rat SOC slices, RH795 was superior when compared to RH414 and Di-8-ANEPPS. Indeed, RH795 was used in several other brain regions of difference species, i.e., monkey visual cortex (Grinvald et al., 1994), guinea pig auditory cortex (Fukunishi et al., 1992), rat somatosensory cortex (Grinvald et al., 1994; London et al., 1989), human neocortical tissue (Köhling et al., 2000), ferret visual cortex (Nelson and Katz, 1995), and respiratory brainstem (Onimaru et al., 1996). But, this is the first study to show the usage of RH795 in auditory brainstem. Another interesting characteristic feature of RH795 is its negligible phototoxicity (Grinvald et al., 1994). The 100 µM dye concentration with 50 min pre-wash enabled me to record SOC slices for more than an hour. With pre-wash, where the unbound dye molecules are likely to be washed away, the amplitude of the optical signal reduced only slightly over recording time. This could be explained by the possibility that, as time passes, even the tightly bound dye molecules to the membrane are also washed away slowly.

**Characteristic features of the optical signals**

In the present study, the stimulus-evoked optical signals were sensitive to TTX, demonstrating that they were AP-driven. In general, neurotransmission comprises presynaptic and postsynaptic events. These components were segregated with calcium replacement experiments, compared to those shown in other imaging studies, like in vagal nuclei of the brainstem (Sato et al., 1998), and neurons from spinal cord (Arai et al., 1999). Between the peak amplitudes of pre- and postsynaptic

responses, there was a delay of 2-3 milliseconds (Fig 2.12). Thus, the separation of pre- and postsynaptic response was possible by a sample rate of at least 1.66 kHz. Depending on the objective of the microscope, a given photodiode detects voltage-dependent fluorescence changes from a varying number of neuronal and non-neuronal structures, such as presynaptic and postsynaptic membranes, membranes of neuronal somata, dendrites, and axons as well as of glial cells. Moreover, these pre- and postsynaptic components matched with the anatomical structures. For example, in the MSO, the location of pre- and postsynaptic response components indeed corresponds to the location of neuropil and somata regions.

**Merits and demerits of VSD recordings**

Optical recordings with VSDs have been successfully performed in many different brain regions, e.g., auditory cortex (Fukunishi and Murai, 1995), squid giant axon (Salzberg et al., 1993), spinal cord (Arai et al., 1999), vagal brainstem nuclei (Momose-Sato et al., 1994; Sato et al., 1998), inferior olive (Leznik et al., 2002), hippocampus (Barish et al., 1996), piriform cortex (Demir et al., 1999), somatosensory barrel cortex (Laaris et al., 2000; Petersen and Sakmann, 2001), visual cortex (Arieli et al., 1995; Nelson and Katz, 1995), olfactory system (Kauer and White, 2001), and human neocortical tissue (Köhling et al., 2000). The technique has several merits and demerits.

*Merits*: In contrast to conventional patch-clamp pipettes, the cell interior is not disturbed during optical recordings. Thus, optical recordings are considered to be a non-invasive technique. Optical recordings allow one simultaneously to record several hundreds of neurons in a single experiment. Therefore, regional differences within a nucleus can be studied. One of the main advantage of this technique is its

high temporal resolution i.e., while using all 464 photodiodes of the array, the fastest sample rate is 1.66 kHz which is necessary for identifying APs, excitatory post synaptic potentials, and inhibitory post synaptic potentials. By reducing the number of photodiodes, the sample rate can even be increased. For example, when using 116 photodiodes, the sample rate is 6.64 kHz. Therefore, one can achieve a high temporal resolution by reducing the diodes.

*Demerits*: Although VSD imaging was proved to be a good method, it has some drawbacks (Ebner and Chen, 1995). For enhancing the signal-to-noise ratio, averaging the optical signals is inevitable. Therefore, one has to take several trials which increase the exposure time of fluorescence light on the slice and which may lead to phototoxicity and dye bleaching.

In conclusion, the technique of voltage-sensitive dye recordings is a powerful tool for studying neural ensemble activity with high spatial and temporal resolution. In this part of the present study, I could demonstrate that this technique is applicable to auditory brainstem preparations of young rats and that it enables one to image the neuronal activity in a population of neurons with a high temporal resolution.

# 3 Functional glutamatergic and glycinergic inputs to several superior olivary nuclei of the rat revealed by optical imaging

## 3.1 INTRODUCTION

The superior olivary complex (SOC) in the mammalian brainstem is composed of several nuclei. The main nuclei are the lateral superior olive (LSO), the medial superior olive (MSO), and the medial nucleus of the trapezoid body (MNTB), all known to be involved in binaural hearing and in the localization of sound sources (review: Irvine, 1992). Among the remaining nuclei of the SOC, the superior paraolivary nucleus (SPN) is a prominent ensemble of neurons whose physiological role is only barely understood. The two major excitatory and inhibitory neurotransmitters in the SOC are glutamate and glycine, respectively (Fig. 3.1). The glycinergic MNTB receives glutamatergic input from the contralateral cochlear nucleus (CN) and acts as a relay by innervating LSO, MSO, and SPN on the same side (Wu and Kelly, 1991, 1992b; Grothe and Sanes, 1993; Smith et al., 2000; Brand et al., 2002; Behrend et al., 2002). In addition to the inhibitory input from the MNTB, the LSO receives an excitatory input from the ipsilateral CN (Fig. 3.1; Wu and Kelly, 1992b). An inhibitory, glycinergic input to the LSO from ipsilateral (Wu and Kelly, 1995), and an excitatory input from contralateral (Glendenning et al., 1985; Wu and Kelly, 1991) have also been described. So far, the latter LSO input has not been pharmacologically identified. In addition to the above-mentioned inhibitory input from the contralateral ear, the MSO receives an inhibitory, glycinergic input from ipsilateral (Brand et al., 2002), as well as excitatory, glutamatergic inputs from ipsi- and contralateral (Fig. 3.1; Smith et al., 2000). In the SPN, excitatory inputs from ipsi- and contralateral (Behrend et al., 2002; Dehmel et al., 2003; Kulesza et al., 2003) as well

as inhibitory inputs from ipsi- and contralateral (Behrend et al., 2002; Dehmel et al., 2003) were described. A pharmacological identification of the SPN inputs still needs to be done, except for the glycinergic contralateral input (Fig. 3.1; Behrend et al., 2002).
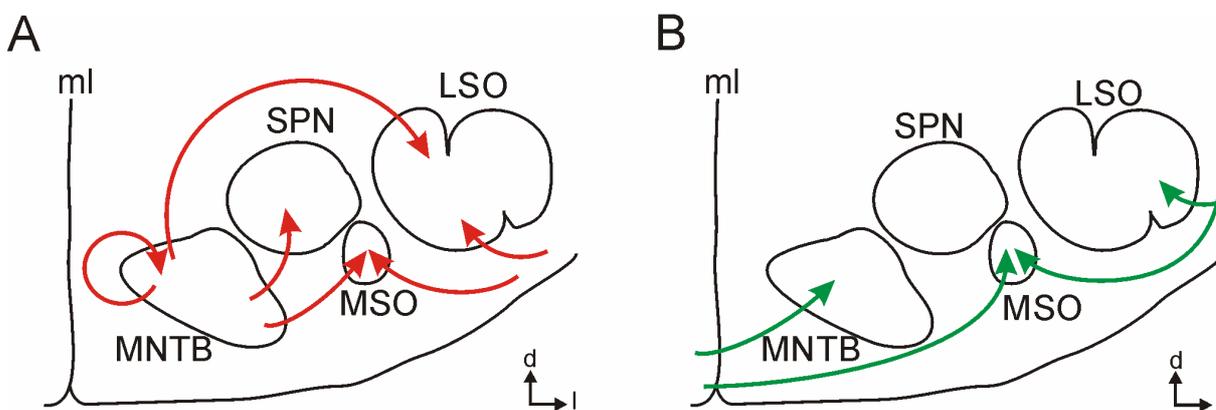


**Fig. 3.1: Inhibitory and excitatory inputs to the SOC**

(A) Schematic diagram of the SOC with its major nuclei and their glycinergic inputs (red arrows). (B) Schematic diagram of the SOC with its major nuclei and their glutamatergic inputs (green arrows). d = dorsal; l = lateral; ml = midline.

Although the neural circuit of the SOC is quite well investigated, there are still several open issues. Three of them are addressed in this Chapter 3 of the present study: (1) the pharmacological identification of most SPN inputs as well as of the excitatory, contralateral LSO inputs, (2) the quantitative characterization of the different inputs to LSO, MSO, and SPN, and (3) the existence of regional differences within a given nucleus. To tackle these issues, I performed optical imaging recordings with the fast voltage-sensitive dye RH795 (reviews: Ebner and Chen, 1995; Momose-Sato et al., 2001) on acute brainstem slices in combination with electrical stimulation of SOC inputs. This approach allows the comparative measurement of electrical activity of cell ensembles with high spatio-temporal resolution. Glycine receptor-mediated inputs and AMPA/kainate glutamate receptor-mediated inputs were identified by applying strychnine and CNQX, respectively. Results obtained in this Chapter show

that the inputs to several SOC nuclei can be simultaneously characterized and pharmacologically identified by VSD recordings. The spatial distribution of inputs within a given nucleus can be detected in a single experiment.

Data presented in this Chapter has been accepted for publication (Srinivasan et al., 2004b).

## 3.2 MATERIALS AND METHODS

### Acute brainstem slice preparation

A total of 63 acute brainstem slices were prepared from Sprague-Dawley rat pups of both gender between P3 and P13 as described in Chapter 2.2. The composition of solutions used for preparation, storage of slices, and recording as well as the dye loading procedures with RH795 were identical to those described in Chapter 2.2. The slices were then transferred to recording solution supplemented with 100 µM of the voltage-sensitive dye RH795. After dye incubation for 30 min, the slices were placed in a chamber with carboxygenated recording solution for 50 min to wash out unbound dye molecules. Finally they were transferred to the recording chamber.

### Drug applications

To pharmacologically separate excitatory and inhibitory inputs to the SOC nuclei, the AMPA/kainate glutamate receptor blocker CNQX (6-cyano-7-nitroquinoxaline-2,3-dione, 20 µM) and the glycine receptor blocker strychnine (0.5 µM) were added to the recording solution (both from Sigma-RBI, Deisenhofen, Germany). Drug solutions were bath applied 15 minutes before the recording started.

**Optical recording**

Recording conditions and experimental setup were identical to those described in Chapter 2.2.

**Data acquisition and analysis**

The data acquisition and analysis were identical to those described in Chapter 2.2. Optical signals were amplified, digitized by an analog-to-digital converter, and low-pass filtered at 1 kHz before storage. The frame rate was 1.66 kHz. To increase signal-to-noise ratio, 10 subsequent trials were temporally averaged in the stimulation – no stimulation mode (Figs. 2.7 and 2.8). I averaged the recordings from several spatially related diodes. Such recordings are considered as `multiple diode recordings´. In Figs. 3.3 – 3.6 and 3.8 – 3.11, the different nuclei of the SOC are illustrated as light gray areas and the regions of `multiple diode recordings´ are marked as dark gray areas. Response amplitudes are given in percentage of fluorescence changes ($\Delta$F/F). When quantitatively comparing $\Delta$F/F values within a nucleus or between nuclei, data were first tested for normal distribution and then the appropriate statistical test was used. In case of normally distributed data, the mean ± standard error of mean is given; otherwise the median and range is listed.

**Electrical stimulation of SOC input fibres**

Stimulus positions were identical to those described in Chapter 2.2. Single current shock of 0.2 ms duration and 3 mA amplitude was used. This was done because in control experiments (3 slices with ipsilateral stimulation; 2 slices with contralateral stimulation) with increasing stimulus amplitudes from 0.5 mA to 4.5 mA with 0.5 mA-increments, 3 mA-pulses always resulted in saturated postsynaptic responses (Fig.

3.2). Only experiments where presynaptic components occurred, implying a successful stimulation of the input fibers, were subjected to a quantitative analysis.

## 3.3 RESULTS

## Pharmacology of ipsilateral inputs to the LSO and MSO

In order to pharmacologically identify the neurotransmitter receptor types mediating
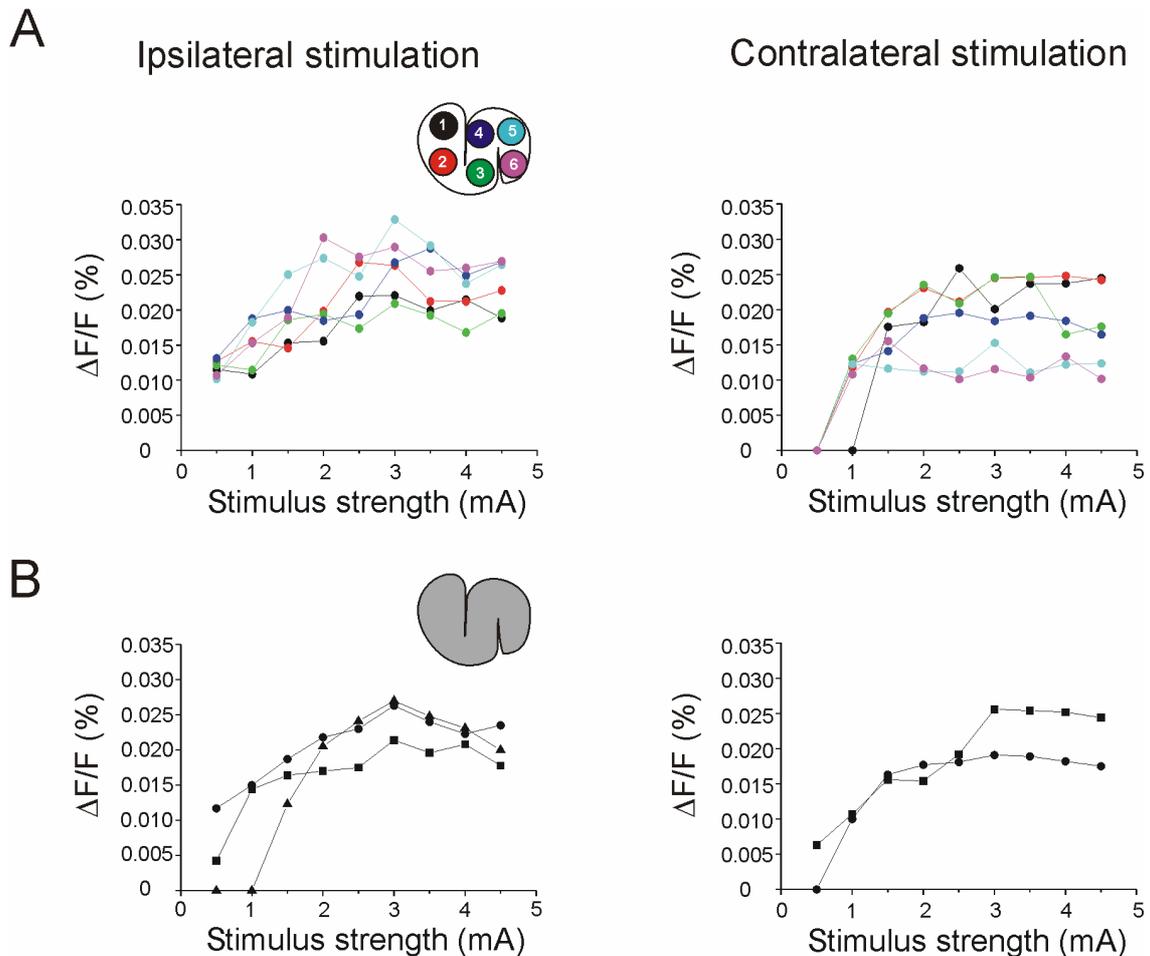


**Fig. 3.2: 3 mA stimulus strength elicites maximum postsynaptic response**
(A) Relation of peak amplitude of the postsynaptic response elicited in 6 different LSO regions (inset with color code) and different stimulus strength upon ipsilateral and contralateral stimulation. Shown are the data from a P8 slice. The inset scheme illustrates the position of the 6 LSO areas, each detected by 7 diodes, from which `multiple diode recordings´ were obtained. (B) Relation of peak amplitude of the postsynaptic response elicited in the entire LSO slice (inset figure) is plotted against different stimulus strength upon ipsilateral (3 slices) and contralateral stimulation (2 slices). The amplitude of the postsynaptic response was measured by spatial averaging of responses from entire LSO.

the postsynaptic response components, the AMPA/kainate glutamate receptor blocker CNQX and the glycine receptor blocker strychnine were bath-applied at 20 µM and 0.5 µM, respectively. To observe possible regional differences of LSO inputs, 6 circular regions (Fig. 3.2) were selected from dorsomedial to ventrolateral, each with a size of ~10,000 µm$^2$ (panel A of Figs. 3.3-3.6). In the MSO, only one region of the same size was selected. Thus, each of these LSO and MSO regions was scanned by 7 diodes. The `multiple diode recordings´ of these diodes are shown in panel B of Figs. 3.3-3.6 and were used for further analysis.

*CNQX-sensitive ipsilateral input*

The effect of CNQX on ipsilateral inputs to the LSO was tested in 42 LSO regions from 12 slices; 11 slices were used for the MSO. In each case, the postsynaptic responses were reduced by CNQX. Under control conditions, the response pattern in the 6 LSO regions was heterogeneous upon ipsilateral stimulation (upper row in Fig. 3.3B). In the presence of CNQX, the postsynaptic response component was altered in every LSO region (middle row in Fig. 3.3B). A clear hyperpolarizing response occurred in regions 2-6, whereas no postsynaptic component was visible in region 1. Digital subtraction of the response traces under CNQX from the response traces under control conditions revealed a CNQX-sensitive component in every LSO region (lower row in Fig. 3.3B). The peak amplitudes of the CNQX-sensitive components varied, yet the variations did not correlate with the variations in peak amplitude of the presynaptic components. For example, the peak amplitudes of the CNQX-sensitive component of regions 3 and 4 were similar, whereas the peak amplitude of the presynaptic component of region 3 was larger than that of region 4. Like in the LSO
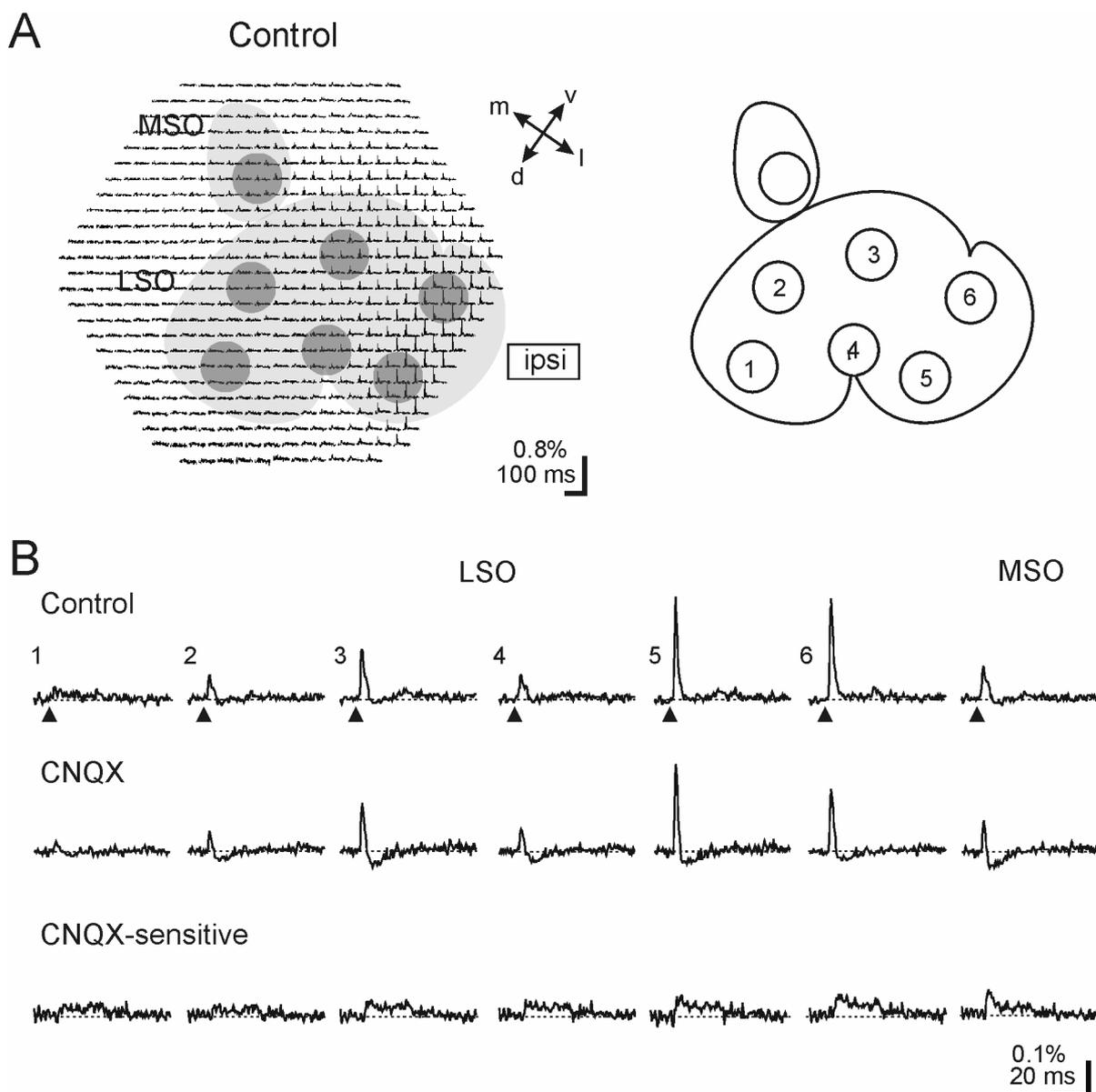
**Fig. 3.3: Ipsilateral, glutamatergic inputs to the LSO and MSO**

(A) Distribution of optical signals in the LSO and the MSO in a coronal section evoked by ipsilateral stimulation. The scheme on the right shows the graphical representation of the LSO and the MSO as well as the position of 7 selected circular regions, each containing 7 diodes, from which `multiple diode recordings´ were obtained (6 in LSO, 1 in MSO). These `multiple diode recordings´ are shown at higher magnification in B. (B) `Multiple diode recordings´ from LSO (1-6) and MSO under control conditions and in the presence of 20 μM CNQX. Arrow head = stimulus. The CNQX-sensitive component was obtained by subtracting the response under CNQX from the response under control conditions. The horizontal dotted lines represent the baseline fluorescent level. This way of data presentation and analysis is also used in figures 3.4-3.6, and 3.8-3.11. ipsi = site of stimulation; v = ventral; d = dorsal; l = lateral; m = medial.

regions, a postsynaptic hyperpolarization in the presence of CNQX and a CNQX-sensitive depolarization were also observed in the MSO (Fig. 3.3B).

*Strychnine-sensitive ipsilateral input*

The effect of strychnine on ipsilateral inputs to the LSO was tested in 69 LSO regions from 15 slices; 12 slices were used for the MSO. In 68% of the LSO regions (47/69), strychnine affected the postsynaptic responses. Similarly, in 75% of the MSO slices/regions, postsynaptic responses were affected by strychnine. The application of strychnine clearly changed the postsynaptic responses in every LSO region and in the MSO: depolarizations became apparent or increased in amplitude (upper and middle row in Fig. 3.4B; appearance in regions 1-3, 6; increase in regions 4 and 5). These depolarizations were attributable to the CNQX-sensitive ipsilateral input described above (cf. lower row in Fig. 3.3). In every LSO region as well as in the MSO, the strychnine-sensitive postsynaptic component was of hyperpolarizing nature (lower row in Fig. 3.4B). Similar to the CNQX-sensitive depolarizations described above, the strychnine-sensitive hyperpolarizations varied in amplitude across the different LSO regions. Again, there was no correlation between the variations in postsynaptic hyperpolarization amplitudes and the variations in presynaptic amplitudes (compare `Control´ and `Strychnine-sensitive´ traces of region 3 and 4 in Fig. 3.4). In the MSO and in region 4 of the LSO, the postsynaptic component contained an action potential in the presence of strychnine, indicative of the abolishment of inhibition (arrows in middle row of Fig. 3.4B). After digital subtraction, such action potentials appeared as downward deflections (arrows in lower row of Fig. 3.4B), which were always excluded from further quantitative analysis (see below).
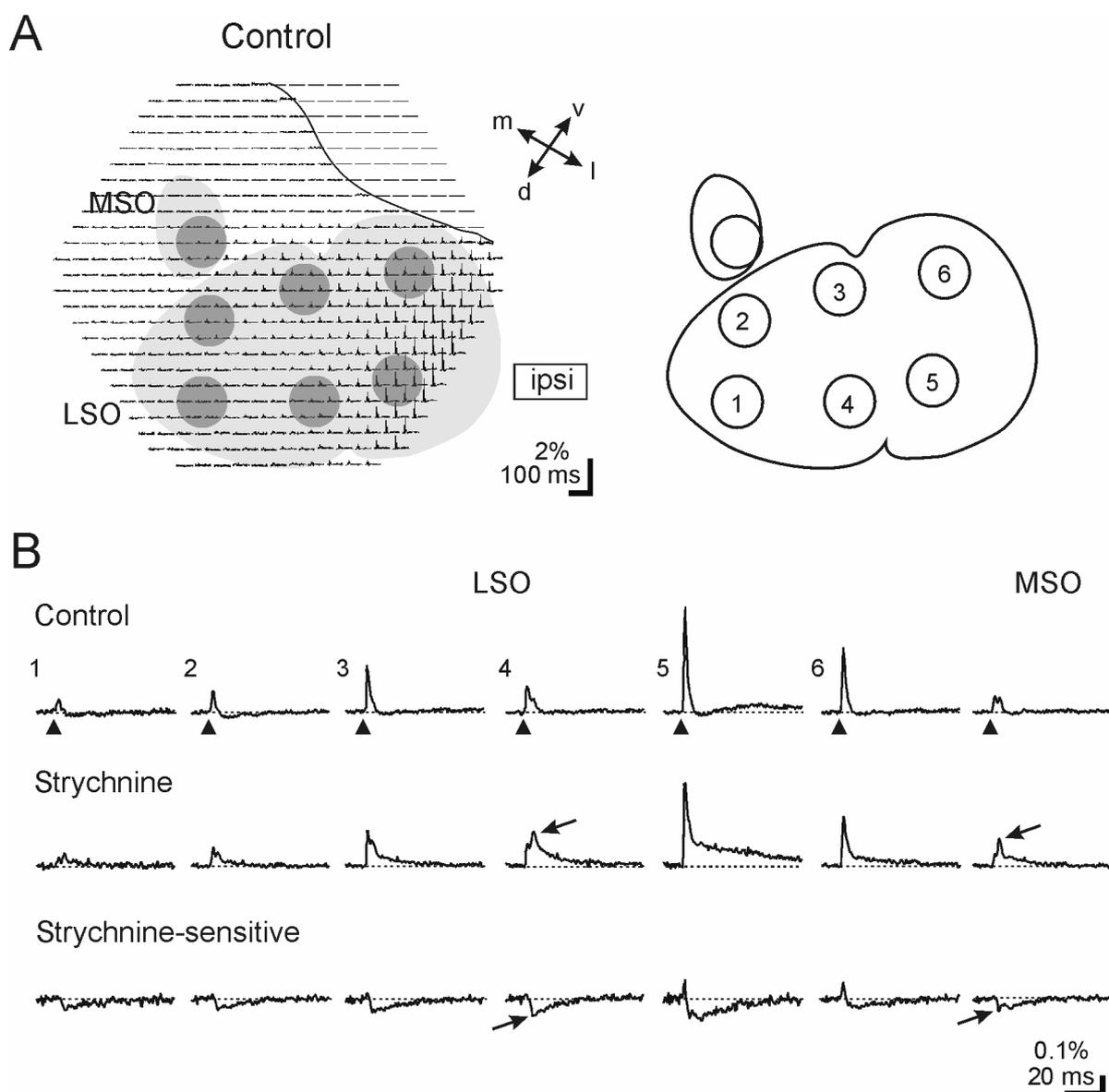
**Fig. 3.4: Ipsilateral, glycinergic inputs to the LSO and MSO**

Data presentation and analysis are the same as described in the legend of Fig. 3.3. (A) Distribution of optical signals within the LSO and the MSO evoked by ipsilateral stimulation. (B) `Multiple diode recordings´ from LSO (regions 1-6) and MSO under control conditions and in the presence of 0.5 µM strychnine. The small upward deflections before the strychnine-sensitive hyperpolarization in regions 5 and 6 possibly reflect time-dependent rundown effects due to washout of dye. In the MSO and region 4 of the LSO, postsynaptic action potentials were elicited in the presence of strychnine (arrows in middle row), which caused a contamination in the strychnine-sensitive responses (arrows in lower row). ipsi = site of stimulation; v = ventral; d = dorsal; l = lateral; m = medial.

Together, the results obtained with the application of CNQX and strychnine show that the LSO and MSO neurons receive functional glutamatergic as well as glycinergic inputs originating from the ipsilateral side.

**Pharmacology of contralateral inputs to the LSO and MSO**

In analogy to the analysis of ipsilateral inputs, strychnine and CNQX were also used to pharmacologically identify the nature of the contralateral inputs to the LSO and the MSO.

*Strychnine-sensitive contralateral input*

An effect of strychnine on postsynaptic responses in the LSO and the MSO was observed in all slices tested (n = 11); the effect was present in 98% (42/43) of the LSO regions analyzed. The representative control traces in Fig. 6 depict differences in the responses among 5 analyzed LSO regions. The presynaptic component was largest in region 2 and smallest in region 5. Under control condition, a postsynaptic hyperpolarization occurred in every region except region 1, which showed a slight postsynaptic depolarization (upper row in Fig. 3.5B). However, after digital subtraction, a strychnine-sensitive hyperpolarization became obvious in every LSO region (lower row in Fig. 3.5B). Furthermore, a residual postsynaptic depolarization occurred in the presence of strychnine in every LSO region (middle row in Fig. 3.5B). Similar to the LSO, a hyperpolarization and a postsynaptic depolarization occurred in the MSO in the presence of strychnine (Fig. 3.5B). As already seen upon ipsilateral stimulation, the postsynaptic component drastically increased in the presence of strychnine in the MSO and gave rise to an action potential (arrow in middle row of Fig. 3.5B). Consequently, the large peak amplitude of the strychnine-sensitive

component (arrow in lower row of Fig. 3.5B) is a contamination and was therefore excluded from further analysis.
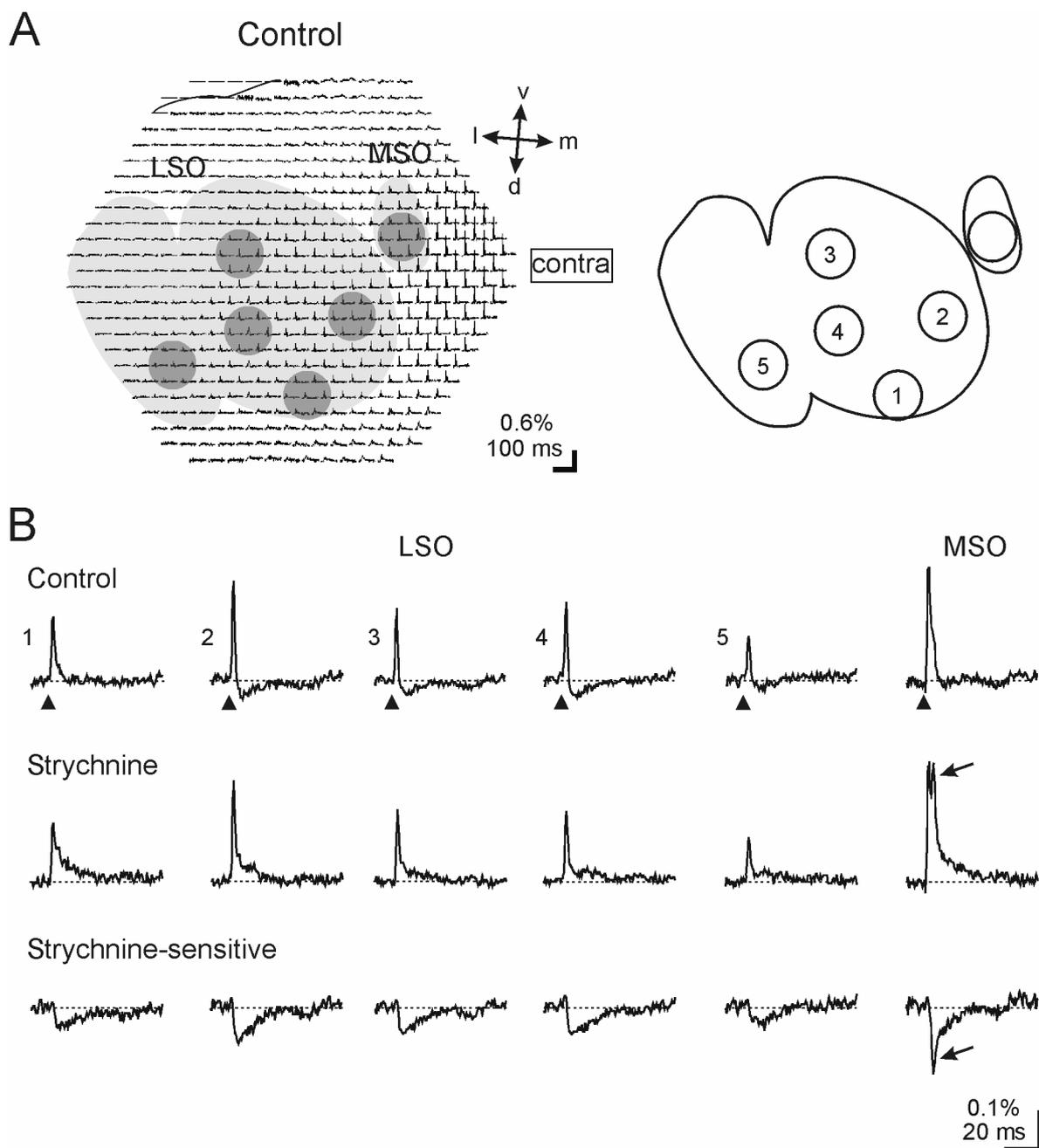


**Fig. 3.5: Contralateral, glycinergic input to the LSO and MSO**

Data presentation and analysis are the same as described in the legend of Fig. 3.3. (A) Distribution of optical signals within the LSO and the MSO evoked by contralateral stimulation. (B) `Multiple diode recordings´ from LSO (regions 1-5) and MSO under control conditions and in the presence of 0.5 µM strychnine. In the MSO, a postsynaptic action potential was elicited in the presence of strychnine (arrow in middle row), which caused a contamination in the strychnine-sensitive response (arrow in lower row). contra = site of stimulation; v = ventral; d = dorsal; l = lateral; m = medial.

*CNQX-sensitive contralateral input*

To identify the origin of the residual postsynaptic depolarization obvious in the presence of strychnine (middle row in Fig. 3.5B), the effect of CNQX on responses evoked by contralateral stimulation was analyzed. Recordings were obtained from 11 slices, comprising 48 LSO regions and the MSO. Regarding the LSO, in 77% of the regions tested (37/48), the postsynaptic component was affected by CNQX. In the MSO, a CNQX-sensitive component was detected in all 11 slices. In the example illustrated in Fig. 3.6, every LSO region as well as the MSO region showed a CNQX-sensitive postsynaptic depolarization (lower row in Fig. 3.6B). The fast transient component of the CNQX-sensitive response in the MSO reflects an action potential, which was already evident in the control trace (see hump in decay phase of presynaptic component, upper row in Fig. 3.6B). In the presence of CNQX, a clear postsynaptic hyperpolarization occurred in the LSO and the MSO (middle row of Fig. 3.6B). This hyperpolarization was attributable to the strychnine-sensitive input described above (cf. lower row of Fig. 3.6B). As in the case of recordings obtained upon ipsilateral stimulation, at contralateral stimulations there was also no correlation between the amplitudes of pre- and postsynaptic components. In Fig. 3.6, the amplitude of the CNQX-sensitive component of region 1 was higher than that of region 2 (lower row in panel B), although the amplitude of the presynaptic component of region 1 was clearly smaller than that of region 2 (upper and middle row in panel B).

Together, the results obtained following strychnine and CNQX application demonstrate the presence of functional contralateral glycinergic as well as glutamatergic inputs to the LSO and the MSO.
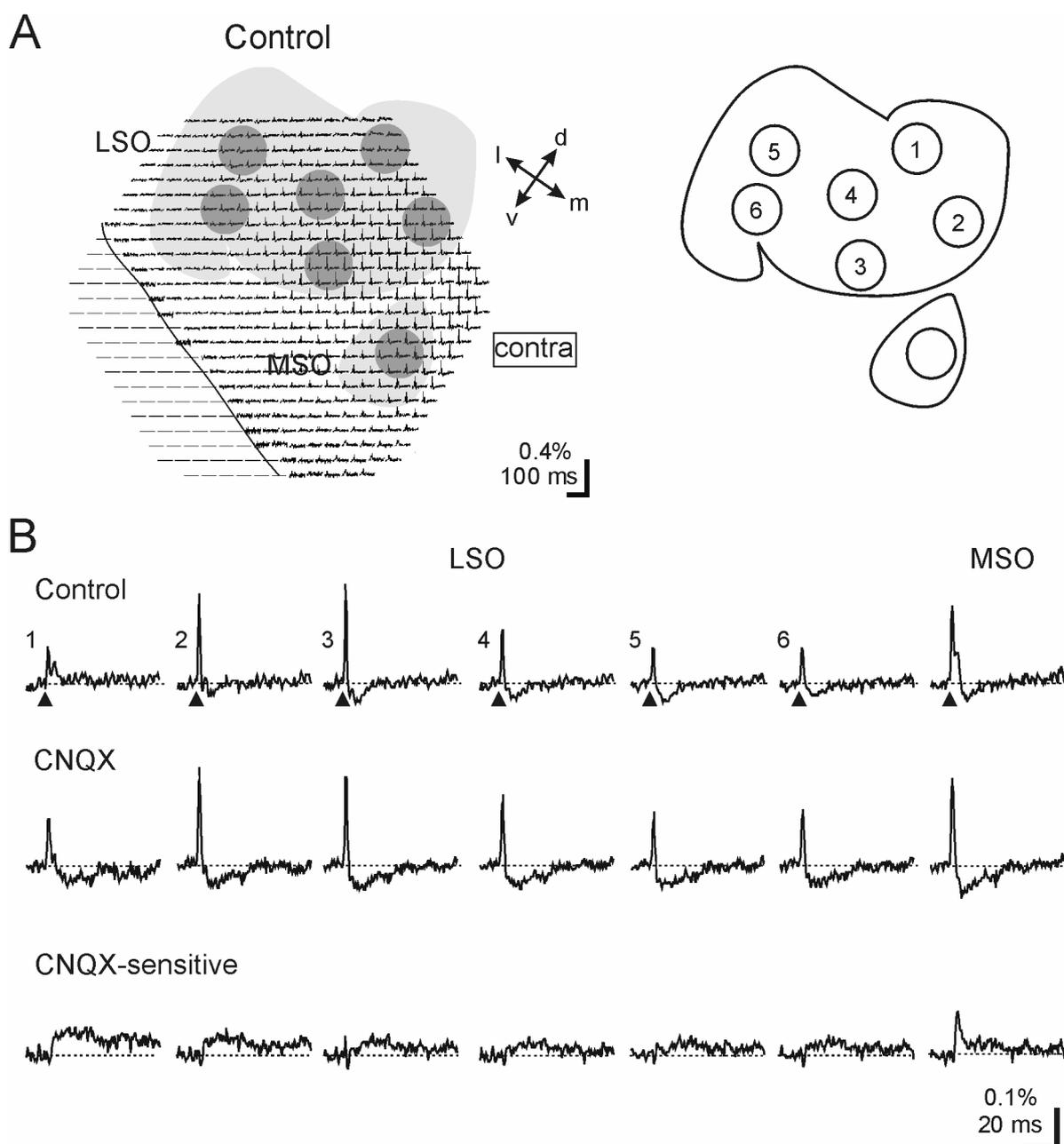
**Fig. 3.6: Contralateral, glutamatergic inputs to the LSO and MSO**

Data presentation and analysis are the same as described in the legend of Fig. 3.3. (A) Distribution of optical signals within the LSO and the MSO evoked by contralateral stimulation. (B) `Multiple diode recordings´ from LSO (regions 1-6) and MSO under control conditions and in the presence of 20 μM CNQX. contra = site of stimulation; v = ventral; d = dorsal; l = lateral; m = medial.

## Comparative analysis of LSO and MSO inputs

The regional distribution of ipsi- and contralateral inputs to both the LSO and MSO is schematically summarized in Fig. 3.7. Panel A represents a *qualitative* analysis, in so

far as each symbol describes the nature of the postsynaptic potentials under control conditions. In the LSO, a depolarization was dominant in every region upon ipsilateral stimulation. On the other hand, a hyperpolarization dominated upon contralateral stimulation in every LSO region except region 1, which showed a depolarization in 68% (15/22) of the cases. In the MSO, 83% (19/23) of the ipsilaterally evoked postsynaptic responses and 86% (19/22) of the contralaterally evoked postsynaptic responses were of depolarizing nature. Fig. 3.7B shows a summary of the *quantitative* analysis of all slices by demonstrating the mean value of CNQX- and strychnine-sensitive $\Delta F/F$ obtained in the 6 different LSO regions and the MSO. Every LSO region and the MSO received a CNQX- and a strychnine-sensitive input in response to ipsilateral or contralateral stimulation.

In the LSO, I found no significant difference between the $\Delta F/F$ of the 6 regions for any of the 4 tested inputs analyzed. Therefore, the values from all 6 LSO regions for the following analysis were pooled. Regarding the ipsilateral LSO inputs, the CNQX-sensitive responses were significantly larger than the strychnine-sensitive responses (median$_{CNQX}$: 0.05%, range: 0.01-0.2%, n = 42 pooled regions; and median$_{strychnine}$: -0.02%, range: -0.1-0%, n = 69 pooled regions, respectively; p = $1.2*10^{-5}$). In contrast, regarding the contralateral LSO inputs, no significant difference between the CNQX- and strychnine-sensitive responses was found (mean$_{CNQX}$ ± S.E.M.: 0.03 ± 0.004%, n = 48 pooled regions; and mean$_{strychnine}$ ± S.E.M.: -0.03 ± 0.001%, n = 43 pooled regions, respectively; p = 0.8). Between the strychnine-sensitive responses of the ipsi- and contralateral LSO inputs, there was also no significant difference (median$_{ipsi}$: -0.02%, range: -0.1-0%, n = 69 pooled regions; and median$_{contra}$: -0.03%, range: -0.07-0%, n = 43 pooled regions, respectively; p = 0.09). In contrast, the ipsilateral CNQX-sensitive LSO input was significantly stronger than the contralateral one
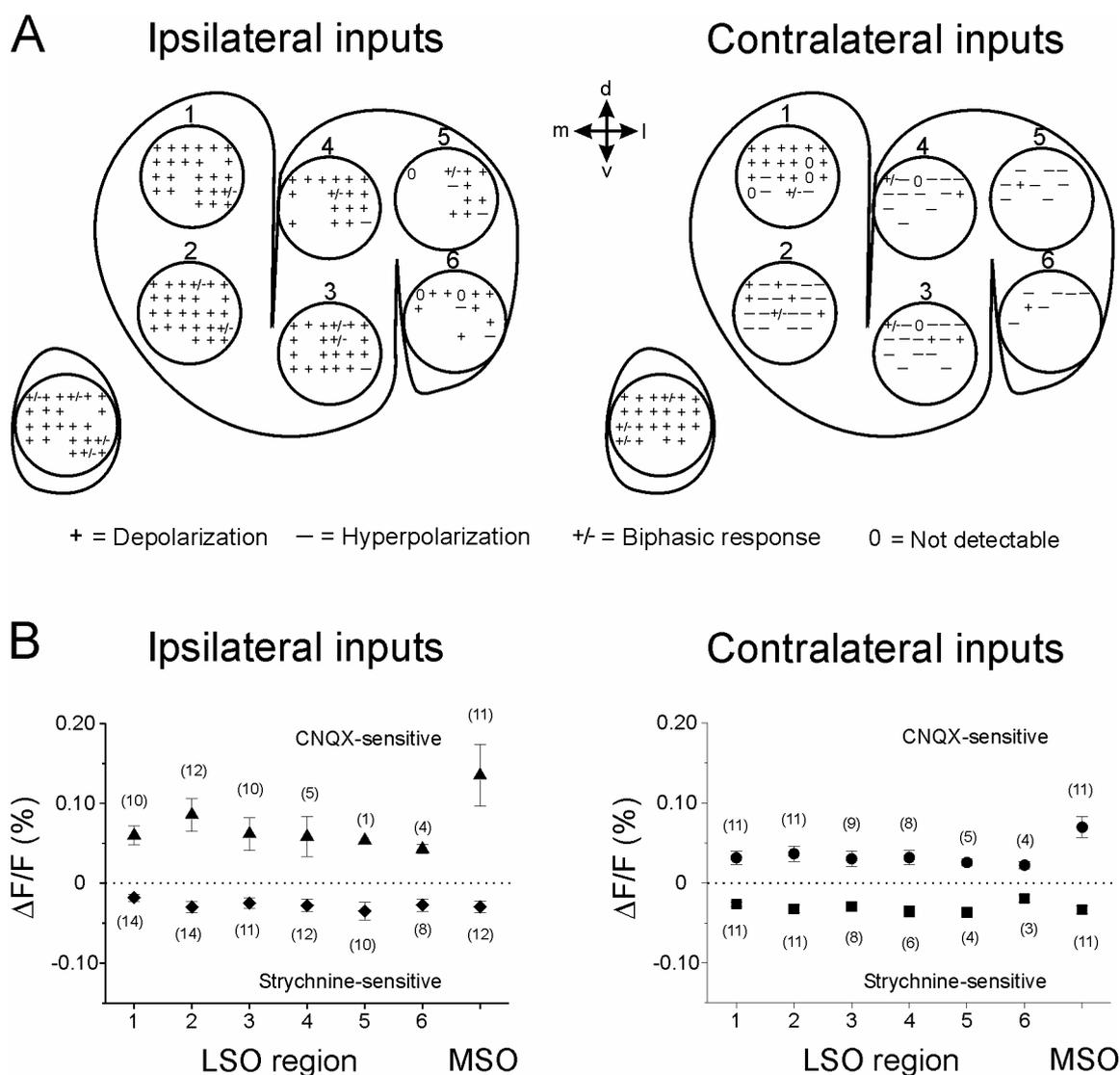
**Fig. 3.7: Regional distribution of ipsi- and contralateral inputs to the LSO and ipsi- and contralateral inputs to the MSO**

(A) Qualitative analysis of postsynaptic components in 6 LSO regions and 1 MSO region, observed under control conditions. In the LSO, depolarizations dominated in every region upon ipsilateral stimulation. Upon contralateral stimulation, hyperpolarizations dominated in every LSO region except of region 1 which shows mostly depolarizations. Occasionally, biphasic responses occurred upon ipsilateral stimulation. In the MSO, depolarizations dominated upon ipsi- and contralateral stimulation. In some cases, biphasic responses were observed upon ipsi- and contralateral stimulation. Note that each position of a symbol in the circular regions corresponds to results obtained from a single experiment. For each experiment, the responses from different regions can be compared with each other. (B) Quantitative analysis of the CNQX- and strychnine-sensitive inputs to the 6 LSO regions and the MSO region. Positive values represent depolarizations, whereas negative values represent hyperpolarizations. Numbers in brackets represent number of experiments/slices. Error bar = standard error of mean.

(median$_{ipsi}$: 0.05%, range: 0.01-0.2%, n = 42 pooled regions; and median$_{contra}$: 0.03%, range: 0-0.09%, n = 48 pooled regions, respectively; p = 0.7*10$^{-3}$).

In the MSO, CNQX-sensitive inputs reached significantly larger average peak values than strychnine-sensitive inputs, from both ipsilateral (mean$_{CNQX}$ ± S.E.M.: 0.1 ± 0.003%, n = 11; and mean$_{strychnine}$ ± S.E.M.: -0.03 ± 0.005%, n = 12, respectively; p = 0.02) and contralateral (mean$_{CNQX}$ ± S.E.M.: 0.07 ± 0.01%, n = 11; and mean$_{strychnine}$ ± S.E.M.: -0.02 ± 0.009%, n = 11, respectively; p = 0.008). In contrast, there was no difference between response amplitudes evoked from ipsilateral vs. contralateral, both for the CNQX-sensitive inputs (p = 0.14) and the strychnine-sensitive inputs (p = 0.55).

Together, the comparative analysis showed no regional differences of the CNQX-sensitive as well as the strychnine-sensitive inputs in the LSO. From the ipsilateral side, the CNQX-sensitive input to LSO neurons was dominant. Interestingly, from the contralateral side, the strength of the strychnine-sensitive input to LSO was similar to the CNQX-sensitive input. In the MSO, the CNQX-sensitive input was always stronger than the strychnine-sensitive input from both the ipsilateral and the contralateral side.

**Pharmacology of ipsilateral inputs to the SPN**

The pharmacological identification of SPN inputs was done in analogy to the above-described experiments. To observe possible regional differences of SPN inputs, 4 circular regions were selected: ventral (1), lateral (2), dorsal (3), and medial (4), each with a size of ~10,000 µm$^2$ (panel A of Figs. 3.8-3.12). As in the LSO and MSO, each SPN region was scanned by 7 diodes. The `multiple diode recordings´ obtained from

these diodes are shown in the figures and were used for further analysis (panel B of Figs. 3.8-3.12).

The presence of ipsilateral inputs to the SPN and their pharmacology in a total of 19 slices, equivalent to 39 regions, were tested. In 16 out of these 19 slices, the stimulus electrode was placed lateral to the LSO as shown in Fig. 2.3A,B. Under this standard ipsilateral stimulus condition, 10 experiments were performed with CNQX and 6 experiments with strychnine. In another set of 3 experiments performed with CNQX, the stimulus electrode was placed dorsal to the standard position, still corresponding to an ipsilateral stimulation.

*CNQX-sensitive ipsilateral input*

In 85% of the SPN regions (33/39), no clear CNQX-sensitive postsynaptic component was detected under standard stimulus conditions. In the example illustrated, a presynaptic depolarization occurred in every region (upper row in Fig. 3.8B). At best, a postsynaptic component was seen in region 2 and 3 in form of a hyperpolarization. CNQX slightly reduced the noise in every region (middle row in Fig. 3.8B), but no clear CNQX-sensitive postsynaptic depolarization was found (lower row in Fig. 3.8B). In the 3 experiments with more dorsally placed stimulus electrodes, no CNQX-sensitive component was seen. Moreover, even a presynaptic component did not occur at this stimulus condition (not shown).
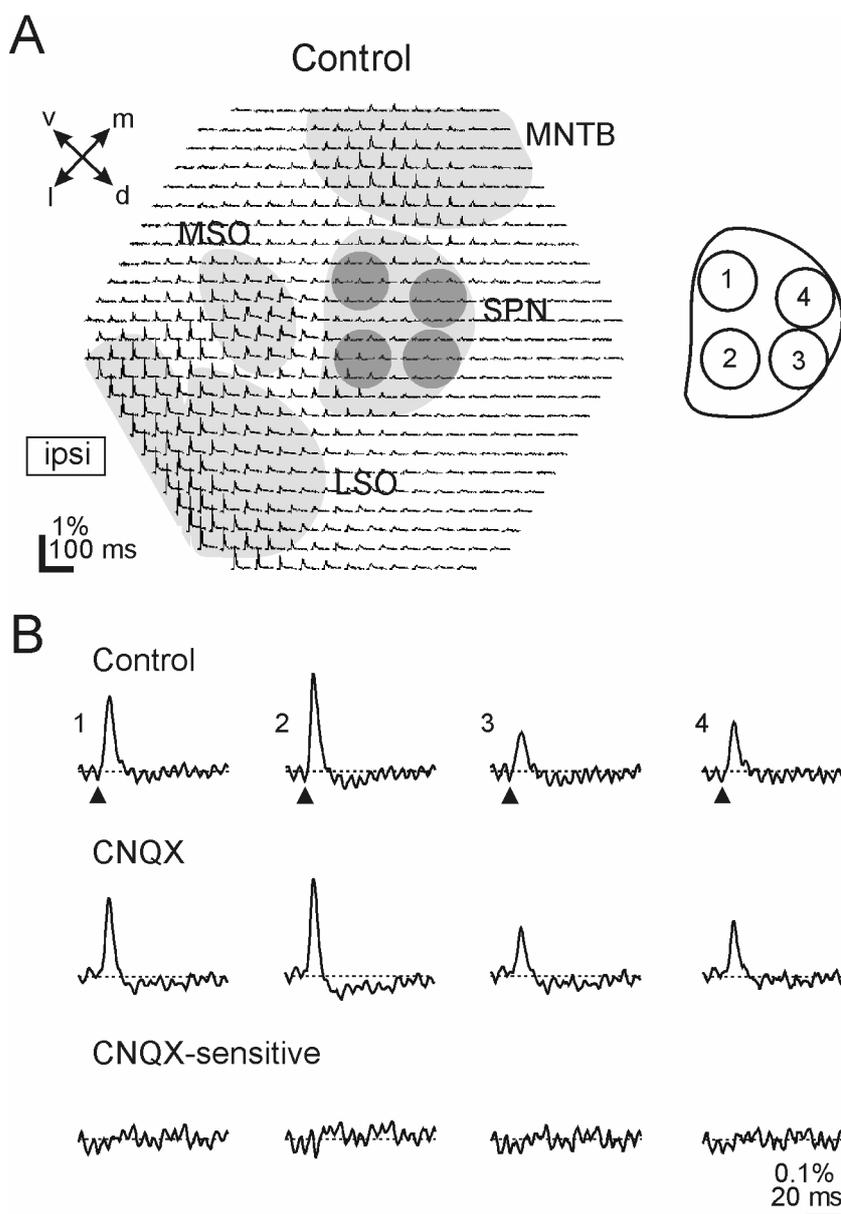
**Fig. 3.8: Absence of ipsilateral, CNQX-sensitive inputs to the SPN**

Data presentation and analysis are the same as described in the legend of Fig. 3.3. (A) Distribution of optical signals within the SPN evoked by ipsilateral stimulation. Note the relatively small responses within the SPN compared to that within LSO, MSO, MNTB, and in the area between MSO and MNTB. (B) `Multiple diode recordings´ from the SPN under control conditions and in the presence of 20 µM CNQX. ipsi = site of stimulation; v = ventral; d = dorsal; l = lateral; m = medial.

*Strychnine-sensitive ipsilateral input*

In 88% of the SPN regions (21/24), an effect of strychnine on the postsynaptic components elicited by standard ipsilateral stimulation was found. Even under control conditions, a small hyperpolarization was seen, at least in region 2 (upper row in Fig. 3.9B). In the presence of strychnine, this hyperpolarization totally disappeared (middle row in Fig. 3.9B). After digital subtraction, a strychnine-sensitive hyperpolarization became obvious in all 4 SPN regions (lower row in Fig. 3.9B).
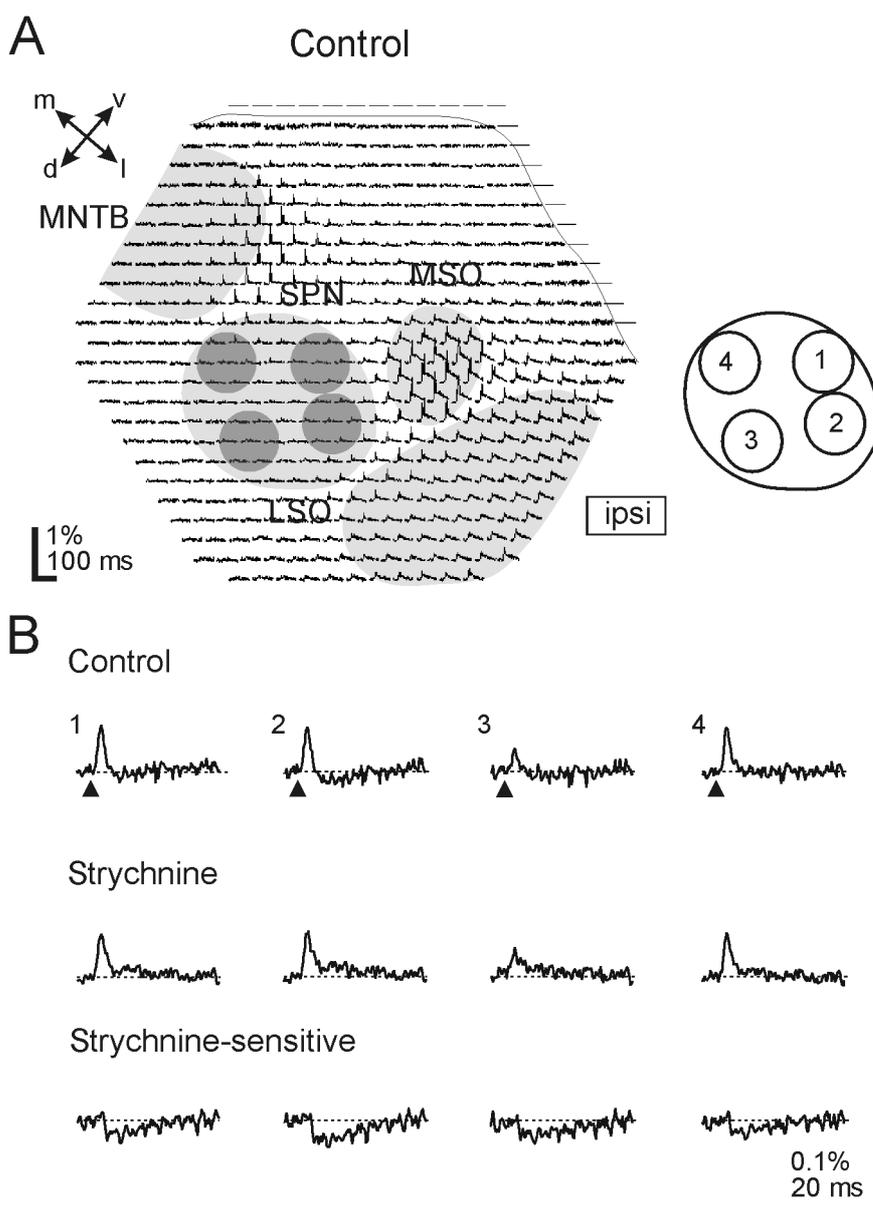
**Fig. 3.9: Ipsilateral, glycinergic inputs to the SPN**

Data presentation and analysis are the same as described in the legend of Fig. 3.3. (A) Distribution of optical signals within the SPN evoked by ipsilateral stimulation. (B) `Multiple diode recordings´ from the SPN under control conditions and in the presence of 0.5 µM strychnine. ipsi = site of stimulation; v = ventral; d = dorsal; l = lateral; m = medial.

Together, the results obtained with the application of CNQX and strychnine show that the SPN neurons receive no, or only a small, glutamatergic input yet a glycinergic input from the ipsilateral side.

**Pharmacology of contralateral inputs to SPN**

In analogy to the ipsilateral SPN inputs, strychnine and CNQX were also used to pharmacologically identify the contralateral SPN inputs. Again, 4 SPN regions were defined as described above. The effect of strychnine on 5 slices, and that of CNQX on 6 slices were tested.

*Strychnine-sensitive contralateral input*

In 100% of the SPN regions (20/20), the contralaterally evoked postsynaptic component was affected by strychnine. The representative example depicted in Fig. 3.10 shows stimulus-evoked responses in the entire SPN (panel A). Under control conditions, depolarizing and hyperpolarizing postsynaptic components appeared (upper row in Fig. 3.10B).
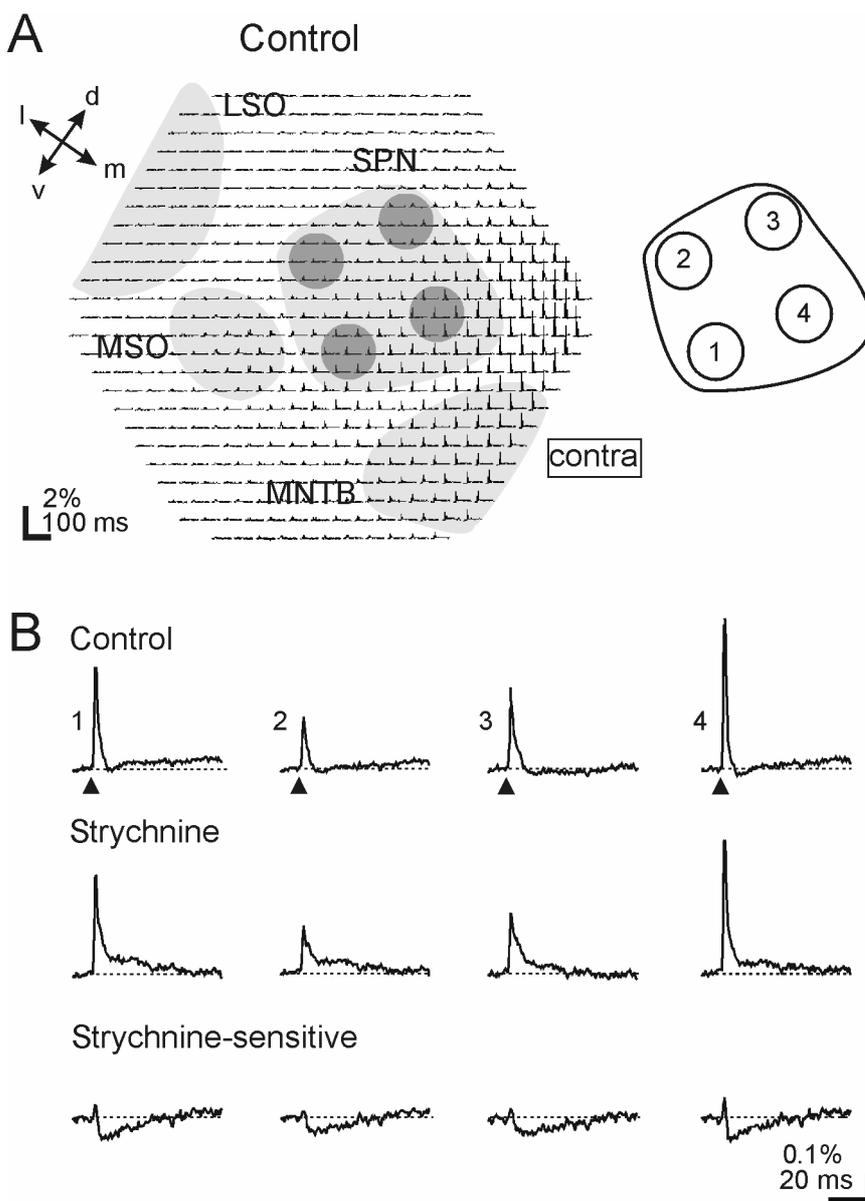


**Fig. 3.10: Contralateral, glycinergic input to the SPN**

Data presentation and analysis are the same as described in the legend of Fig. 3.3. (A) Distribution of optical signals within the SPN evoked by contralateral stimulation. (B) `Multiple diode recordings´ from the SPN under control conditions and in the presence of 0.5 µM strychnine. Note the small upward deflection before the strychnine-sensitive hyperpolarization. They possible reflect time-dependent rundown effects due to washout of dye. contra = site of stimulation; v = ventral; d = dorsal; l = lateral; m = medial.

When strychnine was applied, the postsynaptic responses in all 4 regions displayed a long-lasting depolarization (middle row in Fig. 3.10B). Finally, in every SPN region, a strychnine-sensitive hyperpolarization was present (lower row in Fig. 3.10B).

*CNQX-sensitive contralateral input*

In 100% of the SPN regions (24/24), the postsynaptic component was affected by CNQX.
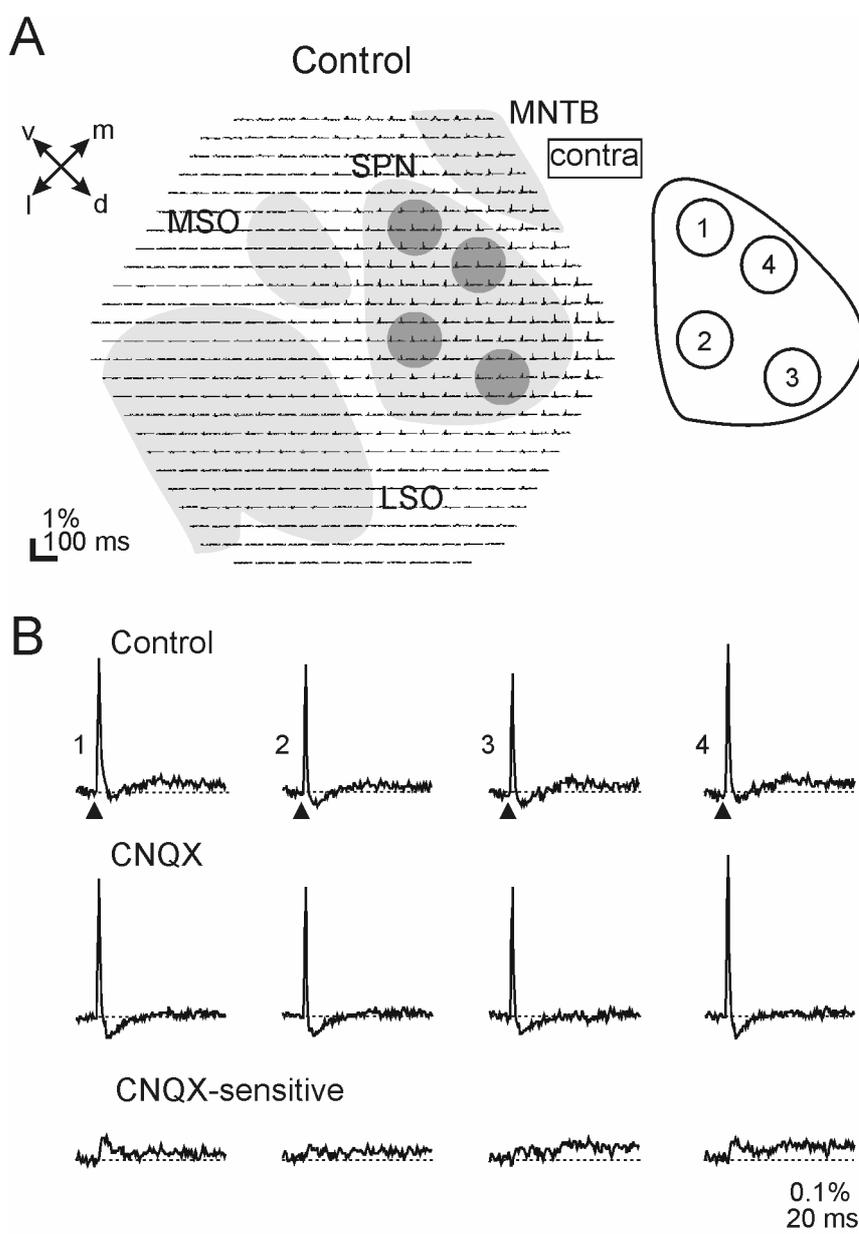


**Fig. 3.11: Contralateral, glutamatergic input to the SPN**

Data presentation and analysis are the same as described in the legend of Fig. 3.3. (A) Distribution of optical signals within the SPN evoked by contralateral stimulation. (B) `Multiple diode recordings´ from the SPN under control conditions and in the presence of 20 µM CNQX. contra = site of stimulation; v = ventral; d = dorsal; l = lateral; m = medial.

In the presence of CNQX, a clear hyperpolarization became obvious in all 4 regions (middle row in Fig. 3.11B). In every region, the CNQX-sensitive component corresponded to a long-lasting depolarization (lower row in Fig. 3.11B).

Together, the results obtained with strychnine and CNQX application demonstrate the presence of functional glycinergic and glutamatergic inputs to the SPN from the contralateral side.

**Comparative analysis of SPN inputs**

The *qualitative* and *quantitative* results of the ipsi- and contralateral inputs to the SPN are summarized in Fig. 3.12. Upon ipsilateral stimulation, almost no postsynaptic component was detectable in regions 1, 3, and 4 (63%, 81%, and 93%, respectively). In contrast, hyperpolarizations dominated in region 2, i.e., in the lateral part of the SPN (63%; Fig. 3.12A, left part). Upon contralateral stimulation, postsynaptic components occurred in every SPN region (region 1: 100%, region 2: 100%, region 3: 92%, region 4: 91%). They were mainly of depolarizing nature or consisted of biphasic responses (Fig. 3.12A, right part).

Concerning the pharmacological identification of the SPN inputs, a strychnine-sensitive input, yet no clear CNQX-sensitive input, was observed in all 4 SPN regions upon ipsilateral stimulation (Fig. 3.12B, left). In contrast, a CNQX- and a strychnine-sensitive input were observed upon contralateral stimulation (Fig. 3.12B, right). Neither the ipsilateral nor the contralateral inputs to the SPN showed significant regional differences. Therefore, I pooled the values from all 4 SPN regions for each input for further analysis. Ipsilaterally, the peak amplitude of the CNQX-sensitive input was significantly smaller than that of the strychnine-sensitive input (median$_{CNQX}$: 0%, range: 0-0.01%, n = 39 pooled regions; and median$_{strychnine}$: -0.02%, range: -

0.03-0%, n = 24 pooled regions, respectively; p = $2.5*10^{-10}$). Contralaterally, no significant difference between the CNQX- and the strychnine-sensitive input was observed (mean$_{CNQX}$ ± S.E.M.: 0.03 ± 0.004%, n = 24 pooled regions; and mean$_{strychnine}$ ± S.E.M.: -0.04 ± 0.004%, n = 20 pooled regions, respectively; p = 0.14). The peak amplitude of the CNQX-sensitive input from contralateral was significantly larger than that from ipsilateral (median$_{ipsi}$: 0.03%, range: 0.01-0.07%, n = 24 pooled regions; and median$_{contra}$: 0%, range: 0-0.01%, n = 39 pooled regions, respectively; p = $5.1*10^{-13}$). Furthermore, the average peak amplitude of the strychnine-sensitive input elicited from the contralateral side was significantly larger than that from the ipsilateral side (mean$_{contra}$ ± S.E.M.: -0.04 ± 0.004%, n = 20 pooled regions; and mean ± S.E.M.: -0.02 ± 0.00001%, n = 24 pooled regions, respectively; p = $3.7*10^{-6}$).

Together, the results demonstrate the presence of CNQX- and strychnine-sensitive inputs to the SPN with similar strength, originating from the contralateral side. From the ipsilateral side, a strychnine-sensitive input dominated a CNQX-sensitive one, which was barely, if at all, detectable. Moreover, the contralateral inputs were stronger than the ipsilateral.

**A**

**Ipsilateral inputs**     **Contralateral inputs**

+ = Depolarization    − = Hyperpolarization    +/− = Biphasic response    0 = Not detectable

**B**

**Ipsilateral inputs**     **Contralateral inputs**
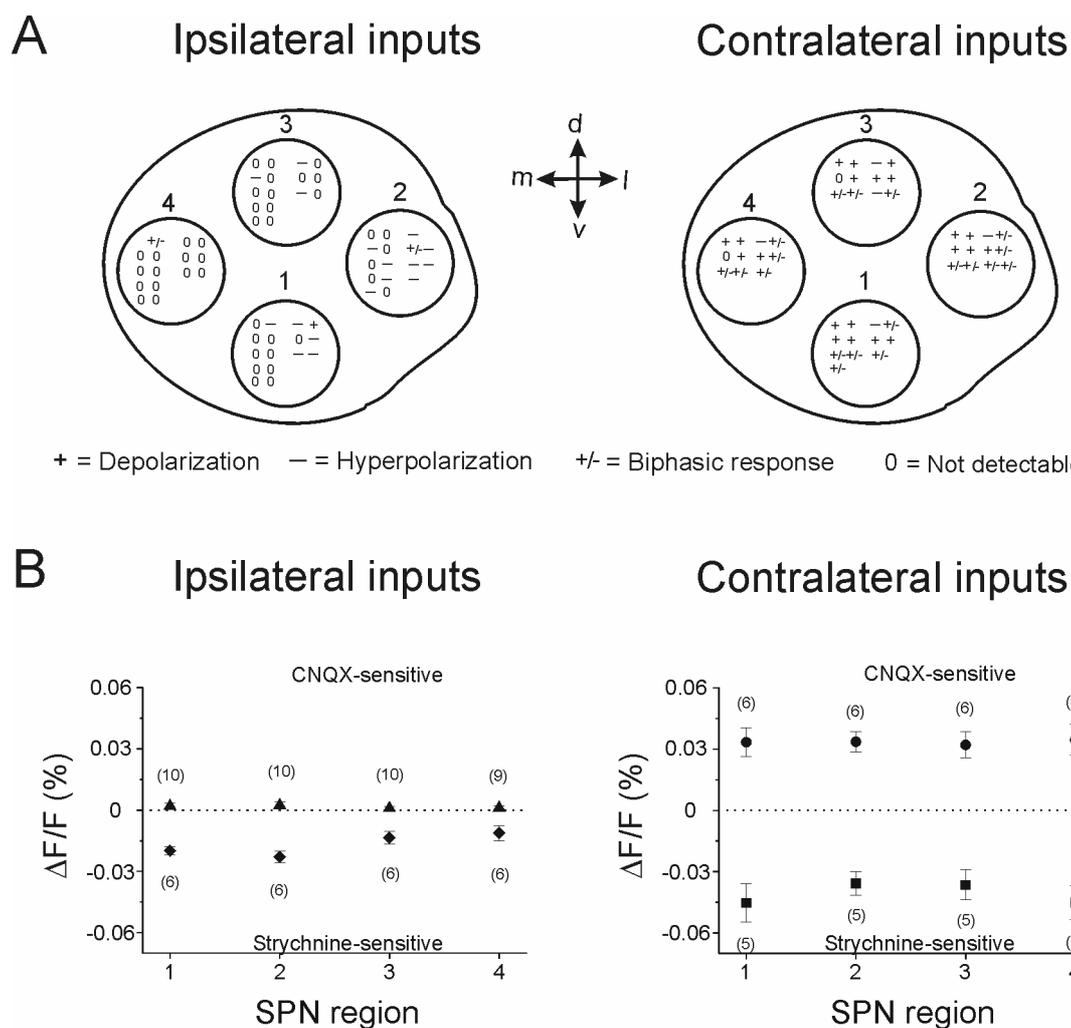
**Fig. 3.12: Regional distribution of ipsi- and contralateral inputs to the SPN**

(A) Qualitative analysis of postsynaptic components observed in 4 SPN regions. Upon ipsilateral stimulation, no postsynaptic component was detected in regions 1, 3, and 4 in most experiments. In contrast, a hyperpolarization dominated in region 2. Upon contralateral stimulation, mainly depolarizations and biphasic responses occurred in every SPN region. (B) Quantitative analysis of the CNQX- and strychnine-sensitive inputs to the 4 SPN regions introduced in panel A. Positive values represent depolarizations, whereas negative values represent hyperpolarizations. Numbers in brackets represent number of experiments/slices. Error bar = standard error of mean.

In summary, a total of 12 inputs to the LSO, MSO, and SPN have been described so far in the literature by a variety of anatomical, immunohistochemical, and physiological methods (Fig. 3.13). To my knowledge, 4 of these 12 inputs (marked by asterisks in Fig. 3.13) are characterized pharmacologically for the first time in the present study.
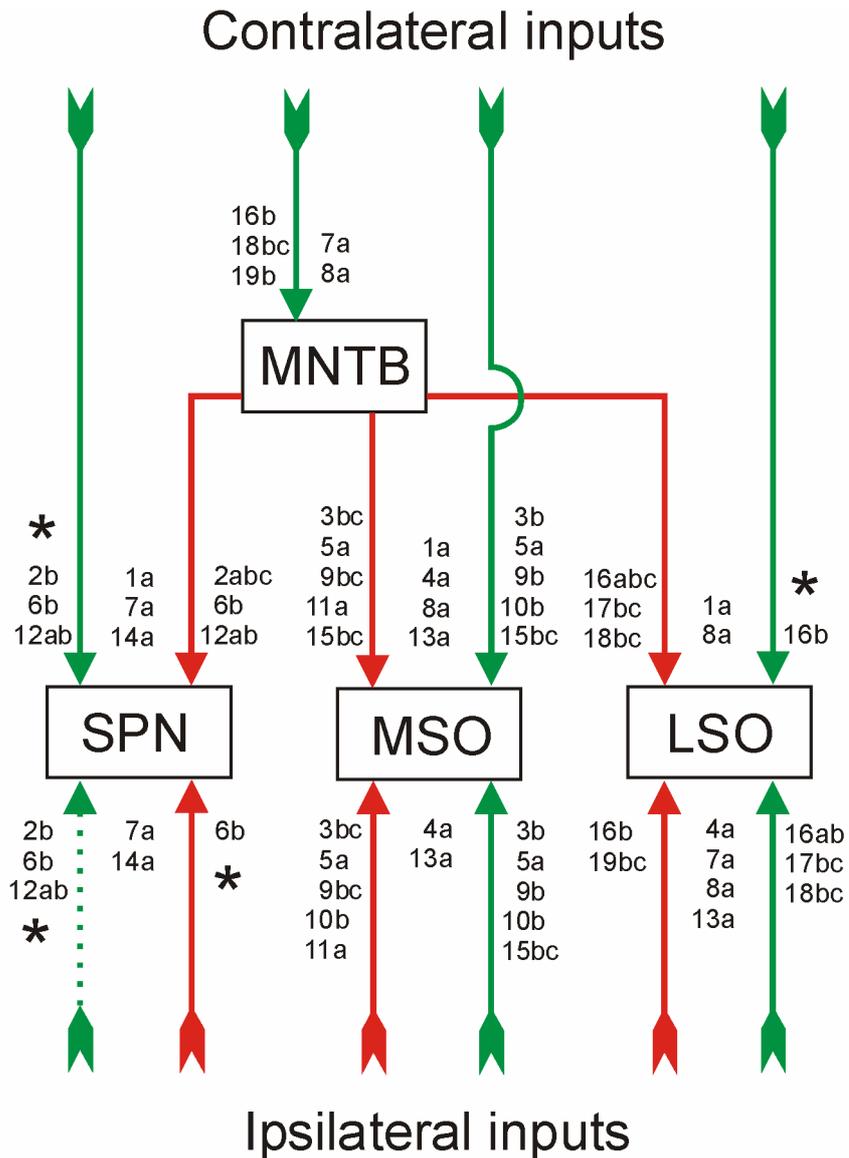
**Fig. 3.13: Summary of characterized glutamatergic and glycinergic inputs to SOC nuclei**

Numbers refer to previous studies which have characterized these inputs. Letters indicate that these studies have employed (a) anatomy, e.g., axonal tracing or immunohistochemistry, (b) electrophysiology, e.g., recording excitatory or inhibitory postsynaptic potentials, or (c) electrophysiology in combination with pharmacology. Asterisks mark inputs which, in the present study, were characterized for the first time as CNQX-sensitive (green arrows) or strychnine-sensitive (red arrows). The dotted green arrow illustrates the weak ipsilateral input to the SPN (cf. Figs. 3.8, 3.9, and 3.12). Studies listed between the arrows did not characterize the inputs as excitatory or inhibitory. 1, (Banks and Smith, 1992); 2, (Behrend et al., 2002); 3, (Brand et al., 2002); 4, (Cant and Casseday,

1986); 5, (Cant and Hyson, 1992); 6, (Dehmel et al., 2003); 7, (Friauf and Ostwald, 1988); 8, (Glendenning et al., 1985); 9, (Grothe and Sanes, 1994); 10, (Inbody and Feng, 1981); 11, (Kapfer et al., 2002); 12, (Kulesza et al., 2003); 13, (Kuwabara and Zook, 1992); 14, (Schofield, 1995); 15, (Smith et al., 2000); 16, (Wu and Kelly, 1991); 17, (Wu and Kelly, 1992a); 18, (Wu and Kelly, 1992b); 19, (Wu and Kelly, 1995).

## 3.4 DISCUSSION

The major results obtained in this Chapter 3 expanded the knowledge concerning the pharmacological identification of excitatory and inhibitory inputs to the LSO, the MSO, and the SPN. Moreover, postsynaptic components could be pharmacologically isolated, and subsequently quantified.

Postsynaptic action potentials could be separated from subthreshold EPSPs (e.g., Fig. 3.4). There was no correlation between the peak amplitude of the pre- and postsynaptic components: a small presynaptic component could be followed by a large postsynaptic component, or a large presynaptic component could be followed by a small postsynaptic component. Therefore, the amplitude of the postsynaptic component could not be predicted from the strength of the presynaptic component. The composition of optical signals reflects mainly the variable assembly of membrane types (e.g., pre- and postsynaptic membranes). Additionally, transmitter release rate, receptor activation, and receptor desensitization also contribute to the optical signals. Regarding the origins of the SOC inputs observed under electrical stimulation situation, I made the following considerations. The bipolar stimulus electrodes and their ipsilateral and contralateral position in the slices were comparable to those used previously (Wu and Kelly, 1991, 1992b; Kandler and Friauf, 1995; Kullmann et al., 2002). In their report on postsynaptic responses of LSO neurons, Wu and Kelly, (1991) discussed the possibility of indirect synaptic activity by antidromic stimulation of axon collaterals in the trapezoid body. For example, an electrical stimulation lateral to the LSO (cf. Fig. 2.3) could activate collaterals of MNTB neurons antidromically,

which then orthodromically conduct inhibition to the LSO via further collaterals. I cannot exclude this possibility, in particular because I indeed detected in one recording antidromic action potentials in the MNTB following ipsilateral stimulation (cf. Fig. 2.12). Nevertheless, because I activated CNQX- and strychnine-sensitive inputs from ipsilateral as well as from contralateral in the absence of antidromic action potentials, I conclude that these inputs really reflect direct synaptic activity elicited from the corresponding stimulation side.

**Glutamatergic and glycinergic inputs to the LSO**

With the usage of CNQX and strychnine, I was able to selectively identify glutamatergic, AMPA/kainate inputs and glycinergic inputs, respectively. I found that LSO neurons receive these two types of inputs from the ipsilateral and contralateral side (Fig. 3.13). The ipsilateral excitatory input as well as the contralateral inhibitory input to the LSO were already described in several electrophysiological studies (Wu and Kelly, 1992a,b, 1995); therefore, the results confirm these previous findings. I also confirm an ipsilateral, inhibitory input to the LSO (Wu and Kelly, 1991, 1994, 1995). An excitatory LSO input from the contralateral side was also known from an earlier study (Wu and Kelly, 1991). However, in the present study, this contralateral LSO input is described to be CNQX-sensitive for the first time. The quantitative analysis of the voltage-sensitive dye data showed that ipsilaterally, the CNQX-sensitive input was stronger than the strychnine-sensitive one. This is in accordance with the observation that under control conditions (i.e., no receptor antagonists in the recording solution), ipsilateral stimulations elicited postsynaptic depolarizations in the entire LSO (Fig. 3.13).

Contralaterally, the strength of CNQX- and strychnine-sensitive inputs to the LSO was similar. However, this was not seen under control conditions in the postsynaptic responses. They were mainly of hyperpolarizing nature, which imply the dominance of contralateral inhibitory inputs (Fig. 3.7). The discrepancy between the results obtained with and without specific receptor antagonists can be explained by the existence of additional, strychnine-insensitive, inhibitory LSO inputs from contralateral, such as the known GABAergic input (Wu and Kelly, 1995; Kotak et al., 1998; Kullmann et al., 2002; Nabekura et al., 2004), which was not investigated in the present study.

Another mismatch concerning pharmacologically identified inputs and postsynaptic responses under control conditions was restricted to a certain LSO area, namely the dorsomedial region 1 (Fig. 3.13). There, postsynaptic depolarizations dominated upon contralateral stimulations, whereas the CNQX- and strychnine-sensitive inputs were similar in amplitude. It is possible that the dorsomedial LSO region receives an additional excitatory input from contralateral, which is CNQX-insensitive.

**Glutamatergic and glycinergic inputs to the MSO**

Similar to the LSO, I found that the MSO receives glutamatergic, AMPA/kainate inputs and glycinergic inputs from both the ipsilateral and contralateral side (Fig. 3.13). Excitatory inputs from both sides were described earlier (Inbody and Feng, 1981; Grothe and Sanes, 1993); their pharmacological identification was done recently (Smith et al., 2000) and confirmed in the present study. Inhibitory, glycinergic inputs from both sides have also been described previously (Grothe and Sanes, 1994). It is generally accepted that the MSO plays a role in sound localization by processing interaural time differences (review: Joris et al., 1998). Recently, the

proposed model of Jeffress (1948), favoring the coincidence detection of bilateral excitatory inputs, was challenged by experimental evidence showing that the detection of interaural time differences within the MSO is achieved by a combination of converging excitatory and inhibitory inputs (review: Grothe, 2003). Quantitative analysis of the four tested MSO inputs showed that the CNQX-sensitive inputs were always stronger than the strychnine-sensitive ones, both ipsilaterally and contralaterally (Fig. 3.7). Accordingly, under control conditions, I obtained exclusively postsynaptic depolarizations or biphasic responses, both in response to ipsilateral and contralateral stimulation. This is in contrast to the situation in the LSO, i.e., the indication for the presence of additional, inhibitory inputs from contralateral. I have not investigated the existence of further inputs to the MSO, yet such an analysis can be performed with other specific receptor antagonists, such as those against NMDA and GABA receptors. Interestingly, Smith and co-workers (2000) described NMDA and $GABA_A$ receptors in MSO neurons (besides non-NMDA and strychnine receptors), which participated in synaptic transmission elicited from the contralateral side.

**Glutamatergic and glycinergic inputs to the SPN**

Similar to the LSO and MSO, I found glutamatergic and glycinergic inputs to the SPN originating from ipsi- and contralateral side. To my knowledge, with the exception of the known glycinergic input to the SPN originating from the ipsilateral MNTB (thus representing a disynaptic input from the contralateral cochlear nucleus), the other inputs were pharmacologically identified for the first time in the present study (Fig. 3.13). The ipsilateral CNQX-sensitive input was the weakest of all four inputs analyzed (cf. Fig. 3.12). It is very unlikely that the weak CNQX-sensitive responses from ipsilateral were due to inadequate stimulation conditions, because I failed to

evoke stronger responses by changing the ipsilateral stimulation loci. The ipsilateral strychnine-sensitive input was significantly smaller than that elicited from contralateral. Together, the contralateral inputs dominated the ipsilateral inputs in the SPN. This is in accordance with anatomical tracing studies, which showed predominantly contralateral inputs to this nucleus (Friauf and Ostwald, 1988; Schofield, 1995). Moreover, Kulesza and co-workers (2003) demonstrated with extracellular *in vivo* recordings obtained from single rat SPN neurons that most of the cells responded to contralateral stimulation alone, whereas none of them responded to ipsilateral stimulation alone. In the same paper, only a few SPN neurons responded best at binaural stimulation. Interestingly, in an earlier *in vivo* study, Finlayson and Adam (1997) characterized the majority of the cells as binaurally excited. Of course, voltage-sensitive dye recordings from brainstem slices cannot address this issue, yet the present work shows that this imaging method can also be used to address issues of how bilateral inputs are integrated in the SOC. Thus, the role of the SPN in bilateral information processing may well be further investigated *in vitro.*

The pharmacologically identified SPN inputs were not in accordance with the postsynaptic responses observed under control conditions (cf. Fig. 3.12), similar to the above-discussed situation in the LSO. Ipsilaterally, the strychnine-sensitive input was stronger than the CNQX-sensitive one, although mainly no postsynaptic responses were detected under control conditions. Contralaterally, strychnine- and CNQX-sensitive inputs were not significantly different in amplitude, although mainly postsynaptic depolarizations were detected under control conditions. These discrepancies can be explained by the existence of further excitatory inputs.

**Functional inputs to the major SOC nuclei**

In the present study, voltage-sensitive dye recordings were performed in order to identify ipsi- and contralateral inputs into different SOC nuclei. All three nuclei investigated, the LSO, the MSO, and the SPN, received glycinergic and AMPA/kainate receptor-mediated glutamatergic inputs from both sides. These results corroborated findings obtained with different preparations and methods (cf. Fig. 3.13) and provided additional information on the pharmacological nature of the inputs.

# 4 Differential timing of the development of inhibition within the superior olivary complex revealed by optical imaging

## 4.1 INTRODUCTION

The superior olivary complex (SOC) is the first binaural station in the auditory system where the inputs from both ears converge. It is comprised of four major nuclei, namely the medial nucleus of the trapezoid body (MNTB), the lateral superior olive (LSO), the medial superior olive (MSO) and the superior paraolivary nucleus (SPN; Fig. 4.1A). Glutamatergic, excitatory and glycinergic, inhibitory inputs to the SOC are important for processing and conveying auditory signals to higher order nuclei (review: Thompson and Schofield, 2000). Through balance of excitation and inhibition, the LSO and the MSO localize sound with respect to interaural level difference (ILD) and interaural time difference (ITD), respectively (review: Irvine, 1986).

Inhibitory and excitatory connections are equal partners in determining neuronal response properties. Compared to the understanding of the development and plasticity of excitatory networks, less is known about inhibitory circuits. Inhibitory synapses mature via excitation (review: Cherubini et al., 1991). During the early development, inhibitory neurotransmitters are excitatory and induce $Ca^{2+}$ influx through voltage-dependent $Ca^{2+}$ channels (Owens et al., 1996; Kullmann et al., 2002). This $Ca^{2+}$ influx triggers various cascades to promote the maturation of inhibitory synapses (review: Ben-Ari et al., 1997). GABA- and glycine- induced depolarizations have been observed in several brain structures, e.g. the hippocampus (Ben-Ari et al., 1989; Ganguly et al., 2001), the neocortex (Dammerman et al., 2000; Owens et al., 1996), the hypothalamus (Chen et al., 1996), the spinal cord (Huang and Redburn,

1996; Billups and Attwell, 2002), the ventral tegmental area (Ye, 2000), and the LSO (Kandler and Friauf, 1995).

The present study was addressed to elucidate the development of inhibitory neurotransmission in the SOC. In all four major nuclei of the SOC, glycinergic inhibitory inputs shape the synaptic output. Anatomical and physiological studies have shown the existence of inhibitory inputs to the LSO, the MSO and the SPN from the MNTB (Thompson and Schofield, 2000). Thus, the MNTB acts as a relay station providing inhibitory inputs into adjacent nuclei, in addition to recurrent inhibition on itself (Banks and Smith, 1992; Fig. 4.1A).
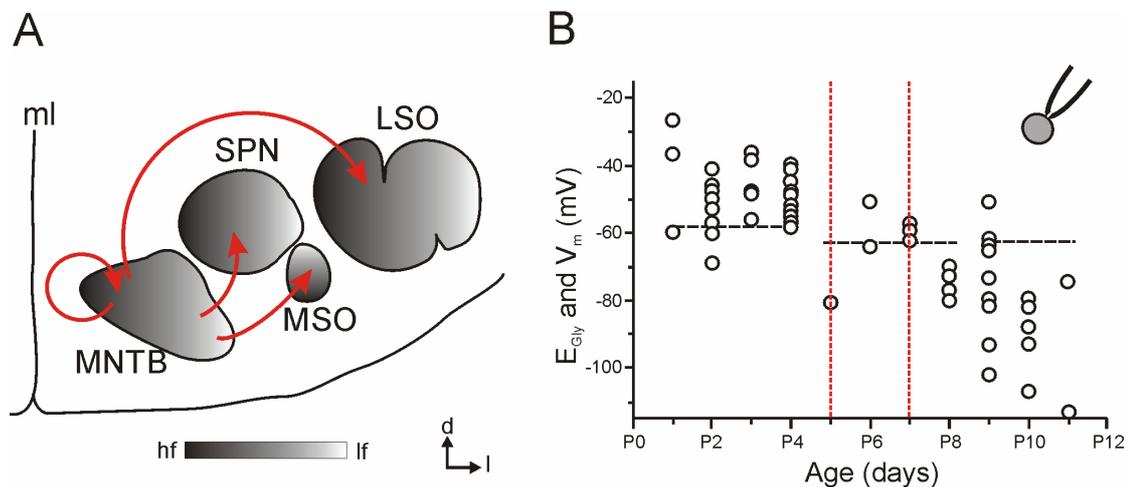


**Fig. 4.1: Inhibitory inputs within the SOC and change in glycine reversal potential ($E_{Gly}$) during LSO development**

(A) Schematic diagram of the SOC with its major nuclei and their glycinergic inputs (red arrows) which arise from the MNTB. hf = high frequency region, lf = low frequency region, d = dorsal, and v = ventral, ml = midline. (B) $E_{Gly}$ values from 57 rat LSO neurons aged P1-11 are plotted against age. After P5-7, the majority of $E_{Gly}$ values were more negative than the membrane resting potential ($V_m$; horizontal broken lines). The day of shift in the $E_{Gly}$ is denoted between P5-7 (vertical broken lines; Modified from Ehrlich et al., 1999).

Developmental studies on LSO neurons addressing the maturation of inhibitory synapses demonstrated a shift in the polarity of glycine-evoked responses (Kandler and Friauf, 1995; Ehrlich et al., 1999; Kakazu et al., 1999). In gramicidin-perforated

patch-clamp recordings, glycine application on to LSO neurons provoked depolarization and hyperpolarization during the first and second postnatal week, respectively (Ehrlich et al., 1999). The difference in polarity is due to a change in the reversal potential of glycine ($E_{Gly}$). When the $E_{Gly}$ is more positive than the resting membrane potential ($V_m$), the LSO neurons display depolarizations due to $Cl^-$ efflux. When the $E_{Gly}$ is more negative than $V_m$, the neurons display hyperpolarizations due to $Cl^-$ influx (Fig. 4.1B; Ehrlich et al., 1999; Balakrishnan et al., 2003). To my knowledge, nothing is known about the development of inhibitory synapses in other SOC nuclei. Chapter 4 of this present study was therefore addressed to elucidate the development of inhibition in the MSO, the SPN, and the MNTB. Furthermore, the LSO was reinvestigated in order to check if there is any regional development of inhibition within the nucleus. In the present study, voltage-sensitive dye imaging served as a tool to examine the voltage changes upon glycinergic synaptic neurotransmission at different ages. The advantages of this imaging method are: (1) the native intracellular chloride concentration ($[Cl^-]_i$) is not disturbed; (2) glycine receptor-mediated responses of entire nuclei, encompassing several hundreds of neurons, can be detected in a single experiment; (3) it is a time saving method.

This work was presented previously in an abstract form (Srinivasan et al., 2004a).


## 4.2 MATERIALS AND METHODS

### Acute brainstem slice preparation

A total of 154 acute brainstem slices were prepared from Sprague-Dawley rat pups of both gender between embryonic day (E) 18 and P10 as described in Chapter 2. For embryonic brainstem slice preparations, young adult rats were paired overnight and the first 24 hr period following the commencement of pairing was considered as E1.

Timed-pregnant females were anesthetized by intramuscular injections of the following anesthesia one by one, ketamine (0.1 mg g $^{-1}$ body weight), mixture of ketamine (0.1 mg g $^{-1}$ body weight) and xylazine hydrochloride (0.005 mg g $^{-1}$ body weight), Acepromazinemalate (0.01 mg g $^{-1}$ body weight). The embryos were removed by Cesarean section. The composition of solutions used for preparation, storage of slices, and recording as well as the dye loading procedures with RH795 were identical to those described in Chapters 2 and 3.

**Drug application**

To pharmacologically separate glycinergic inhibitory inputs to the SOC nuclei, 0.5 µM strychnine was bath applied for 15 min to the recording solution before the recordings began.

**Optical recording**

The experimental setup and the recording conditions were identical to those described in Chapter 2.

**Data acquisition and analysis**

The data acquisition and analysis were identical to those described in Chapters 2 and 3. To study regional differences within a given nucleus, they were separated into different regions regarding their tonotopic order, i.e., from high frequency (hf) to low frequency (lf; Fig. 4.1). Spatially related diodes were averaged in each region. For the LSO, depending on the magnification of the objective, at 40x, 24 diodes (for A, B, & C) and at 20x, 6 diodes (for D) were used for averaging. But the area covered for the multiple diode recordings from each region was same for both objectives (8,438 µm$^2$).

For the MSO, 12 diodes for 40x and 3 diodes for 20x were averaged. The area covered from each region was also same for both objectives and amounted to 4,219 $\mu m^2$. For the SPN, 20 diodes for 40x and 5 diodes for 20x were averaged. Again, the area covered from each region was same for both objectives, amounting to 7,031 $\mu m^2$. For the MNTB, 32 diodes for 40x and 8 diodes for 20x were averaged. The area covered from each region was 11,250 $\mu m^2$ for both objectives.

Strychnine-sensitive components were isolated by the digital subtraction of the strychnine-sensitive response traces under strychnine from the response traces under control conditions. For quantiative analysis, the peak amplitudes of responses were measured. Response amplitudes are given in percentage of fluorescence changes ($\Delta$F/F). The data were first tested for normal distribution, and then peak amplitudes for glycine-evoked fluorescence changes were plotted against age, and the data were analyzed for best-fitting regression functions by software (Winstat für Excel – Fitch software). The point of intersection of regression line to the baseline ($\Delta$F/F = 0%) is determined as the day of shift.

**Electrical stimulation of SOC input fibres**

For recordings in the SPN, the MSO, and the LSO, electrodes were placed within the MNTB to stimulate the inputs as described in Chapter 2 (Fig. 2.3B). To stimulate fibers innervating MNTB, the stimulus electrode was placed at the midline (ml in Fig. 4.1A).

**4.3 RESULTS**

**Regional development of glycine-evoked responses in LSO**

A total of 52 slices were used to study the developmental change in the polarity of glycine-evoked responses in the LSO between P2 and P9. A minimum of 5 slices

were analyzed at each age. Depending on the age, and thus, on the size of the LSO, the entire LSO was focused with different objectives. For younger than P9, a 40x objective was used, and at P9, a 20x objective was employed. At P2, the MNTB simulation provoked strong strychnine-sensitive depolarizations in all four regions of the LSO (Fig. 4.2A). At P5, hyperpolarizations appeared in region 1 and 2 (Fig. 4.2B), also sometimes in region 3 and 4 (Fig 4.3). Mostly, region 3 and 4 displayed no strychnine-sensitive response (Fig. 4.2B). This can be explained by the following arguments: (1) If $V_m = E_{Gly}$, there is no driving force for glycine-evoked (strychnine-sensitive) responses, (2) If both de- and hyperpolarizations are detected by the same diode, the responses will nullify each other, as a result there could be no change of fluorescence. At P7, regions 1, 2, and 3 displayed hyperpolarizing responses, but no prominent hyperpolarization could be detected in region 4 (Fig. 4.2C). At P9, all four regions showed hyperpolarizing responses (Fig. 4.2D). In regions 3 and 4, the postsynaptic response displayed a sharp downward deflection, which was assumed to be an action potential in the presence of strychnine, indicative of the abolishment of inhibition. After digital subtraction, such action potentials appeared logically as downward deflections (asterisks), which were always excluded from further quantitative analysis. The latency, from stimulus to peak response, decreased over age as shown in the typical examples in Fig. 4.2 (20 ms at P2, 6.6 ms at P9).

The optical responses from 52 slices, obtained from animals aged between P2 and P9, were used for quantitative analysis (Fig. 4.3). Region 1 and 2 demonstrated the shift in polarity of glycine-evoked responses at P4 (Fig. 4.3A and B), whereas region 3 at about P5, and region 4 at about P6 (Fig. 4.3C and D). The glycine-evoked responses in the lateral part of the LSO (regions 3 and 4) showed depolarizations for some longer time i.e., until P7, when compared to the medial part (regions 1 and 2)
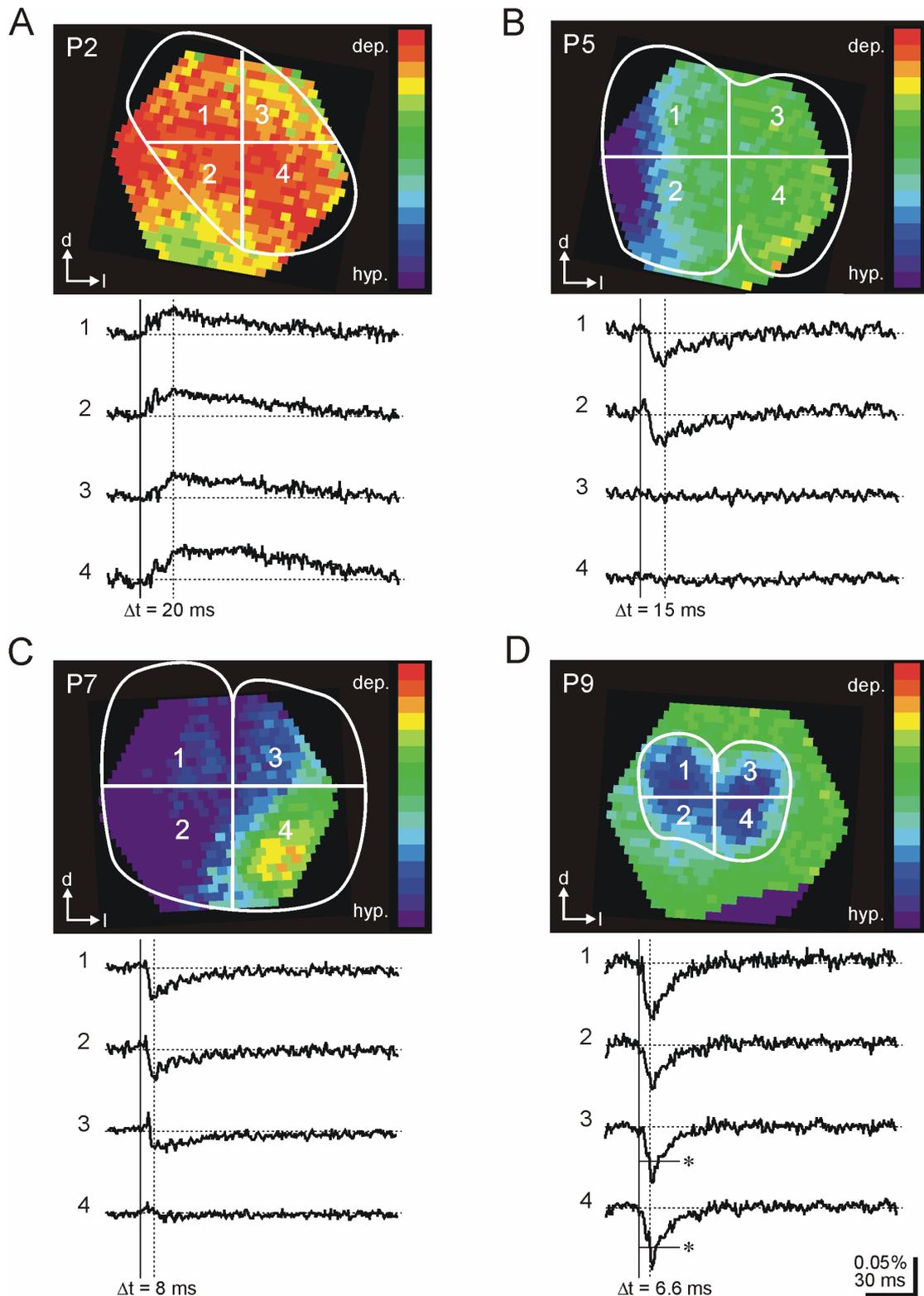
**Fig. 4.2: Age-dependent and region-specific strychnine-sensitive responses in LSO**

Pseudocolor images (top) showing glycine-evoked responses (strychnine-sensitive) and the corresponding `multiple diode recordings´ (bottom) from the four LSO regions (separated from medial to lateral along the frequency line) indicated by numbers. (A) At P2, the entire LSO displays strychnine-sensitive depolarizations (warm colors). (B) At P5, regions 1 & 2 display hyperpolarizations (cold

colors), whereas region 3 & 4 show no change of fluorescence. (C) At P7, regions 1, 2 & 3 display hyperpolarizations, whereas region 4 shows no change of fluorescence. (D) At P9, the entire LSO displays hyperpolarizations. The LSO is outlined by a white line. Solid line = stimulus. Dotted vertical line = peak of the postsynaptic glycine response and the time of the corresponding pseudocolor image shown above. The corresponding latency from the stimulus onset to the peak response ($\Delta t$) is indicated in each panel. Asterisks = reversed action potential.
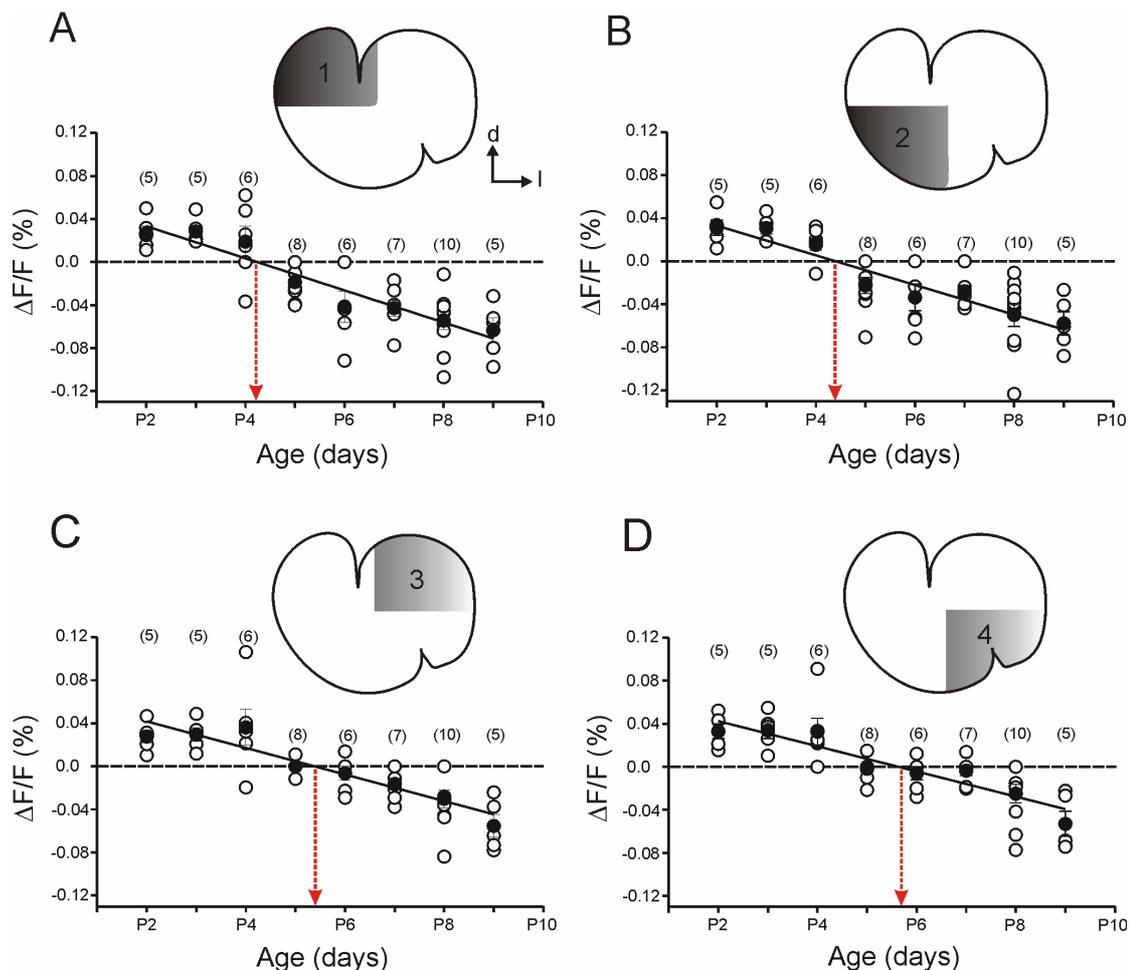


**Fig. 4.3: LSO displays regional differences in the development of glycinergic inhibition**

Peak amplitudes of glycine-evoked fluorescence changes, with positive values equal to depolarizations and negative values equal to hyperpolarizations, are plotted against age. Data from four different LSO regions (inset; see also Fig. 4.2) are displayed in separate diagrams. Relation between $\Delta F/F$ values and age was tested for the best fit regression. The point of the intersection of the regression line with the baseline (horizontal broken line) represents the day of shift, which was denoted by a red dotted arrow. LSO regions 1 & 2 display a shift at around P4 (A, B). Region 3 displays a shift at about P5 (C), whereas region 4 displays it at around P6 (D). Open symbols = glycine responses from individual slices; filled symbols = mean glycine responses; error bars = standard error of mean; number in brackets = number of slices; meaning of symbols and presentation of data holds also for figures 4.4, 4.5, & 4.6.

which showed depolarizations only until P4 (Fig. 4.3A and B). Together, the results obtained with the application of strychnine show that the LSO displays regional difference in the developmental shift of glycine-evoked responses in a tonotopic order i.e., the high frequency region matures earlier than the low frequency region in the LSO.

## In the MSO, the change in the polarity of glycine responses occurs at P5

A total of 62 slices obtained from animals aged between E18–20 and P9 were used to
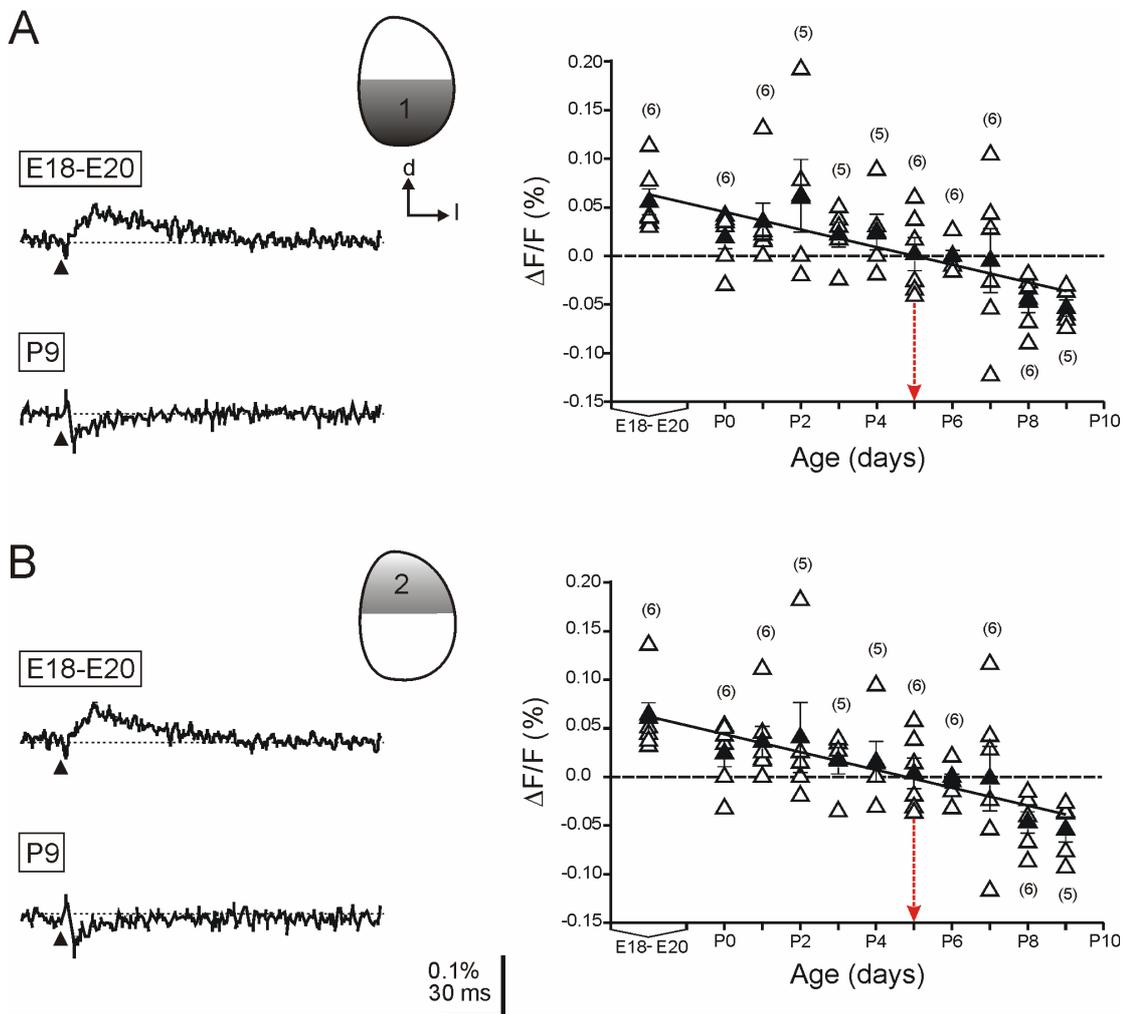


**Fig. 4.4: Developmental shift of glycinergic response in MSO**

The MSO is separated into two regions from ventral to dorsal along the hf and lf region, respectively. (A) The ventral part of the MSO (region 1) displayed early depolarizations and late hyperpolarizations. (B) The dorsal part of the MSO (region 2) also displayed early depolarizations and late

hyperpolarizations. Left panels in A and B show typical examples of multiple diode recordings from E18-E20 and P9. Black arrow heads = stimulus. Right panels in A and B show peak amplitudes of glycine-evoked fluorescence changes from all MSO regions tested. Positive values, equal to depolarizations, and negative values, equal to hyperpolarizations, are plotted against age. The point of intersection of regression line in each graph represents the day of shift which was P5 in both regions (red dotted arrow).

study the glycine developmental shift in the MSO. The MSO was divided into two regions according to the tonotopic organization, i.e., region 1 corresponds to the high frequency region, and region 2 corresponds to the low frequency region. At E18-20, MSO neurons displayed exclusively glycine-evoked depolarizations in both regions (n = 6; Fig. 4.4). At P8 and P9, MSO neurons displayed exclusively glycine-evoked hyperpolarizations in both regions (n = 6 and 5, respectively; Fig. 4.4). Quantitative analysis reveals the day of shift in the polarity of glycine-evoked responses at P5. In contrast to the LSO, no regional difference was observed in the MSO (Fig. 4.4).

**In the SPN, the change in the polarity of glycine responses occurs at E18-20**

A total of 43 slices obtained from animals aged between E18–20 and P6 were used to study the glycine developmental shift in the SPN. The SPN was divided into two regions according to the tonotopic organization, i.e., region 1 corresponds to the high frequency region, and region 2 corresponds to the low frequency region. Only at embryonic ages between E18 and E20, SPN neurons displayed strychnine-sensitive depolarizations in both regions (Fig 4.5). From P0 onwards, the polarity of glycine-evoked responses changed to hyperpolarizations in both regions (Fig. 4.5). Quantitative analysis reveals the shift in the polarity of glycine-evoked responses during E18-20 (Fig 4.5). Thus, the developmental shift from depolarizing to hyperpolarizing glycine responses occur before birth in the SPN.
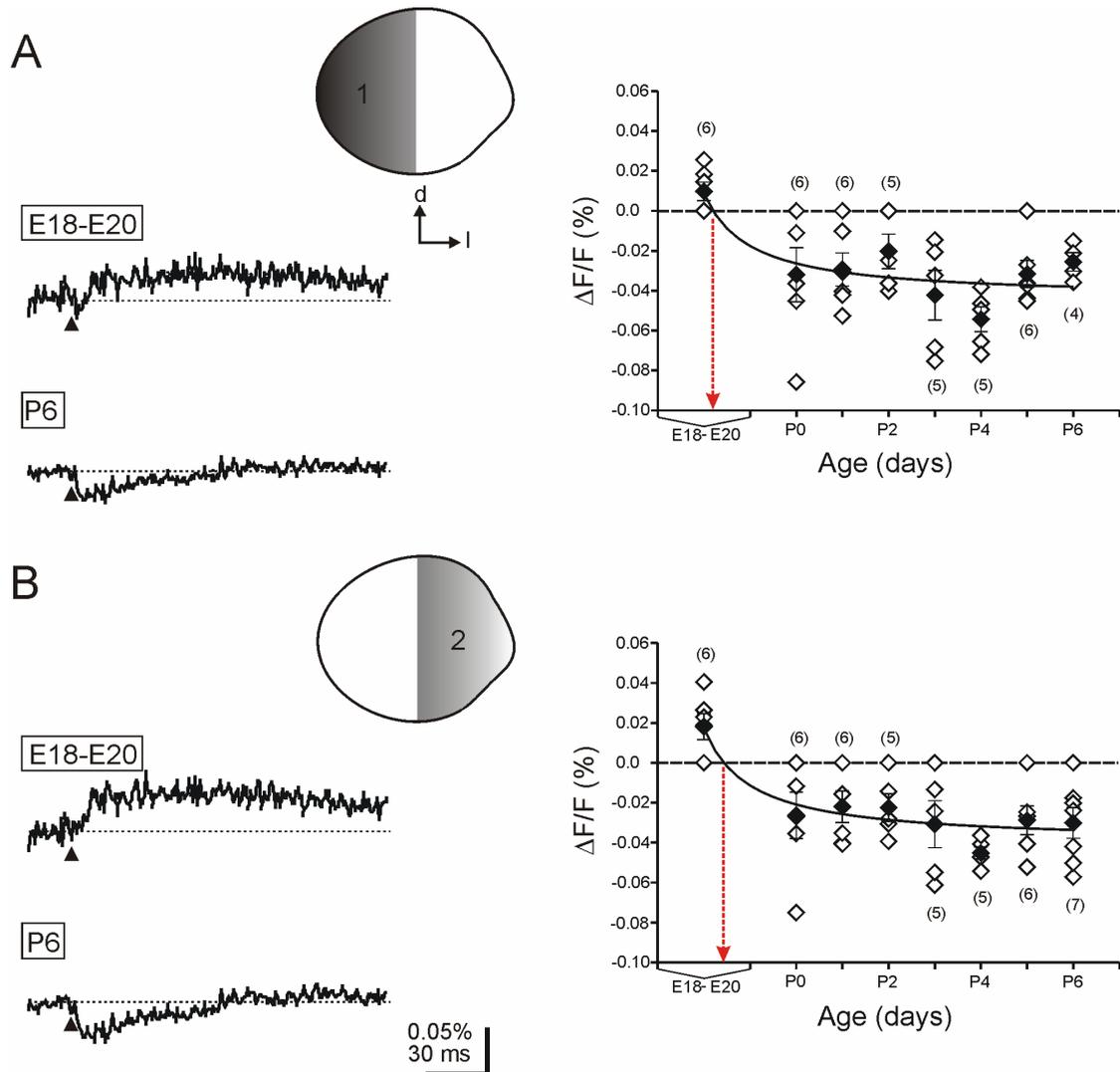
**Fig. 4.5: Developmental shift of glycinergic response in SPN**

The SPN is separated into two regions from medial to lateral along the hf and lf region, respectively. (A) The medial part of the SPN (region 1) displayed early depolarizations and late hyperpolarizations. (B) The lateral part of the SPN (region 2) also displayed early depolarizations and late hyperpolarizations. Left panels in A and B show typical examples of multiple diode recordings from E18-E20 and P6. Black arrow heads = stimulus. Right panels in A and B show peak amplitudes of glycine-evoked fluorescence changes from all SPN regions tested. Positive values, equal to depolarizations, and negative values, equal to hyperpolarizations, are plotted against age. The point of intersection of regression line in each graph represent the day of shift which was E18-E20 in both regions (red dotted arrow).

## Characterization of strychnine-sensitive responses in the MNTB

A total of 40 slices obtained from animals aged between P3 and P10 were used to
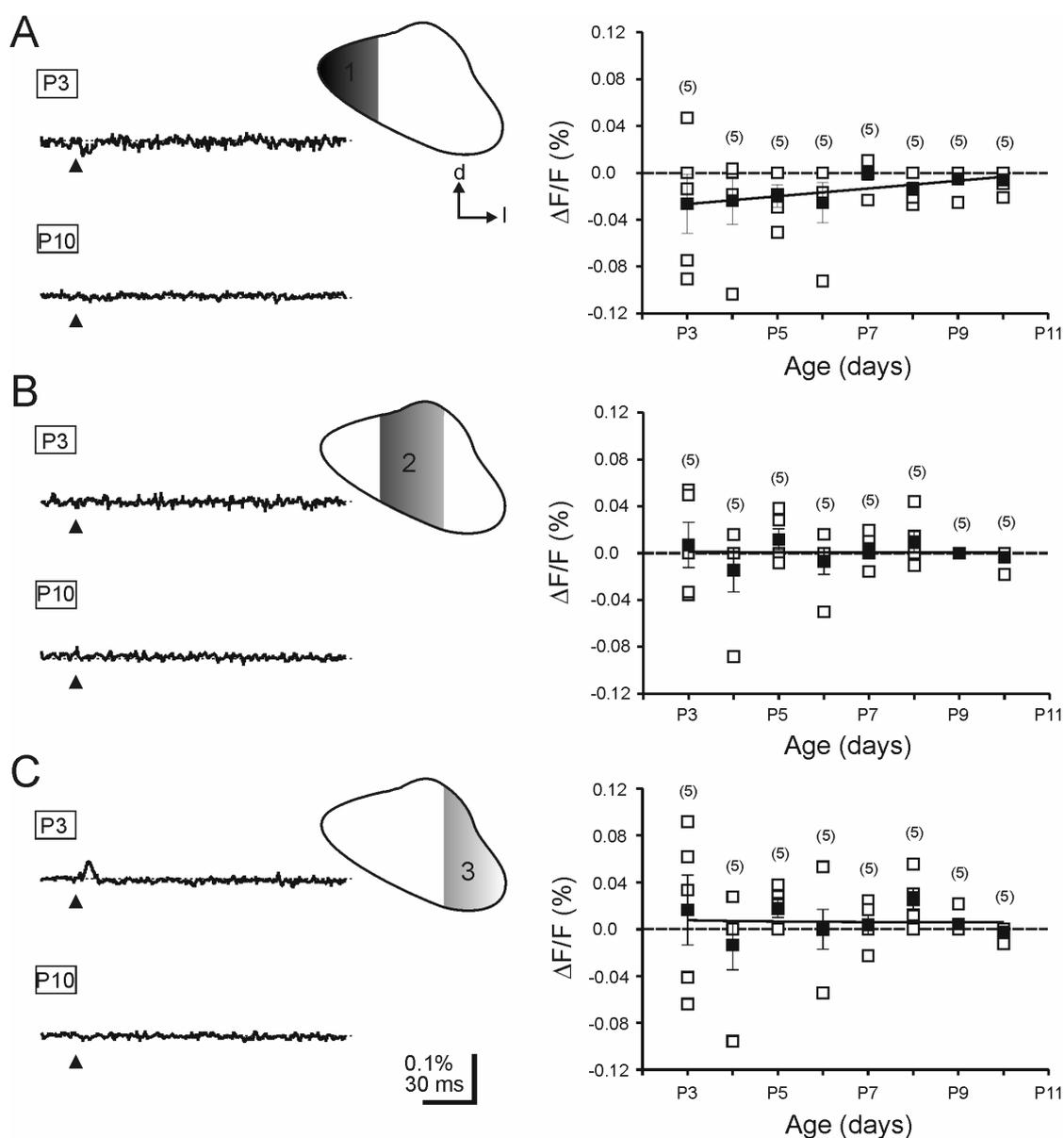


**Fig. 4.6: Development of strychnine-sensitive responses in the MNTB**

The MNTB is separated into three regions from medial to lateral along the hf to the lf region. (A) The medial part of the MNTB (region 1) displayed early hyperpolarizations which decline with age. (B) The central part of the MNTB (region 2) displayed both depolarizing and hyperpolarizing responses. (C) The lateral part of the MNTB (region 3) also displayed both depolarizations and hyperpolarizations. Left panels in A, B, and C show typical examples of multiple diode recordings from P3 and P10. Black arrow heads = stimulus. Right panels in A, B, and C show peak amplitudes of glycine-evoked fluorescence changes from all MNTB regions analyzed. Positive values, equal to depolarizations, and negative values, equal to hyperpolarizations, are plotted against age. The regression line shows no point of intersection, so the MNTB diplays no age-dependent shift in glycine activity between P3-P10.

study glycine developmental shift in the MNTB. Glycinergic input to the MNTB was provoked by stimulating nerve fibres innervating the MNTB, and was pharmacologically isolated with strychnine. The MNTB was divided into three regions ascending from the high frequency to the low frequency regions. In region 1, strychnine-sensitive responses were predominantly hyperpolarizations early from the first postnatal week and declined over age (Fig 4.6A). In region 2 and 3, mixed responses comprising depolarizations and hyperpolarizations were observed (Fig 4.6B and C).
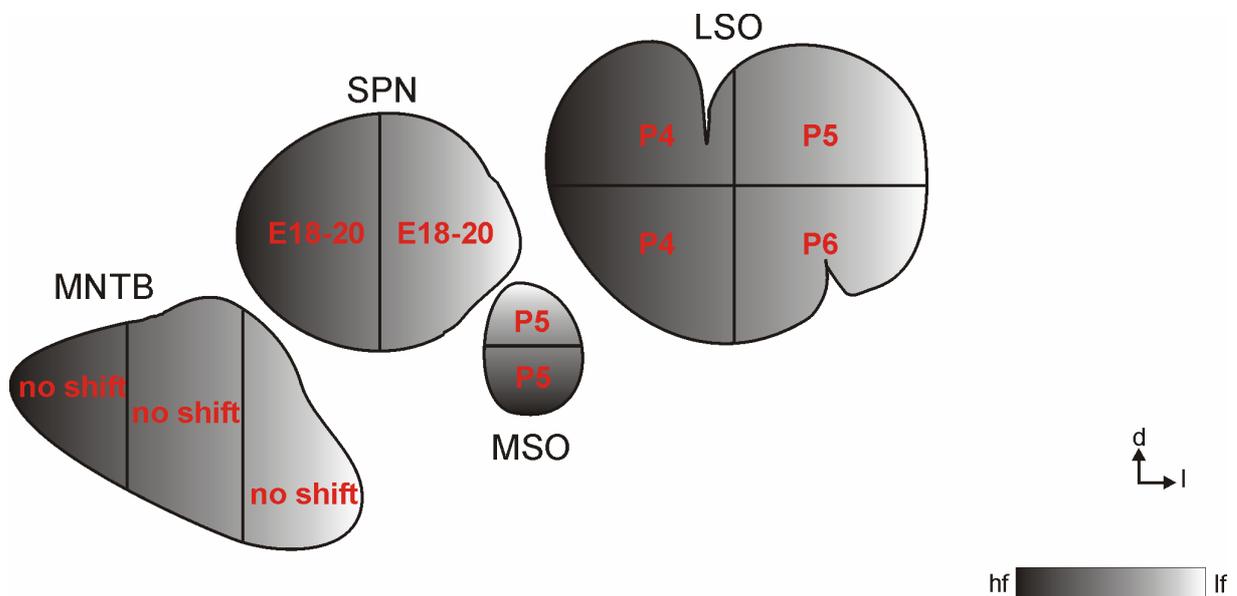


**Fig. 4.7: Differential timing in the development of inhibition within the SOC**

The nuclei of the SOC display a differential timing reagarding the shift of glycinergic responses from depolarization to hyperpolarization. Schematic diagram of the SOC nuclei and their region-specific day of shift. In the MNTB, a shift in glycine activity was not detected between P3-P10, the period investigated in the present study.

The results from the LSO, the MSO, the SPN, and the MNTB were summarized in Fig. 4.7. Differential timing in the development of inhibition in these nuclei was illustrated. Among the nuclei analyzed, the LSO and the MSO shifted postnatally, whereas SPN shifted already prenatally, only the MNTB lacked a developmental shift of glycine

responses from depolarization to hyperpolarization during the period analyzed. Among the nuclei analyzed only the LSO displayed region specific changes in the shift.

## 4.4 DISCUSSION

Four major results were obtained from Chapter 4 of this present study (Fig. 4.7).

(1) The LSO displays a tonotopic development of strychnine-sensitive responses i.e., the high frequency region matures at P4, whereas the low frequency region matures at P6. (2) The MSO developed shift in the polarity of strychnine sensitive responses at P5, without any regional differences. (3) Among the nuclei analyzed, the SPN displayed an earlier development of hyperpolarizing strychnine-sensitive responses, namely during E18-20 with no regional differences. (4) In contrast to the LSO, the MSO, and the SPN, the MNTB lacked a shift from depolarization to hyperpolarization between P3 to P10.

**Tonotopic maturation of inhibitory synapses in the LSO**

A developmental shift from depolarizing to hyperpolarizing glycine/GABA-evoked responses has been reported in several regions of the brain, e.g., in the cerebral cortex (Luhmann and Prince, 1991; Yuste and Katz, 1991; Lo Turco et al., 1995; Owens et al., 1996), the hippocampus (Mueller et al., 1984; Janigro and Schwartzkroin, 1988a,b; Ben-Ari et al., 1989; Cherubini et al., 1990; Zhang et al., 1990), the hypothalamus (Chen et al., 1996), the spinal cord (Wu et al.,1992; Reichling et al., 1994; Rohrbough and Spitzer, 1996), the retina (Huang and Redburn, 1996; Billups and Attwell, 2002), and the LSO ( Kandler and Friauf, 1995; Kotak et al., 1998; Nabekura et al., 2004). In the SOC, the MNTB projection conveys inhibitory input to the LSO from the contralateral ear, where it is integrated with the excitatory

information from the ipsilateral ear. Thus, inhibitory input to the LSO plays a significant role in shaping the neuronal responses. Studies focussing on the maturation of inhibitory synapses have revealed a shift from early GABAergic to late glycinergic neurotransmission in the gerbil and the rat LSO (Kotak et al., 1998; Nabekura et al., 2004). However, in the gerbil, there are differences between the lateral (low fequency region) and the medial (high frequency region) limb in this aspect (Kotak et al., 1998). The lateral limb lacks the shift from GABAergic to glycinergic neurotransmission, at the age between P3 to P16, at which it was analyzed, and it is glycinergic earlier. Moreover, in the lateral limb, inhibitory postsynaptic current reversal potentials are relatively negative compared to the medial limb. Thus, early maturation occurs in the low frequency lateral limb in this low frequency hearing animal. Furthermore, several regional differences within the gerbil LSO have been reported. In the medial limb, neurons have more narrow dendritic arbors (Sanes et al., 1990), there is a greater density of [$^3$H] strychnine binding (Sanes et al., 1987), and there is a distinct complement of glial markers (Hafidi et al., 1994, 1996). In a previous study, Ehrlich and coworkers (1999) reported no significant regional difference in the developmental glycine action in rat LSO neurons. It can be reasoned that the authors analyzed few cells, with which a conclusive evidence for a regional gradient was not drawn. Here, I show that in rats, a high frequency hearing animal, the LSO displayed maturation of inhibitory synapses from the high frequency region to the low frequency region during the first postnatal week.

**Differential maturation of inhibitory synapses in the SOC**

The SOC is composed of several nuclei, which plays a major role in sound localization using different cues. In high frequency animals, ILD is considered to be the main cue

processed by the LSO, whereas in low frequency hearing animals, ITD is considered to be the main cue, and processed by the MSO. The functional role of the SPN is not clearly defined. It is evident that the MNTB plays a major role in sound localization, being a relay center to convey the information to several ipsilateral nuclei from the contralateral ear. Thus, each nucleus in the SOC differs from each other in its function. The present study reveals the difference in the development of inhibiton in the SOC. To my knowledge, this is the first study that addresses the inhibitory synapse maturation in the MSO, the SPN, and the MNTB with respect to a shift in polarity of glycine responses. In the MNTB, a shift in the polarity of glycine responses was not observed, in contrast to the situation seen in other SOC nuclei. However, in the mature MNTB, gramicidin perforated patch-clamp recording reveals $E_{Gly} < V_m$ ($E_{Gly}$ of -75 to -80 mV; Awatramani et al., 2004). The authors did not provide the $V_m$ values, and the specific age of the animals. Limitations of the optical recording allowed me to record only until P10 in the MNTB, presumably due to the huge presynaptic calyx masking the postsynaptic structure or overgrowth of glial cells. Experiments after P10 are needed to track the developmental shift in the polarity of glycine responses in the MNTB. Among the nuclei analyzed in SOC, the SPN displays the earliest shift in the polarity of glycine-evoked responses i.e., before birth. The functional implication of early inhibitory synapse maturation in the SPN is not known. It can be speculated that the maturation of one nucleus may influence the other. A regional difference in the maturation of inhibitory synapse was not observed in the SOC nuclei, except for the LSO. Although this discussion does not explain why there is a regional difference in the maturation of inhibitory synapse in the LSO, it does suggest that the high frequency region may display a distinct pattern of differentiation, because their functional properties differ from low frequency region.

**Chloride homeostasis determines the development of inhibitory synapse**

Chloride ion plays a vital role in cell physiology. Intracellular chloride concentration ($[Cl^-]_i$) determines the polarity of response evoked by inhibitory neurotransmitter (GABA/glycine) in neurons (Owens et al., 1996; Rohrbough and Spitzer, 1996; Ehrlich et al., 1999). The depolarization is due by $Cl^-$ efflux, because of relatively high $[Cl^-]_i$ above equilibrium, thereby generating an outward-directed electrochemical gradient for $Cl^-$. In this study, all the analyzed SOC nuclei display glycine-evoked depolarizations. Glycine-evoked depolarizations might increase intracellular calcium concentration through voltage dependent calcium channels and NMDA channels in all the other SOC nuclei similar to its effect in the LSO (Kullmann et al., 2002; Ene et al., 2003). Thus, inhibitory synapse mature through the activation of calcium induced secondary messenger cascades. In mature neurons, the $[Cl^-]_i$ is reduced below equilibrium, thus rendering glycine activity hyperpolarizing. The maintenance of chloride gradient was achieved by different chloride transporting mechanisms (review: Delpire, 2000). For example, in the LSO, $[Cl^-]_i$ was maintained below the equilibrium by the $K^+$- dependent chloride co-transporter (KCC2; Balakrishnan et al., 2003), with its consequent hyperpolarizing IPSP as well as shunting inhibition (Funabiki et al., 1998). This is very important for LSO neurons in auditory information processing. The development of glycinergic or GABAergic inhibition is well correlated with the functional expression of KCC2 (Rivera et al., 1999; Hübner et al., 2001; Balakrishnan et al., 2003). The reason for the differential timing in the maturation of inhibitory synapse in the SOC nuclei could be due to differential expression pattern of functional KCC2. From the present study, a differential functional expression pattern of KCC2 is expected within each SOC nuclei and also within the LSO.

**Functional implications of inhibitory synapse maturation**

For normal brain functioning, appropriate inhibitory and excitatory synaptic transmission is necessary. Malfunctioning of inhibitory synaptic transmission is associated with several disorders like epilepsy (Köhling et al., 2000; Cohen et al., 2002), anxiety disorders, schizophrenia (review: Wong et al., 2003). Likewise, auditory functioning relies on precise inhibition for proper hearing. The role of inhibition in processing ILD and ITD has been demonstrated (Tollin and Yin, 2002; Brand et al., 2002). The LSO integrates auditory information from both ears. The probability of action potentials in the LSO is determined by the differences of arrival from the ipsilateral (glutamatergic) and contralateral (glycinergic) inputs. This process, which encodes ILD, supplies the cues to localize sound in azimuthal space (Koyano and Ohmori, 1996; Sanes and Rubel, 1988).

In low frequency hearing mammals, the MSO is focussed to process ITD. Spherical bushy cells from each cochlear nucleus provide binaural excitatory input to MSO neurons (Smith et al., 1993; Grothe, 2000), and *in vivo* recordings in the MSO have demonstrated the sensitivity to ITDs (Yin and Chan, 1990; Spitzer and Semple, 1995). However, MSO neurons also receive glycine inputs, arising mainly from the MNTB, and partly from the LNTB (Cant and Hyson, 1992; Kuwabara and Zook, 1992; Grothe and Sanes, 1993; Smith et al., 2000). Brand and coworkers (2002) addressed the contribution of these glycinergic inhibitory inputs to ITD processing and found precise inhibition to be essential for microsecond ITD coding. Furthermore, inhibition has been reported to play a significant role in auditory processing in other structures like the inferior colliculis (Jen, 2003) and the cochlear nucleus (Rhode and Greenberg, 1994; Babalian et al., 2002). Thus, the maturation of inhibition through excitation plays a

major role in proper functioning of these nuclei in auditory pathways to enable sound localization.

In conclusion, this study by optical imaging sheds some light on the differential development of glycinergic inhibition within the SOC nuclei.

# 5 Characterization of rat MSO by optical imaging: A possible role in sound localization

## 5.1 INTRODUCTION

One of the primary tasks of the auditory system is to localize sounds in space. There are two primary cues for sound localization, 1) interaural time differences (ITD), and 2) interaural level differences (ILD). Sounds arriving at the two ears from different locations (except of midline) in the azimuthal plane differ in both arrival time and sound level. Psychoacoustical studies have determined that low and high frequency sounds are localized based primarily on ITD and ILD, respectively (review: Erulkar, 1972). ILD caused by the head, which acts as an obstacle for reflecting and shadowing sound waves, enable vertabrates with small heads, to localize high frequency sounds with high precision (reviews: Erulkar, 1972; Simmons, 1987; Heffner and Heffner, 1990). In contrast, at low frequencies, e.g., in cats, gerbils, when the wavelength is equal or longer than the inter ear distance, the head does not efficiently reflect sound waves. Thus, the ILDs are not available for localizing low frequency sounds. ITDs are the cue available to localize sounds of low frequencies, which are in the range of microseconds (Erulkar, 1972; Goldberg and Brown, 1969; Yin and Chan, 1990). The basic structures that enable mammals to encode ILD is the lateral superior olive (LSO) and to encode ITD is the medial superior olive (MSO).

## 5.1.1 The principles of ITD coding

The MSO contains neurons which are arranged like a pile of coins with bipolar dendrites that extend medially and laterally (Cajal, 1907). In 1948, Lloyd Jeffress proposed an elegant model that suggests how the auditory neurons process ITD, and

how it represents the particular ITD that is received at the ears (Fig. 5.1). The important feature of the Jeffress model is coincidence detection by neurons when binaural excitatory inputs arrive simultaneously. It was suggested that the MSO neurons can work as coincidence detectors, only responding with action potentials when both excitatory signals arrive at the same time. This is based on several lines of evidence derived mainly from studies of cat and dog MSO (Cajal, 1907; Goldberg and Brown, 1969; Caird and Klinke, 1983; Joris et al., 1998). For a coincidence mechanism to be useful in localizing sound, different neurons must be maximally sensitive to different ITDs. The axons that project from the anteroventral cochlear nuclei (AVCN) to the MSO vary systematically in length to create delay lines (Fig. 5.1; review: Grothe, 2000). Consequently, for different azimuthal positions of a sound source, coincidence of inputs will occur at different neurons. Thereby, an ITD map that encodes the position of the sound in the azimuthal plane can be created. Processing ITDs by the nucleus laminaris in birds (equivalent to the MSO in mammals) has been confirmed (Overholt et al., 1992; Carr and Konishi, 1988). However, for mammals the direct confirmation of such an arrangement to process ITD is still lacking.

Apart from the binaural excitatory glutamatergic inputs from AVCN, MSO neurons also receive glycinergic inputs via the medial and the lateral nucleus of the trapezoid body (MNTB and LNTB; Grothe, 2000; Cant and Hyson, 1992; Grothe and Sanes, 1994). Brand and coworkers (2002) found that ITD tuning in the gerbil MSO is the product of interactions of precisely timed excitatory and inhibitory inputs.

Even though the rat is a high frequency hearing animal, it has a prominent MSO with its anatomical structures (column like arrangement of bipolar cells) and physiological inputs (receives both excitatory and inhibitory inputs from ipsilateral and contralateral

sides) related to low frequency hearing animals like cats, dogs, and gerbils (Goldberg and Brown, 1969; Yin and Chan, 1990; Spitzer and Semple, 1995; Rogowski and Feng, 1981). The role of the rat MSO is not known. This chapter of the present study is focussed on the possible role of ITD coding in the rat. The detection of fast time-dependent processes, such as the integration of ipsi- and contralateral inputs during bilateral information processing, will be an interesting endeavor. To do so,
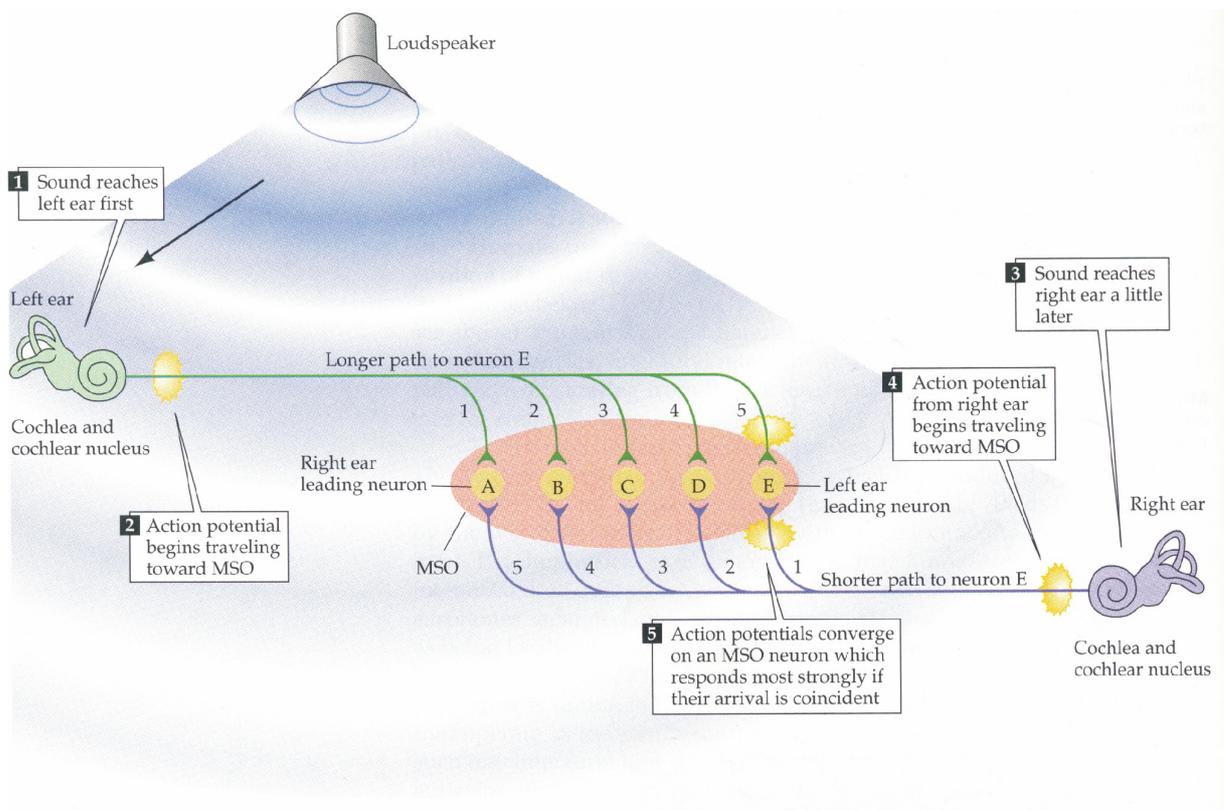


**Fig. 5.1: Jeffress model of sound location**

Diagram illustrating how the MSO computes the location of sound by ITD. A given MSO neuron responds most strongly when the inputs from the two ears arrive simultaneously. The systematic variation of axonal length of the input causes different travelling times of the neural activity to the coincidence detector neurons (so-called delay lines). Consequently, for different azimuthal positions of a sound source (= different ITDs) coincidence of inputs will occur at different neurons. Thereby, a systematic place code of azimuthal position could be created. In this model, neuron E (left ear leading neuron) would be most sensitive to sounds arriving earlier to the left ear, and neuron A (right ear leading neuron) would be most sensitive to sounds arriving earlier to the right ear (from Cant, 1997).

simultaneous recording of neuronal activity in the MSO with high temporal resolution is needed. This can be achieved by optical recordings with fast voltage-sensitive dyes. Optical imaging might visualize orientation of coincidence in the MSO.

## 5.2 MATERIALS AND METHODS

### Acute brainstem slice preparation

Acute brainstem slices were prepared from Sprague-Dawley rat pups of both gender between P8 and P10. Slices were prepared as described in Chapter 2. The composition of solutions used for preparation, storage of slices, and recording as well as the dye loading procedures with RH795 were identical to those described in Chapters 2 and 3.

### Drug application

In some experiments to pharmacologically block glycinergic inhibitory inputs to the MSO, strychnine (0.5 µM) was added to the recording solution. This was bath applied continuously throughout the recording time. The usage of strychnine is mentioned in the appropriate sections.

### Optical recording

Recording conditions and experimental setup were identical to those described in Chapter 2.

### Data acquisition and analysis

The data acquisition and analysis were identical to those described in Chapters 2 and 3. To study regional differences within the MSO, it was divided into 3 different

regions along the dorso-ventral axis, as region 1, 2, and 3. Scaling of pseudocolor imaging was done by setting the maximum and minimum values obtained during 0 $\Delta$t condition.

**Electrical stimulation of SOC input fibres**

Stimulus positions and durations were identical to those described in Chapter 2. Stimulus amplitude ranged between 20 µA and 2 mA. The time difference of ipsi- and contralateral stimulation is referred to as $\Delta$t, rather than ITD, because the stimulation time difference doesn't reflect the real time conditions for ITD. For example, the results could be influenced by electrode positioning (Fig. 5.5). Moreover, in these *in vitro* experiments there is no involvement of the ears. $\Delta$t of -50 µs, 0 µs, and +50 µs denote contralateral stimulation 50 µs before ipsilateral stimulation, contralateral and ipsilateral stimulations at the same time, and ipsilateral stimulation 50 µs before contralateral stimulation, respectively.

**5.3 RESULTS**

**Summation of postsynaptic-responses in the MSO**

As described in Chapter 3, MSO neurons receive glutamatergic inputs from the AVCN of both sides and glycinergic inputs from the contralateral side MNTB and the ipsilateral side LNTB. To study the summation of these postsynaptic responses in the MSO, the ipsilateral and contralateral inputs were stimulated as illustrated in Fig. 5.2A. A total of 10 brainstem slices were used for this study and a typical example is shown in Fig. 5.2.

Upon contralateral and ipsilateral stimulation, the MSO displayed optical responses which are shown in pseudocolor (Fig. 5.2B, C top). Multidiode recordings from the
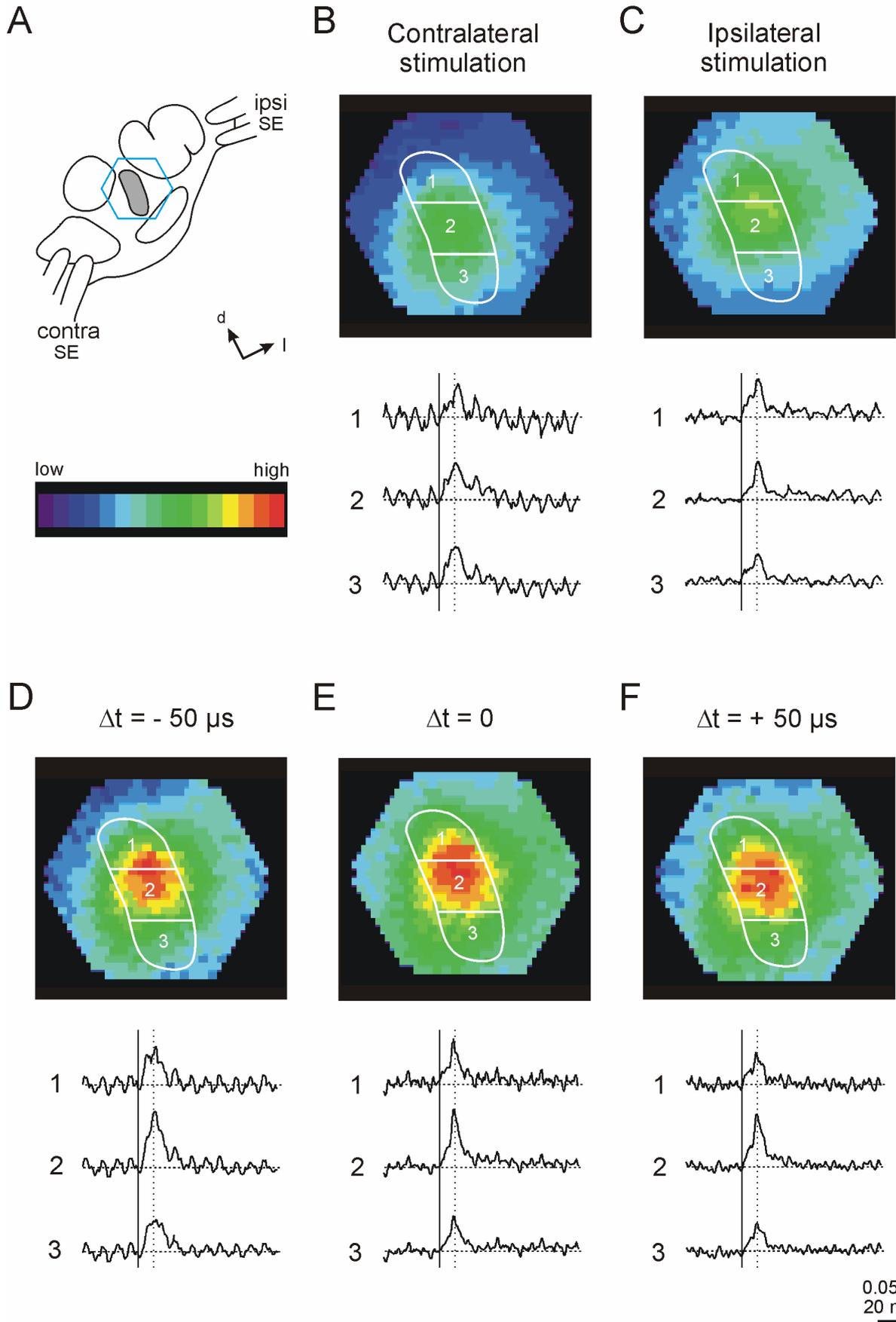
**Fig. 5.2: Summation of postsynaptic responses in bilaterally stimulated MSO**

(A) Schematic diagram of a P8 SOC with its major nuclei outlined, and positioning of the contralateral (contra) and the ipsilateral (ipsi) stimulus electrode (SE). The PDA (blue hexagon) covers the entire MSO (shaded region) at 40x. The 16 colors from purple to red represent the scale that was used for the pseudocolor presentation of fluorescence signals (top panel in B-F). Purple represents the minimum fluorescence change (low) and red represents the maximum fluorescence change (high). Scaling of the colors holds for all pseudocolor images in a set of experiments which were compared. (B) Pseudocolor image showing the distribution of responses within the entire MSO upon contralateral stimulation (top). The corresponding multidiode recordings obtained from the 3 regions (labeled 1-3) are shown below. 40, 43, and 37 diodes were averaged for regions 1, 2, and 3, respectively. Solid vertical lines = stimulus. Dotted vertical lines = time of the pseudocolor image shown above. The corresponding latency from stimulus onset to the peak response (indicated by the dotted vertical lines) is 7 ms (B-F). Scale bar holds for B-F. (C) Optical signals evoked upon ipsilateral stimulation. (D) Optical signals evoked upon bilateral stimulation with contralateral stimulation 50 µs before ipsilateral stimulation ($\Delta$t = -50 µs). (E) Optical signals evoked upon ipsi- and contralateral stimulation at the same time ($\Delta$t = 0). (F) Optical signals evoked upon bilateral stimulation with ipsilateral stimulation 50 µs before contralateral stimulation ($\Delta$t = +50 µs).

three regions show the amplitude of the postsynaptic responses (Fig. 5.2B, C bottom). The effect of ipsi- and contralateral stimulation at different time $\Delta$t values (50 µs, 0 µs and +50 µs) was investigated.

In all the cases ($\Delta$t of -50 µs, 0 µs, and +50 µs) the summation (indicated in red color) of postsynaptic responses were observed preferentially in region 2 and to some extent in region 1. But, the summation was not observed in region 3 (Fig. 5.2D, E, F top). The stimulus strength which I used for these experiments was 2 mA. This high stimulus strength could result in a postsynaptic action potential (AP). Even at single side stimulation e.g. ipsilateral stimulation alone, AP was induced in every region (Fig. 5.2C). But coincidence referred in the Jeffress model means, the summation of two excitatory postsynaptic potential (EPSP) at a same time, resulting in an AP. Therefore, for provoking EPSP, subthreshold stimulus conditions are needed.

## Coincidence of postsynaptic responses evoked by subthreshold stimulus strength in the presence of strychnine

In line with the above conclusion, a reduced stimulus strength was used in further experiments. To achieve subthreshold postsynaptic responses with ipsi- and contralateral stimulations, responses upon different stimulus amplitudes were induced (Fig. 5.3). Subthreshold stimulus conditions were optimized by reducing the stimulus strength of ipsi- and contralateral stimulation until postsynaptic responses of smaller amplitude were evoked (presumably an EPSP). As illustrated in Fig. 5.3, a similar amplitude of postsynaptic responses was achieved by optimizing both ipsilateral (in this example, 20 µA) and contralateral (in this example, 200 µA) stimulation. Brand and coworkers (2002) demonstrated the ITD function in the physiologically relavant range in the absence of inhibition. So, 0.5 µM strychnine was used in further experiments.
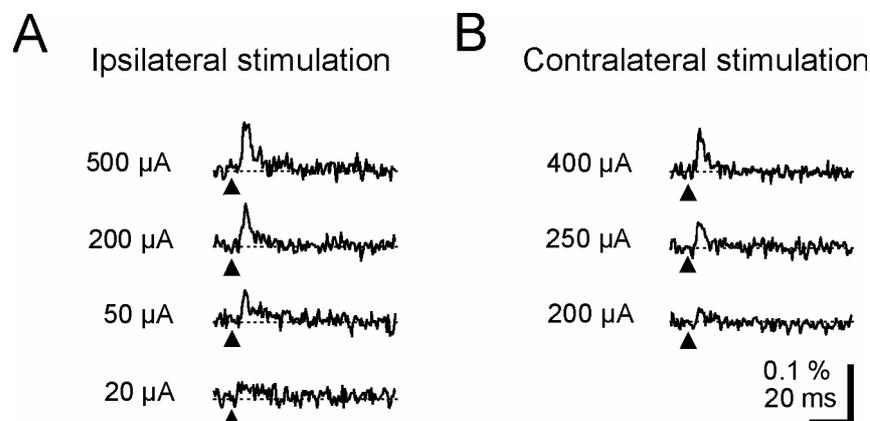


**Fig. 5.3: Determination of subthreshold stimulus strength in MSO**

Single diode recordings from a P10 MSO upon ipsilateral (A) and contralateral (B) stimulation with single rectangular pulses (0.2 ms, onset indicated by arrow heads) of variable strength (current values adjacent to the traces). Here, 20 µA and 200 µA were necessary to evoke subthreshold responses from ipsilateral and contralateral, respectively.

A

contra
SE

ipsi
SE

d

l

low                    high

B    Contralateral
     stimulation

1

2

3

1

2

3

C    Ipsilateral
     stimulation

1

2

3

1

2

3

D    $\Delta t = -50\ \mu s$

1

2

3

1

2

3

E    $\Delta t = 0$

1

2

3

1

2

3

F    $\Delta t = +50\ \mu s$

1

2

3

1

2

3

0.05 %

20 ms
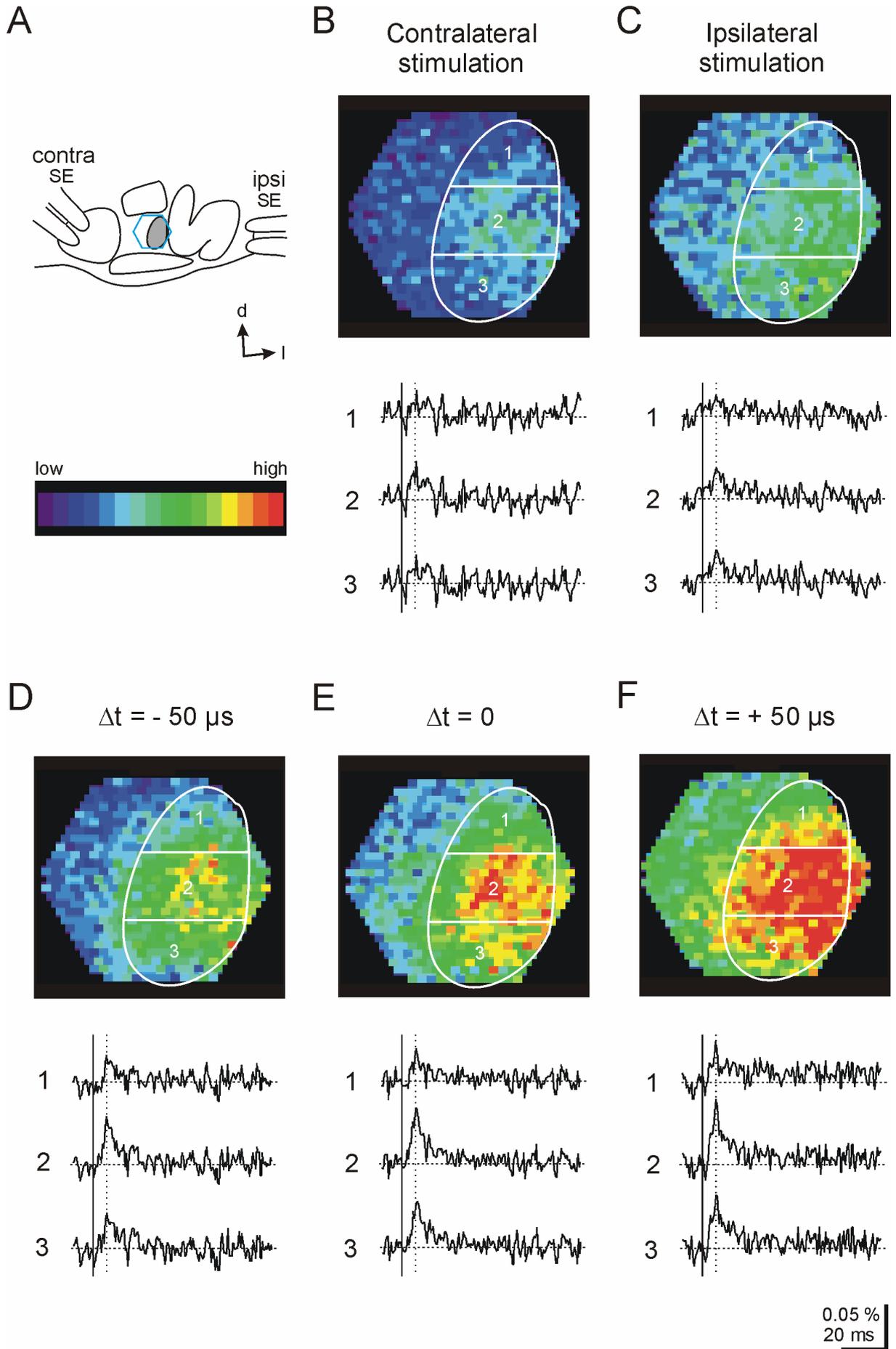
**Fig. 5.4: Coincidence of postsynaptic responses evoked by subthreshold stimulus strength in the presence of strychnine**

(A) Schematic diagram of a P10 SOC with its major nuclei outlined and positioning of the contralateral (contra) and the ipsilateral (ipsi) stimulus electrode (SE). The PDA (blue hexagon) covers the entire MSO (shaded region) at 60x. The 16 colors from purple to red represent the scale that was used for the pseudocolor presentation of fluorescence signals (top panel in B-F). Purple represents the minimum fluorescence change (low) and red represents the maximum fluorescence change (high). Scaling of the colors holds for all pseudocolor images in a set of experiments which were compared. (B) Pseudocolor image showing the distribution of responses within the entire MSO upon contralateral stimulation (top). The corresponding multidiode recordings obtained from the 3 regions (labeled 1-3) are shown below. 83, 97, and 67 diodes were averaged for regions 1, 2, and 3, respectively. Solid vertical lines = stimulus. Dotted vertical lines = time of the pseudocolor image shown above. The corresponding latency from stimulus onset to the peak response (indicated by the dotted vertical line) is 6 ms (B-F). Scale bar holds for B-F. (C) Optical signals evoked upon ipsilateral stimulation. (D) Optical signals evoked upon bilateral stimulation with contralateral stimulation 50 μs before ipsilateral stimulation ($\Delta t$ = -50 μs). (E) Optical signals evoked upon ipsi- and contralateral stimulation at the same time ($\Delta t$ = 0). (F) Optical signals evoked upon bilateral stimulation with ipsilateral stimulation 50 μs before contralateral stimulation ($\Delta t$ = +50 μs).

In order to see the coincidence of the postsynaptic responses in the MSO, ipsilateral and contralateral inputs were stimulated as illustrated in Fig. 5.4A. A total of 6 brainstem slices were used for this study. Upon contralateral and ipsilateral stimulation, the MSO displayed optical responses, which are shown in pseudocolor (Fig. 5.4B, C top). Multidiode recordings from the three regions show the amplitude of the postsynaptic responses (Fig. 5.4B, C bottom). The coincidence of ipsi- and contralateral stimulation at different time in stimulus onset ($\Delta t$; -50 μs, 0 μs and +50 μs) was investigated. In this example, with $\Delta t$ = -50 μs, i.e., contralateral stimulation 50 μs before ipsilateral stimulation, coincidence (indicated by red color) of postsynaptic responses was observed only in few diodes (Fig. 5.4D top). When contralateral and ipsilateral stimulations were given at the same time ($\Delta t$ = 0 μs), the coincidence was prominent in region 2 of the MSO area. But region 1 and 3 displayed no prominent coincidence response (Fig. 5.4E top). With $\Delta t$ = +50 μs, i.e.,

ipsilateral stimulation 50 µs before contralateral stimulation, a high degree of coincidence was observed (Fig. 5.4F top). Out of six slices, two displayed a high degree of coincidence with Δt of +50 µs (as shown above) and another two slices displayed a high degree of coincidence with Δt of -50 µs (Fig. 5.5). And in the remaining two slices, no coincidence was observed with different Δt values used above.
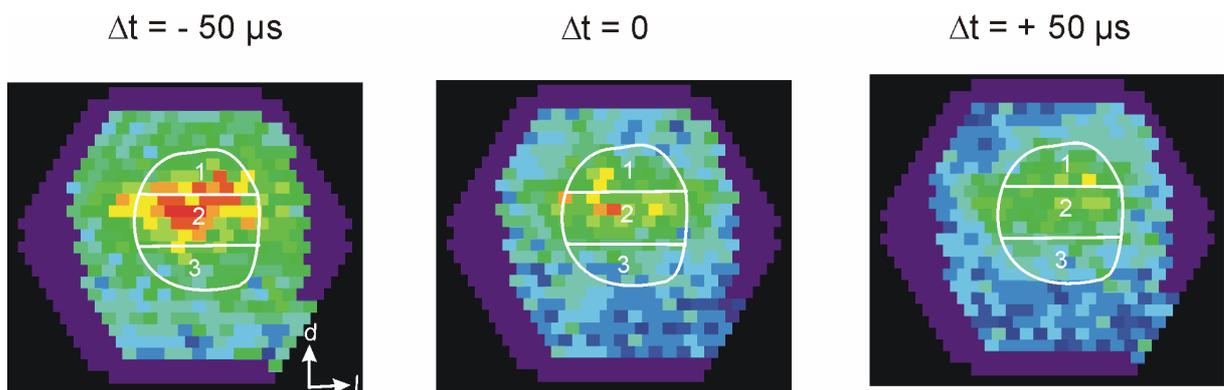


**Fig. 5.5: Coincidence of postsynaptic responses with Δt = -50 µs**
Pseudocolor images showing the distribution of responses within the entire MSO upon bilateral stimulation with contralateral stimulation 50 µs before ipsilateral stimulation (Δt = -50 µs), optical signals evoked upon ipsi- and contralateral stimulation at the same time (Δt = 0), and optical signals evoked upon bilateral stimulation with ipsilateral stimulation 50 µs before contralateral stimulation (Δt = +50 µs).

The results demonstrate the coincidence of postsynaptic responses in the MSO upon subthreshold stimulus strength. With respect to the Jeffress model, one would expect a *shift* in the area of coincidence upon different Δt values. But the results demonstrate an *increase or decrease* in the area of coincidence (differential pattern in the spread of activity) upon different time in ipsi- and contralateral stimulus onset. The possible reason for this result is shown in Fig. 5.6, where a scenario for coincidence responses in MSO with respect to the electrode positioning is shown.
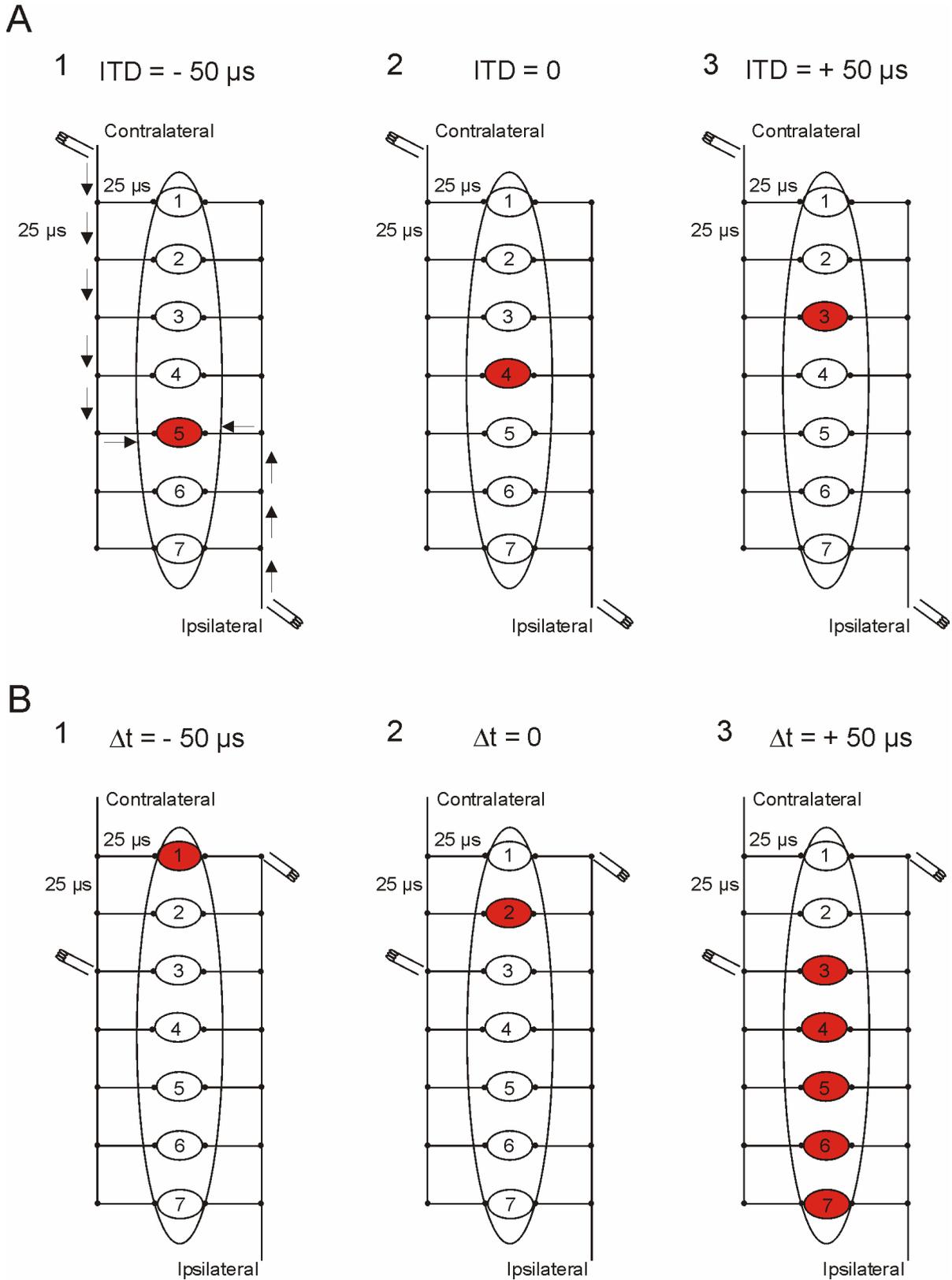
**Fig. 5.6: Scenario for coincidence responses in MSO with respect to electrode positioning**

(A) Optimal stimulus electrode position where the Jeffress model works with different ITD. The red spot represents the possible neuron where coincident detection occurs. For example in Fig. 5.6A1, with ITD of -50 µs, i.e., when contra leads ipsi by 50 µs, both the inputs will coincide in the neuron 5.

The time taken to reach neuron 5 by contralateral stimulation is $6 \times 25$ µs, for ipsilateral stimulation is $4 \times 25$ µs. (B) Interpretation of response pattern observed in the experiment shown in figure 5.4. It illustrates a possible stimulus configuration (position of electrodes ↘), responsible for the findings. Axon travelling time from one point (●) to next point is considered as 25 µs.

## 5.4 DISCUSSION

In this study, subthreshold stimulus strength elicited postsynaptic responses (presumably EPSPs) and they coincide upon different $\Delta t$ values. In addition, a differential pattern in the spread of activity was observed with different $\Delta t$ values.

To a certain extent, some MSO neurons act as coincidence detectors, matching the Jeffress model (1948) of ITD coding in low frequency mammals (Cat: Galambos et al., 1959; Caird and Klinke, 1983; Yin and Chan, 1990; Beckius et al., 1999; dog: Goldberg and Brown, 1969; bat: Grothe and Park, 1998; and gerbil: Brand et al., 2002). In all the above cases a certain percentage of monaural neurons are also present. These neurons cannot work as coincidence dectectors as proposed by Jeffress. Moreover, Jeffress model does not include binaural inhibitory inputs. But the crucial role of inhibitory inputs to the gerbil MSO is demonstrated by Brand and coworkers (2002). Although, the MSO in rat is related to that in cat, dog, and gerbil with respect to anatomical structures and physiological inputs (Goldberg and Brown, 1969; Yin and Chan, 1990; Spitzer and Semple, 1995), the size of the rat MSO is small (Rogowski and Feng, 1981). It possesses bipolar neurons similar to cat, dog, and gerbil (Feng and Rogowski, 1980). *In vivo* experiments in rat demonstrate that half of the neurons in MSO exhibited binaural excitatory inputs. Thus the other half performs a function other than ITD coding (Inbody and Feng, 1981).

For an inter ear distance of 2 cm, the calculated maximum ITD is $\pm 50$ µs. Thus for an adult rat, maximum ITD is in the range of $\pm 150$ µs (Grothe, 2000). So, in my study I

used $\Delta$t of $\pm$50 µs. Coincidence of postsynaptic responses varied upon different $\Delta$t values (Fig. 5.4 and 5.5). The possible reason for the results obtained with different $\Delta$t experiments is presumably due to electrode positioning. Illustrations representing the model of coincidence detection under Jeffress assumption (Fig. 5.6A), and the model representing the possible stimulus configuration (position of the electrodes) responsible for the findings (Fig. 5.6B) are shown. A model MSO, comprising seven neurons, and its binaural inputs along with stimulation conditions was shown. In this model, time taken from one point to the next point is considered as 25 µs. With respect to the Jeffress model, at ITD of -50 µs, 0 µs and +50 µs, the coincidence will occur at neuron 5, 4 and 3, respectively (Fig 5.6A). Results obtained in the experimental part of this study, were explained in Fig. 5.6B. Under the stimulus condition shown in the illustration, $\Delta$t of -50 µs and 0 µs provokes coincidence in neuron 1 and 2 respectively. But with $\Delta$t of +50 µs, coincidence will occur in all neurons from 3 to 7. Due to electrical stimulation, antidromic conductions are possible which could reason the coincidence shown in $\Delta$t of 0 and +50 µs in the model decribed in Fig. 5.6B. Thus, the stimulus electrode position may interfere with the coincidence detection in MSO in *in vitro* brain slice studies. This is just a model with seven neurons, and in reality, one should consider the neurons which are in the deeper layers. In experimental conditions, the response from the deeper layer will also be detected by the photodiodes.

In conclusion, these experiments demonstrate a difference in the spread of activity upon different $\Delta$t values which indicates a possible delay lines as proposed by Jeffress (1948) in the ITD model of sound localization.

# 6 General summary

In this doctoral thesis, several aspects of neuronal activity in the rat superior olivary complex (SOC), an auditory brainstem structure, were analyzed using optical imaging with voltage-sensitive dyes (VSD). The thesis is divided into 5 Chapters.

Chapter 1 is a general introduction, which gives an overview of the auditory brainstem and VSD imaging.

In Chapter 2, an optical imaging method for the SOC was standardized, using the VSD RH795. To do so, the following factors were taken into consideration and optimized: (1) An extracellular potassium concentration of 5 mM turned out to be necessary during the incubation and recording to observe synaptically evoked responses in the SOC. (2) Employing different power supplies reduced the amplitude of the noise. (3) Averaging of 10 subsequent trials yielded a better signal-to-noise ratio. (4) RH795 of 100 µM with 50 min prewash was optimal to image SOC slices for recording times of more than one hour. (5) The optical signals from VSD imaging were characterized in order to interpret them in terms of neuronal activity. Stimulus-evoked optical signals were TTX sensitive, revealing action potential-driven input.
(6) Synaptically evoked optical signals were characterized to be composed of pre- and postsynaptic components. (7) Optical signals were well correlated with anatomical structures. Overall, this method allows the comparative measurement of electrical activity of cell ensembles with high spatio-temporal resolution.

In Chapter 3, the nature of functional inputs to the main SOC nuclei, namely the lateral superior olive (LSO), the medial superior olive (MSO), and the superior

_____

paraolivary nucleus (SPN) were analyzed using the glycine receptor blocker strychnine and the AMPA/kainate receptor blocker CNQX. In the LSO, the known glutamatergic inputs from the ipsilateral side, and the glycinergic inputs from the ipsilateral and contralateral sides, were confirmed. Furthermore, a CNQX-sensitive input from the contralateral side was identified. In the MSO, the glutamatergic and glycinergic inputs from the ipsilateral and contralateral sides were corroborated. In the SPN, besides the known glycinergic input from the contralateral side, I found a glycinergic input from the ipsilateral side and I also identified CNQX-sensitive inputs from the contralateral and ipsilateral sides. However, the latter was very weak and appeared only in 30% of the experiments. Together, my results thus corroborate findings obtained with different preparations and methods, and provide additional and novel information on the pharmacological nature of the inputs.

In Chapter 4, the development of glycinergic inhibition for the LSO, the MSO, the SPN, and the medial nucleus of the trapezoid body (MNTB) was studied by characterizing the polarity of strychnine-sensitive responses. In the LSO, I observed a regional difference in the developmental shift of glycine-evoked responses i.e., a shift from depolarization to hyperpolarization. The high frequency region displayed a shift in the polarity at P4, whereas the low frequency region displayed the shift at P6. In the MSO, both the high frequency and the low frequency regions displayed the shift in the polarity of glycine-evoked responses at P5. The SPN displayed a shift in the polarity before birth i.e., at E18-20 without any regional differences. In contrast to the LSO, the MSO, and the SPN, the MNTB lacked a shift from depolarization to hyperpolarization between P3 and P10. Together, these results demonstrate a differential timing in the development of glycinergic inhibition in these nuclei.

_____

Finally, in Chapter 5, the role of the MSO in processing bilateral time differences ($\Delta$t) was investigated. This was done by stimulating ipsilateral and contralateral inputs to the MSO with different $\Delta$t values i.e., contralateral stimulation 50 µs before ipsilateral stimulation ($\Delta$t = -50 µs), contralateral stimulation and ipsilateral stimulation given at the same time ($\Delta$t = 0 µs), and ipsilateral stimulation 50 µs before contralateral stimulation ($\Delta$t = +50 µs). In preliminary experiments, under subthreshold stimulus conditions, the postsynaptic responses showed a differential pattern in the spread of activity upon different $\Delta$t values. This data demonstrates a possible presence of delay lines (variation in the axonal length) as proposed by Jeffress in the interaural time difference model of sound localization.

In conclusion, this study demonstrates the usage of VSD imaging to analyze the neuronal activity in auditory brainstem slices. Moreover, this study expands the knowledge of the inputs to the SOC, and has identified one glycinergic and three AMPA/kainate glutamatergic novel inputs to the SOC nuclei.

# 7 Bibliography

Albowitz B, Kuhnt U (1993) The contribution of intracortical connections to horizontal spread of activity in the neocortex as revealed by voltage sensitive dyes and a fast optical recording method. Eur J Neurosci 5: 1349-1359.

Antic S, Major G, Zecevic D (1999) Fast optical recordings of membrane potential changes from dendrites of pyramidal neurons. J Neurophysiol 82: 1615-1621.

Arai Y, Momose-Sato Y, Sato K, Kamino K (1999) Optical mapping of neural network activity in chick spinal cord at an intermediate stage of embryonic development. J Neurophysiol 81: 1889-1902.

Arieli A, Shoham D, Hildesheim R, Grinvald A (1995) Coherent spatiotemporal patterns of ongoing activity revealed by real-time optical imaging coupled with single-unit recording in the cat visual cortex. J Neurophysiol 73: 2072-2093.

Awatramani GB, Turecek R, Trussell LO (2004) Inhibitory control at a synaptic relay. J Neurosci 24: 2643-2647.

Babalian AL, Jacomme AV, Doucet JR, Ryugo DK, Rouiller EM (2002) Commissural glycinergic inhibition of bushy and stellate cells in the anteroventral cochlear nucleus. Neuroreport 13: 555-558.

Balakrishnan V, Becker M, Lohrke S, Nothwang HG, Guresir E, Friauf E (2003) Expression and function of chloride transporters during development of inhibitory neurotransmission in the auditory brainstem. J Neurosci 23: 4134-4145.

Banks MI, Smith PH (1992) Intracellular recordings from neurobiotin-labeled cells in brain slices of the rat medial nucleus of the trapezoid body. J Neurosci 12: 2819-2837.

Barish ME, Ichikawa W, Tominaga T, Matsumoto G, Iijima T (1996) Enhanced fast synaptic transmission and a delayed depolarization induced by transient potassium current blockade in rat hippocampal slice as studied by optical recording. J Neurosci 16: 5672-5687.

Beckius GE, Batra R, Oliver DL (1999) Axons from anteroventral cochlear nucleus that terminate in medial superior olive of cat: Observations related to delay lines. J Neurosci 19: 3146-3161.

Behrend O, Brand A, Kapfer C, Grothe B (2002) Auditory response properties in the superior paraolivary nucleus of the gerbil. J Neurophysiol 87: 2915-2928.

Ben Ari Y, Cherubini E, Corradetti R, Gaiarsa JL (1989) Giant synaptic potentialsin immature rat CA3 hippocampal neurones. J Physiol (Lond) 416: 303-325.

Ben Ari Y, Khazipov R, Leinekugel X, Caillard O, Gaiarsa JL (1997) GABAA, NMDA and AMPA receptors: a developmentally regulated `menage a trois´. Trends Neurosci 20: 523-529.

Billups D, Attwell D (2002) Control of intracellular chloride concentration and GABA response polarity in rat retinal ON bipolar cells. J Physiol (Lond) 545: 183-198.

Borst JGG, Helmchen F, Sakmann B (1995) Pre- and postsynaptic whole-cell recordings in the medial nucleus of the trapezoid body of the rat. J Physiol (Lond) 489: 825-840.

Brand A, Behrend O, Marquardt T, Mcalpine D, Grothe B (2002) Precise inhibition is essential for microsecond interaural time difference coding. Nature 417: 543-547.

Caird D, Klinke R (1983) Processing of binaural stimuli by cat superior olivary complex neurons. Exp Brain Res 52: 385-399.

Cant NB, Casseday JH (1986) Projections from the anteroventral cochlear nucleus to the lateral and medial superior olivary nuclei. J Comp Neurol 247: 457-476.

Cant NB (1991) Projections to the lateral and medial superior olivary nuclei from the spherical and globular bushy cells of the anteroventral cochlear nucleus. In: neurobiology of hearing: The central auditory system (Altschuler RA, Bobbin RP, Clopton BM, Hoffman DW, eds), pp 99-119. New York: Raven Press, Ltd.

Cant NB, Hyson RL (1992) Projections from the lateral nucleus of the trapezoid body to the medial superior olivary nucleus in the gerbil. Hearing Res 58: 26-34.

Cant NB (1997) Neuroscience: The auditory system (Purves D, Augustine GJ, Fitzpatrick D, Katz LC, Lamantia AS, Mcnamara JO, eds), pp 238. Massachusetts: Sinauer Publishers.

Carr CE, Konishi M (1988) Axonal delay lines for time measurement in the owl's brainstem. Proc Natl Acad Sci USA 85: 8311-8315.

Chen G, Trombley PQ, van den Pol AN (1996) Excitatory actions of GABA in developing rat hypothalamic neurones. J Physiol (Lond) 494: 451-464.

Cherubini E, Rovira C, Gaiarsa JL, Corradetti R, Ben-Ari Y (1990) GABA mediated excitation in immature rat CA3 hippocampal neurons. Int J Dev Neurosci 8: 481-490.

Cherubini E, Gaiarsa JL, Ben-Ari Y (1991) GABA: an excitatory transmitter in early postnatal life. Trends Neurosci 14: 515-519.

Clark GM (1969a) The ultrastructure of nerve endings in the medial superior olive of the cat. Brain Res 14: 293-305.

Clark GM (1969b) Vesicle shape versus type of synapse in the nerve endings of the cat medial superior olive. Brain Res 15: 548-551.

Cohen I, Navarro V, Clemenceau S, Baulac M, Miles R (2002) On the origin of interictal activity in human temporal lobe epilepsy in vitro. Science 298: 1418-1421.

Dammerman RS, Flint AC, Noctor S, Kriegstein AR (2000) An excitatory GABAergic plexus in developing neocortical layer 1. J Neurophysiol 84: 428-434.

deBeer ZJ (1997) Comparison of fluorescent voltage-sensitive dyes for multisite optical recording in hamster cerebral cortex by measurement of bicuculline-induced epileptiform events. Neuroimage 5: 154-163.

Dehmel S, Kopp-Scheinpflug C, Dörrscheidt GJ, Rübsamen R (2002) Electrophysiological characterization of the superior paraolivary nucleus in the mongolian gerbil. Hearing Res 172: 18-36.

Delpire E (2000) Cation-chloride cotransporters in neuronal communication. News Physiol Sci 15: 309-312.

Demir R, Haberly LB, Jackson MB (1998) Voltage imaging of epileptiform activity in slices from rat piriform cortex: onset and propagation. J Neurophysiol 80: 2727-2742.

Ebner TJ, Chen G (1995) Use of voltage-sensitive dyes and optical recordings in the central nervous system. Prog Neurobiol 46: 463-506.

Ehrlich I, Löhrke S, Friauf E (1999) Shift from depolarizing to hyperpolarizing glycine action in rat auditory neurons is due to age-dependent Cl$^-$ regulation. J Physiol (Lond) 520: 121-137.

Ene FA, Kullmann PH, Gillespie DC, Kandler K (2003) Glutamatergic calcium responses in the developing lateral superior olive: receptor types and their specific activation by synaptic activity patterns. J Neurophysiol 90: 2581-2591.

Erulkar SD (1972) Comparative aspects of spatial localization of sound. Physiol Rev 52: 237-360.

Feng AS, Rogowski BA (1980) Effects of monaural and binaural occlusion on the morphology of neurons in the medial superior olivary nucleus of the rat. Brain Res 189: 530-534.

Finlayson PG, Adam TJ (1997) Excitatory and inhibitory response adaptation in the superior olive complex affects binaural acoustic processing. Hear Res 103: 1-18.

Forsythe ID, Barnes-Davies M (1993a) The binaural auditory pathway: membrane currents limiting multiple action potential generation in the rat medial nucleus of the trapezoid body. Proc R Soc Lond [Biol] 251: 143-150.

Forsythe ID, Barnes-Davies M (1993b) The binaural auditory pathway: excitatory amino acid receptors mediate dual timecourse excitatory postsynaptic currents in the rat medial nucleus of the trapezoid body. Proc R Soc Lond [Biol] 251: 151-157.

Friauf E, Ostwald J (1988) Divergent projections of physiologically characterized rat ventral cochlear nucleus neurons as shown by intraaxonal injection of horseradish peroxidase. Exp Brain Res 73: 263-284.

Fukunishi K, Murai N, Uno H (1992) Dynamic characteristics of the auditory cortex of guinea pigs observed with multichannel optical recording. Biol Cybern. 67: 501-509.

Fukunishi K, Murai N (1995) Temporal coding in the guinea-pig auditory cortex as revealed by optical imaging and its pattern-time-series analysis. Biological Cybernetics 72: 463-473.

Funabiki K, Koyano K, Ohmori H (1998) The role of GABAergic inputs for coincidence detection in the neurones of nucleus laminaris of the chick. J Physiol (Lond) 508: 851-869.

Galambos R, Schwartzkopff J, Rupert A (1959) Microelectrode study of superior olivary nuclei. Am J Physiol 197: 527-536.

Ganguly K, Schinder AF, Wong ST, Poo M (2001) GABA itself promotes the developmental switch of neuronal GABAergic responses from excitation to inhibition. Cell 105: 521-532.

Glendenning KK, Hutson KA, Nudo RJ, Masterton RB (1985) Acoustic chiasm II: Anatomical basis of binaurality in the lateral superior olive of the cat. J Comp Neurol 232: 261-285.

Goldberg JM, Brown PB (1968) Functional organization of the dog superior olivary complex: an anatomical and electrophysiological study. J Neurophysiol 31: 639-656.

Goldberg JM, Brown PB (1969) Response of binaural neurons of dog superior olivary complex to dichotic tonal stimuli: Some physiological mechanism of sound localization. J Neurophysiol 32: 613-636.

Grinvald A, Frostig RD, Lieke E, Hildesheim R (1988) Optical imaging of neuronal activity. Physiological Reviews 68: 1285-1366.

Grinvald A, Lieke EE, Frostig RD, Hildesheim R (1994) Cortical point-spread function and long-range lateral interactions revealed by real-time optical imaging of macaque monkey primary visual cortex. J Neurosci 14: 2545-2568.

Grothe B, Vater M, Casseday JH, Covey E (1992) Monaural interaction of excitation and inhibition in the medial superior olive of the mustached bat: An adaptation for biosonar. Proc Natl Acad Sci USA 89: 5108-5112.

Grothe B, Sanes DH (1993) Bilateral inhibition by glycinergic afferents in the medial superior olive. J Neurophysiol 69: 1192-1196.

Grothe B, Sanes DH (1994) Synaptic inhibition influences the temporal coding properties of medial superior olivary neurons: An in vitro study. J Neurosci 14: 1701-1709.

Grothe B (1994) Interaction of excitation and inhibition in processing of pure tone and amplitude-modulated stimuli in the medial superior olive of the mustached bat. J Neurophysiol 71: 706-721.

Grothe B, Park TJ (1998) Sensitivity to interaural time differences in the medial superior olive of a small mammal, the Mexican free-tailed bat. J Neurosci 18: 6608-6622.

Grothe B (2000) The evolution of temporal processing in the medial superior olive, an auditory brainstem structure. Prog Neurobiol 61: 581-610.

Grothe B (2003) New roles for synaptic inhibition in sound localization. Nat Rev Neurosci 4: 540-550.

Guinan JJ Jr, Li RY (1990) Signal processing in brainstem auditory neurons which receive giant endings (calyces of Held) in the medial nucleus of the trapezoid body of the cat. Hearing Res 49: 321-334.

Hafidi A, Sanes DH, Hillman DE, Kedeshian P (1994) Structural and molecular heterogeneity of astrocytes and oligodendrocytes in the gerbil lateral superior olive. Neuroscience 60: 503-519.

Hafidi A, Katz JA, Sanes DH (1996) Differential expression of MAG, MBP and L1in the developing lateral superior olive. Brain Res 736: 35-43.

Heffner RS, Heffner HE (1990) The evolution of sound localization. Comparative perception I: Discrimination (Berkley M, Stebbins W, eds), pp 285. New York: Wiley Publications.

Huang BO, Redburn DA (1996) GABA-induced increases in $[Ca^{2+}]_i$ in retinal neurons of postnatal rabbits. Vis Neurosci 13: 441-447.

Hubner CA, Stein V, Hermans-Borgmeyer I, Meyer T, Ballanyi K, Jentsch TJ (2001) Disruption of KCC2 reveals an essential role of K-Cl cotransport already in early synaptic inhibition. Neuron 30: 515-524.

Illing RB, Kraus KS, Michler SA (2000) Plasticity of the superior olivary complex. Microsc Res Tech 51: 364-381.

Inbody SB, Feng AS (1981) Binaural response characteristics of single neurons in the medial superior olivary nucleus of the albino rat. Brain Res 210: 361-366.

Inoue M, Hashimoto Y, Kudo Y, Miyakawa H (2001) Dendritic attenuation of synaptic potentials in the CA1 region of rat hippocampal slices detected with an optical method. Eur J Neurosci 13: 1711-1721.

Irvine RF (1986) Calcium transients: mobilization of intracellular $Ca^{2+}$. Br Med Bull 42: 369-374.

Irvine DRF (1986) Progress in sensory physiology 7. The auditory brainstem. Berlin, Heidelberg, New York: Springer Press, Ltd.

Irvine DRF (1992) Physiology of the auditory brainstem. In: The mammalian auditory pathway: Neurophysiolgy (Popper AN, Fay RR, eds), pp 153-231. New York: Springer Press, Ltd.

Janigro D, Schwartzkroin PA (1988a) Effects of GABA and baclofen on pyramidal cells in the developing rabbit hippocampus: an 'in vitro' study. Brain Res 469: 171-184.

Janigro D, Schwartzkroin PA (1988b) Effects of GABA on CA3 pyramidal cell dendrites in rabbit hippocampal slices. Brain Res 453: 265-274.

Jeffress LA (1948) A place theory of sound localization. J Comp Psychol 41: 35-39.

Jen PH, Feng R, Chen B (2003) GABAergic inhibition and the effect of sound direction on rate-intensity functions of inferior collicular neurons of the big brown Bat, Eptesicus fuscus. Chin J Physiol 46: 83-90.

Joris PX, Smith PH, Yin TCT (1998) Coincidence detection in the auditory system: 50 years after Jeffress. Neuron 21: 1235-1238.

Kakazu Y, Akaike N, Komiyama S, Nabekura J (1999) Regulation of intracellular chloride by cotransporters in developing lateral superior olive neurons. J Neurosci 19: 2843-2851.

Kandler K, Friauf E (1995) Development of glycinergic and glutamatergic synaptic transmission in the auditory brainstem of perinatal rats. J Neurosci 15: 6890-6904.

Kauer JS, White J (2001) Imaging and coding in the olfactory system. Annu Rev Neurosci 24: 963-979.

Kelly JB, Liscum A, Vanadel B, Ito M (1998) Projections from the superior olive and lateral lemniscus to tonotopic regions of the rat's inferior colliculus. Hearing Res 116: 43-54.

Kim G, Kandler K (2003) Elimination and strengthening of glycinergic/GABAergic connections during tonotopic map formation. Nat Neurosci 6: 282-290.

Köhling R, Höhling JM, Straub H, Kuhlmann D, Kuhnt U, Tuxhorn I, Ebner A, Wolf P, Pannek HW, Gorji A, Speckmann EJ (2000) Optical monitoring of neuronal activity during spontaneous sharp waves in chronically epileptic human neocortical tissue. J Neurophysiol 84: 2161-2165.

_____

Kohling R, Vreugdenhil M, Bracci E, Jefferys JG (2000) Ictal epileptiform activity is facilitated by hippocampal GABA$_A$ receptor-mediated oscillations. J Neurosci 20: 6820-6829.

Kotak VC, Korada S, Schwartz IR, Sanes DH (1998) A developmental shift from GABAergic to glycinergic transmission in the central auditory system. J Neurosci 18: 4646-4655.

Koyano K, Ohmori H (1996) Cellular approach to auditory signal transmission. Jpn J Physiol 46: 289-310.

Kulesza RJ, Spirou GA, Berrebi AS (2003) Physiological response properties of neurons in the superior paraolivary nucleus of the rat. J Neurophysiol 89, 2299-2312.

Kullmann PH, Ene FA, Kandler K (2002) Glycinergic and GABAergic calcium responses in the developing lateral superior olive. Eur J Neurosci 15: 1093-1104.

Kuwabara N, Zook JM (1991) Classification of the principal cells of the medial nucleus of the trapezoid body. J Comp Neurol 314: 707-720.

Kuwabara N, Zook JM (1992) Projections to the medial superior olive from the medial and lateral nuclei of the trapezoid body in rodents and bats. J Comp Neurol 324: 522-538.

Laaris N, Carlson GC, Keller A (2000) Thalamic-evoked synaptic interactions in barrel cortex revealed by optical imaging. J Neurosci 20: 1529-1537.

Langford TL (1984) Responses elicited from medial superior olivary neurons by stimuli associated with binaural masking and unmasking. Hear Res 15: 39-50.

Leznik E, Makarenko V, Llinas R (2002) Electrotonically mediated oscillatory patterns in neuronal ensembles: An in vitro voltage-dependent dye-imaging study in the inferior olive. J Neurosci 22: 2804-2815.

Llinas RR, Leznik E, Urbano FJ (2002) Temporal binding via cortical coincidence detection of specific and nonspecific thalamocortical inputs: a voltage-dependent dye-imaging study in mouse brain slices. Proc Natl Acad Sci USA 99: 449-454.

London JA, Cohen LB, Wu JY (1989) Optical recordings of the cortical response to whisker stimulation before and after the addition of an epileptogenic agent. J Neurosci 9: 2182-2190.

Lo Turco JJ, Owens DF, Heath MJS, Davis MBE, Kriegstein AR (1995) GABA and glutamate depolarize cortical progenitor cells and inhibit DNA synthesis. Neuron 15: 1287-1298.

Luhmann HJ, Prince DA (1991) Postnatal maturation of the GABAergic system in rat neocortex. J Neurophysiol 65: 247-263.

Momose-Sato Y, Sakai T, Hirota A, Sato K, Kamino K (1994) Optical mapping of early embryonic expressions of Mg(2+)-/APV-sensitive components of vagal glutaminergic EPSPs in the chick brainstem. J Neurosci 14: 7572-7584.

Momose-Sato Y, Sato K, Kamino K (2001) Optical approaches to embryonic development of neural functions in the brainstem. Prog Neurobiol 63: 151-197.

Moore MJ, Caspary DM (1983) Strychnine blocks binaural inhibition in lateral superior olivary neurons. J Neurosci 3: 237-242.

Mueller AL, Taube JS, Schwartzkroin PA (1984) Development of hyperpolarizing inhibitory postsynaptic potentials and hyperpolarizing response to gamma-aminobutyric acid in rabbit hippocampus studied in vitro. J Neurosci 4: 860-867.

Nabekura J, Katsurabayashi S, Kakazu Y, Shibata S, Matsubara A, Jinno S, Mizoguchi Y, Sasaki A, Ishibashi H (2004) Developmental switch from GABA to glycine release in single central synaptic terminals. Nat Neurosci 7: 17-23.

Nelson DA, Katz LC (1995) Emergence of functional circuits in ferret visual cortex visualized by optical imaging. Neuron 15: 23-34.

Neunlist M, Peters S, Schemann M (1999) Multisite optical recording of excitability in the enteric nervous system. Neurogastroenterology & Motility 11: 393-402.

Oliver DL (2000) Ascending efferent projections of the superior olivary complex. Microsc Res Tech 51: 355-363.

Onimaru H, Kanamaru A, Homma I (1996) Optical imaging of respiratory burst activity in newborn rat medullary block preparations. Neurosci Res. 2: 183-190.

Overholt EM, Rubel EW, Hyson RL (1992) A circuit for coding interaural time differences in the chick brainstem. J Neurosci 12: 1698-1708.

Owens DF, Boyce LH, Davis MB, Kriegstein AR (1996) Excitatory GABA responses in embryonic and neonatal cortical slices demonstrated by gramicidin perforated-patch recordings and calcium imaging. J Neurosci 16: 6414-6423.

Perkins RE (1973) An electron microscopic study of synaptic organization in the medial superior olive of normal and experimental chinchillas. J Comp Neurol 148: 387-415.

Petersen CCH, Sakmann B (2001) Functionally independent columns of rat somatosensory barrel cortex revealed with voltage-sensitive dye imaging. J Neurosci 21: 8435-8446.

Petersen CCH, Grinvald A, Sakmann B (2003) Spatiotemporal dynamics of sensory responses in layer 2/3 of rat barrel cortex measured in vivo by voltage-sensitive dye imaging combined with whole-cell voltage recordings and neuron reconstructions. J Neurosci 23: 1298-1309.

Ramon y Cajal S (1907) Histologie du systeme nerveux de l'homme et des vertebrates. Paris: Malonie.

Reichling DB, Kyrozis A, Wang J, Mac Dermott AB (1994) Mechanisms of GABA and glycine depolarization-induced calcium transients in rat dorsal horn neurons. J Physiol (Lond) 476: 411-421.

Rhode WS, Greenberg S (1994) Lateral suppression and inhibition in the cochlear nucleus of the cat. J Neurophysiol 71: 493-514.

Rietzel HJ, Friauf E (1998) Neuron types in the rat lateral superior olive and developmental changes in the complexity of their dendritic arbors. J Comp Neurol 390: 20-40.

Rivera C, Voipio J, Payne JA, Ruusuvuori E, Lahtinen H, Lamsa K, Pirvola U, Saarma M, Kaila K (1999) The $K^+$/$Cl^-$ co-transporter KCC2 renders GABA hyperpolarizing during neuronal maturation. Nature 397: 251-255.

Rogowski BA, Feng AS (1981) Normal postnatal development of medial superior olivary neurons in the albino rat: A Golgi and Nissl study. J Comp Neurol 196: 85-97.

Rohrbough J, Spitzer NC (1996) Regulation of intracellular $Cl^-$ levels by $Na^+$-dependent $Cl^-$ cotransport distinguishes depolarizing from hyperpolarizing $GABA_A$ receptor-mediated responses in spinal neurons. J Neurosci 16: 82-91.

Saint Marie RL, Baker RA (1990) Neurotransmitter-specific uptake and retrograde transport of [$^3$H]glycine from the inferior colliculus by ipsilateral projections of the superior olivary complex and nuclei of the lateral lemniscus. Brain Res 524: 244-253.

Saldana E, Berrebi AS (2000) Anisotropic organization of the rat superior paraolivary nucleus. Anat Embryol (Berl) 202: 265-279.

Salzberg BM, Obaid AL, Bezanilla F (1993) Microsecond response of a voltage-sensitive merocyanine dye: fast voltage-clamp measurements on squid giant axon. Jpn J Physiol 43: 37-41.

Sanes DH, Geary WA, Wooten GF, Rubel EW (1987) Quantitative distribution of the glycine receptor in the auditory brain stem of the gerbil. J Neurosci 7: 3793-3802.

Sanes DH, Rubel EW (1988) The ontogeny of inhibition and excitation in the gerbil lateral superior olive. J Neurosci 8: 682-700.

Sanes DH, Goldstein NA, Ostad M, Hillman DE (1990) Dendritic morphology of central auditory neurons correlates with their tonotopic position. J Comp Neurol 294: 443-454.

Sanes DH (1993) The development of synaptic function and integration in the central auditory system. J Neurosci 13: 2627-2637.

Sato K, Momose-Sato Y, Hirota A, Sakai T, Kamino K (1998) Optical mapping of neural responses in the embryonic rat brainstem with reference to the early functional organization of vagal nuclei. J Neurosci 18: 1345-1362.

Schofield BR (1995) Projections from the cochlear nucleus to the superior paraolivary nucleus in guinea pigs. J Comp Neurol 360: 135-149.

Schwarz DW (1992) Sound delay lines in the nucleus laminaris of the chicken. J Otolaryngol 21: 202-208.

Simmons JA (1987) Directional hearing and sound localization in echolocating animals.In: Directional hearing (Yost WA, Gourevitch G, eds), pp 214. New York: Springer-verlag.

Smith AJ, Owens S, Forsythe ID (2000) Characterisation of inhibitory and excitatory postsynaptic currents of the rat medial superior olive. J Physiol (Lond) 529: 681-698.

Smith PH, Joris PX, Yin TCT (1993) Projections of physiologically characterized spherical bushy cell axons from the cochlear nucleus of the cat: evidence for delay lines to the medial superior olive. J Comp Neurol 331: 245-260.

Smith PH (1995) Structural and functional differences distinguish principal from nonprincipal cells in the guinea pig MSO slice. J Neurophysiol 73: 1653-1667.

Smith PH, Joris PX, Yin TCT (1998) Anatomy and physiology of principal cells of the medial nucleus of the trapezoid body (MNTB) of the cat. J Neurophysiol 79: 3127-3142.

Sommer I, Lingenhöhl K, Friauf E (1993) Principal cells of the rat medial nucleus of the trapezoid body: An intracellular in vivo study of their physiology and morphology. Exp Brain Res 95: 223-239.

Spangler KM, Warr WB, Henkel CK (1985) The projections of principal cells of the medial nucleus of the trapezoid body in the cat. J Comp Neurol 238: 249-262.

Spitzer MW, Semple MN (1995) Neurons sensitive to interaural phase disparity in gerbil superior olive: Diverse monaural and temporal response properties. J Neurophysiol 73: 1668-1690.

Spors H, Grinvald A (2002) Spatio-temporal dynamics of odor representations in the mammalian olfactory bulb. Neuron 34: 301-15.

Srinivasan G, Friauf E, Löhrke S (2004a) Differential timing of the development of inhibition within the superior olivary complex revealed by optical imaging. Assn Res Otolaryngol Abstr 27: 917.

Srinivasan G, Friauf E, Löhrke S (2004b) Functional glutamatergic and glycinergic inputs to several superior olivary nuclei of the rat revealed by optical imaging. Neuroscience (in press).

Stotler WA (1953) An experimental study of the cells and connections of the superior olivary complex of the cat. J Comp Neurol 98: 401-431.

Suneja SK, Benson CG, Gross J, Potashner SJ (1995) Evidence for glutamatergic projections from the cochlear nucleus to the superior olive and the ventral nucleus of the lateral lemniscus. J Neurochem 64: 161-171.

Thompson AM, Schofield BR (2000) Afferent projections of the superior olivary complex. Microsc Res Tech 51: 330-354.

Tolbert LP, Morest DK (1982) The neuronal architecture of the anteroventral cochlear nucleus of the cat in the region of the cochlear nerve root: Golgi and Nissl methods. Neuroscience 7: 3013-3030.

Tolbert LP, Morest DK, Yurgelun-Todd DA (1982) The neuronal architecture of the anteroventral cochlear nucleus of the cat in the region of the cochlear nerve root: horseradish peroxidase labelling of identified cell types. Neuroscience 7: 3031-3052.

Tollin DJ, Yin TCT (2002a) The coding of spatial location by single units in the lateral superior olive of the cat. I. Spatial receptive fields in azimuth. J Neurosci 22: 1454-1467.

Tollin DJ, Yin TCT (2002b) The coding of spatial location by single units in the lateral superior olive of the cat. II. The determinants of spatial receptive fields in azimuth. J Neurosci 22: 1468-1479.

Vater M, Feng AS (1990) Functional organization of ascending and descending connections of the cochlear nucleus of horseshoe bats. J Comp Neurol 292: 373-395.

Vater M (1995) Ultrastructural and immunocytochemical observations on the superior olivary complex of the mustached bat. J Comp Neurol 358: 155-180.

Waggoner AS (1979a) The use of cyanine dyes for the determination of membrane potentials in cells, organelles, and vesicles. Methods Enzymol 55: 689-695.

Waggoner AS (1979b) Dye indicators of membrane potential. Annu Rev Biophys Bioeng 8: 47-68.

Warr WB (1966) Fiber degeneration following lesions in the anterior ventral cochlear nucleus of the cat. Exp Neurol 14: 453-474.

_____

Warr WB (1972) Fiber degeneration following lesions in the multipolar and globular cell areas in the ventral cochlear nucleus of the cat. Brain Res 40: 247-270.

Wenthold RJ (1991) Neurotransmitters of brainstem auditory nuclei. In: Neurobiology of Hearing: The Central Auditory System (Altschuler RA, Bobbin RP, Clopton BM, Hoffman DW, eds), pp 121-139. New York: Raven Press Ltd.

Wong CG, Bottiglieri T, Snead OC (2003) GABA, gamma-hydroxybutyric acid, and neurological disease. Ann Neurol 54: 3-12.

Wu SH, Kelly JB (1991) Physiological properties of neurons in the mouse superior olive: membrane characteristics and postsynaptic responses studied in vitro. J Neurophysiol 65: 230-246.

Wu SH, Kelly JB (1992a) NMDA, non-NMDA and glycine receptors mediate binaural interaction in the lateral superior olive: physiological evidence from mouse brain slice. Neurosci Lett 134: 257-260.

Wu SH, Kelly JB (1992b) Synaptic pharmacology of the superior olivary complex studied in mouse brain slice. J Neurosci 12: 3084-3097.

Wu SH, Kelly JB (1994) Physiological evidence for ipsilateral inhibition in the lateral superior olive: Synaptic responses in mouse brain slice. Hearing Res 73: 57-64.

Wu SH, Kelly JB (1995) Inhibition in the superior olivary complex: Pharmacological evidence from mouse brain slice. J Neurophysiol 73: 256-269.

Wu WL, Ziskind-Conhaim L, Sweet MA (1992) Early development of glycine- and GABA-mediated synapses in rat spinal cord. J Neurosci 12: 3935-3945.

Wu JY, Lam YW, Falk CX, Cohen LB, Fang J, Loew L, Prechtl JC, Kleinfeld D, Tsau Y (1998) Voltage-sensitive dyes for monitoring multineuronal activity in the intact central nervous system. Histochem J 30: 169-187.

Ye J (2000) Physiology and pharmacology of native glycine receptors in developing rat ventral tegmental area neurons. Brain Res 862: 74-82.

Yin TCT, Chan JCK (1990) Interaural time sensitivity in medial superior olive of cat. J Neurophysiol 64: 465-488.

Yuste R, Katz LC (1991) Control of postsynaptic $Ca^{2+}$ influx in developing neocortex by excitatory and inhibitory neurotransmitters. Neuron 6: 333-344.

Zhang L, Spigelman I, Carlen PL (1990) Whole-cell patch study of GABAergic inhibition in CA1 neurons of immature rat hippocampal slices. Brain Res Dev Brain Res 56: 127-130.

# 8 Appendix

## Abbreviations

| | |
|---|---|
| $[Cl^-]_i$ | Intracellular chloride concentration |
| $[K^+]_e$ | Extracellular potassium concentration |
| AMPA | $\alpha$-Amino-3-hydroxy-5-methyl-4-isoxazol-propionate |
| AP | Action potential |
| AVCN | Antero ventral cochlear nucleus |
| CCD | Charge coupled device |
| CN | Cochlear nucleus |
| CNQX | 6-cyano-7-nitroquinoxaline-2,3- dione |
| DIC | Differential interference contrast |
| E | Embryonic day |
| $E_{Gly}$ | Glycine reversal potential |
| EPSP | Excitatory postsynaptic potential |
| F | Fluorescence baseline level |
| $\Delta F$ | Fluorescence change |
| $\Delta F/F$ | Change in fluorescence / baseline level fluorescence |
| FFT | Fast fourier transformation |
| GABA | $\gamma$-amino-butyric acid |
| HF | High frequency |
| IC | Inferior colliculus |
| ITD | Interaural time difference |
| ILD | Interaural level difference |
| IPSP | Inhibitory postsynaptic potential |

| | |
|---|---|
| KCC2 | Potassium chloride cotransporter isoform 2 |
| LSO | Lateral superior olive |
| LNTB | Lateral nucleus of the trapezoid body |
| LF | Low frequency |
| MNTB | Medial nucleus of the trapezoid body |
| MSO | Medial superior olive |
| NMDA | N-methyl-D-aspartate |
| PDA | Photodiode array |
| PON | Periolivary nucleus |
| P | Postnatal day |
| RLI | Resting light intensity |
| $V_m$ | Resting membrane potential |
| SE | Stimulus electrode |
| SEM | Standard error of mean |
| SOC | Superior olivary complex |
| SPN | Superior paraolivary nucleus |
| TTX | Tetrodotoxin |
| VSD | Voltage-sensitive dyes |
| VNTB | Ventral nucleus of the trapezoid body |

# Curriculum Vitae

**Geetha Srinivasan**

Born in Mayiladuthurai (12.09.1976), Tamilnadu, India, as elder daughter of Thozhudoor Srinivasan Sudarsana Ramanujam and Chandra Srinivasan

| | |
|---|---|
| 2001-present | Ph.D student in the Sensory and Developmental Neurobiology laboratory of Prof. Eckhard Friauf, University of Kaiserslautern, Kaiserslautern, Germany |
| 1999-2000 | Research Assistant in the Cardiovascular Research laboratory of Prof. Lee-Young Chau, Inst. of Biomedical Sciences, Academia Sinica, Taipei, Taiwan |
| | Project: Post-transcriptional regulation of H-ferritin mRNA in human monocytic THP-1 cells |
| 1994-1999 | Obtained 'Master of Science' in Life Sciences (Specialization in Biotechnology – five years integrated course), from Bharathidasan University, Tiruchirappalli, Tamilnadu, India |
| | Thesis: Scope of evolving tissue culture techniques for the production of secondary metabolites in efficient *Withania somnifera* (L.) Dunal strain with reference to the pharmacological studies.<br>Thesis award: Tamilnadu state council for science and technology |
| 1992-1994 | Higher secondary schooling at Jawahar matriculation higher secondary school, Neyveli, Tamilnadu, India |
| 1986-1991 | Elementary schooling at Sabanayaka mudaliar hindu higher secondary school, Sirkali, Tamilnadu, India |
| 1981-1986 | Primary schooling at Thaiyalnayaki primary school, Vaitheeswarankoil, Tamilnadu, India |

# Acknowledgements

Grateful and sincere thanks to Prof. Eckhard Friauf for rendering me an opportunity to do this work in his lab, and for his farsighted guidance and kind support. I thank Prof. Rüdiger Köhling for demonstrating his VSD imaging setup to have a better understanding over the same, and Prof. Joachim Deitmer for his comments during the neurobiology seminar. I also thank these professors for having participated in my dissertation committee.

I am highly indebted to my direct supervisor, Dr. Stefan Löhrke, who taught me the ABC's of neurophysiology. His continual support and valuable guidance in every phase enabled me to complete this work. I also thank Dr. Hansgerd Nothwang for his constructive criticisms and discussions during the lab meetings.

Many thanks to the personals of electronic workshop in the university of Kaiserslautern, for their kind support in fighting against the noise. Thanks to: Sascha for his excellent technical assistance, Petra for her constant help, Dr. Harald Vitten for demonstrating things during my arrival and for his help, and Dennis Daniel for getting me the backups whenever I lost my data. I would like to extend my thanks to Obi for collaborating with me and to all my colleagues (Michael, Peter, Kornelia, Katia, Isa, Nicole, Alex, Jens, Markus, and Anne) for their help and good times in the lab.

I thank Prof. Lee-Young Chau for having me shown the way of research, and Drs. M. Krishnan, S. Karuthapandian, A. Ganapathi for their encouragement and support. To my friends (Shiva, Poongo, Ajay, Ajoy, Kitcha, Leena, and Karthi), I thank you all for having made these years enjoyable.

I feel a deep sense of gratitude for my parents. The happy memory of my mother still provides a persistent inspiration for my journey in this life. I am grateful to my brothers Lord Nan, Bulb Babu, and my sister Thoppai Sumi for their love and support throughout these years! Finally, I thank Veera for his love, encouragement and support over a decade.